Experimental and Numerical Investigation of Dry Turning AISI 1030 Carbon Steel

Gebremichael Haileselasse Alemayoh

A Thesis Submitted to

The Department of Mechanical Engineering

School of Mechanical, Chemical and Materials Engineering

Presented in Partial Fulfillment of the Requirement for the Degree of Master's in Manufacturing Engineering

Office of Graduate Studies

Adama Science and Technology University

November 2022

Adama, Ethiopia

Experimental and Numerical Investigation of Dry Turning AISI 1030 Carbon Steel

Gebremichael Haileselasse Alemayoh

Advisor: Dr Balkeshwar Singh
Professor

A Thesis Submitted to

The Department of Mechanical Engineering

School of Mechanical, Chemical and Materials Engineering

Presented in Partial Fulfillment of the Requirement for the Degree of Master's in Manufacturing Engineering

Office of Graduate Studies

Adama Science and Technology University

November 2022

Adama, Ethiopia

DECLARATION

I hereby declare that this Master Thesis entitled "Experimental and Numerical Investigation of Dry Turning AISI 1030 Carbon Steel" is my original work. That is, it has not been submitted for the award of any academic degree, diploma or certificate in any other university. All sources of materials that are used for this thesis have been duly acknowledged through citation

________________	________________________	________________
Name of student	Signature	Date

RECOMMENDATION

I, the advisors of this thesis, hereby certify that I have read the revised version of the thesis entitled" Experimental and Numerical Investigation of Dry Turning AISI 1030 Carbon Steel" was prepared under our guidance by Gebremichael Haileselasse Alemayoh and submitted in partial fulfilment of the requirements for the degree of Mater's of Science in Manufacturing Engineering. Therefore, I recommend the submission of the revised version of the thesis to the department following the applicable procedures.

Dr Balkeshwar Singh (Professor)

Main Advisor	Signature	Date

APPROVAL SHEET

I, the advisor of the thesis entitled “Experimental and Numerical Investigation of Dry Turning AISI 1030 Carbon Steel” and developed by Gebremichael Haileselasse Alemayoh, hereby certify that the recommendation and suggestions made by the board of examiners are appropriately incorporated into the final version of the thesis.

Dr Balkeshwar Singh (Professor)

______________________	______________________	______________________
Main Advisor	Signature	Date

We, the undersigned, members of the Board of Examiners of the thesis by Gebremichael Haileselasse Alemayoh have read and evaluated the thesis entitled” Experimental and Numerical Investigation of Dry Turning AISI 1030 Carbon Steel” and examined the candidate during the open defence. This is, therefore, to certify that the thesis is accepted for partial fulfilment of the requirement of the degree of Master of Science in Manufacturing Engineering.

______________________	______________________	______________________
Chairperson	Signature	Date
______________________	______________________	______________________
Internal Examiner	Signature	Date
______________________	______________________	______________________
Eternal Examiner	Signature	Date

Finally, approval and acceptance of the thesis are contingent upon the submission of its final copy to the Office of Postgraduate Studies (OPGS) through the Department Graduate Council (DGC) and School Graduate Committee (SGC).

______________________	______________________	______________________
Department Head	Signature	Date
______________________	______________________	______________________
School Dean	Signature	Date
______________________	______________________	______________________
Office of Postgraduate Studies, Dean	Signature	Date

ACKNOWLEDGMENT

First, I would like to express my gratitude to Almighty God for enabling me to complete this thesis. For his continuous support, direction, comments, and recommendations throughout the thesis work, I would especially want to thank my adviser, Dr Balkeshwar Singh, Professor in the Mechanical Design and Manufacturing Engineering Program at Adama Science and Technology University. I also want to express my gratitude to Dr Moera Gutu for his support and advice throughout my master's study. For their kind assistance and for providing the workshop facility and tools needed to carry out the experimental work, I would especially like to thank the management staff, the supervisors of the Mechanical Engineering Department, the management staff of Ethio-Technical University, and the machinists there. I want to express my gratitude to Adama Science and Technology University for giving me the chance to complete my master's degree and conduct this research.

Finally, I would like to express my gratitude to all of my friends for their significant support, encouragement, and contributions to preparing this research. Their advice and suggestions helped me a lot.

TABLE OF CONTENTS

CONTENTS PAGE

LIST OF FIGURES

LIST OF TABLES

ACRONYMS AND ABBREVIATIONS

AISI	American Iron and Steel Institute
Al2O3	Aluminium Oxide
ANOVA	Analysis Of Variance
BUE	Built-up-Edge
CBN	Cubic Boron Nitride
CVD	Chemical Vapour Deposition
CNC	Computer Numerical Control
DOE	Design Of Experiment
DOF	Degree Of Freedom
FEA	Finite Element Analysis
FEM	Finite Element Method
GRA	Grey Relational Analysis
GRG	Grey Relational Grade
HB	Hardness, Brinell
HSS	High-Speed Steel
LN2	Liquid Nitrogen
MPa	Mega Pascal
MRR	Material Removal Rate
MSE	Mean Square Error
MWF	Metal-Working Fluid
OA	Orthogonal Array
PCBN	Polycrystalline Cubic Boron Nitride
PCD	Polycrystalline Diamond
PVD	Physical Vapour Deposition
Ra	Surface Roughness
RSM	Response Surface Methodology
SEM	Scanning Electron Microscope
SFM	Surface Feet Per Minute

ABSTRACT

Nowadays, modern metal industries have difficulty obtaining the required surface quality during machining. This is because various process parameters have an impact on the quality of the surface finish. As a result, optimizing the turning machining parameters such as cutting speed, depth of cut and feed is crucial to improve surface finish that minimizes mechanical failures caused by wear, and corrosion, and increases the productivity of the products. In addition to this, to minimize the limitations of experimental studies of metal cutting, finite element simulation is used, which improves time and cost. This study aims to investigate the dry turning of AISI 1030 carbon steel material experimentally and numerically using finite element simulation, as well as optimizing cutting parameters (cutting speed, depth of cut, and feed) to get a better surface finish, reduce tool wear, minimize tool temperature and maximize material removal rate. The experiment was designed using a Taguchi L9 orthogonal array, and an Analysis of Variance was used to determine the significance of cutting parameters on end responses. Finally, multi-response optimization using grey relational analysis was done, and an optimal parameter combination for the turning operation was obtained via this grey relational analysis. According to the results, cutting speed (67.21%) was the most significant parameter which influences surface roughness followed by feed rate (26.91%). At 250 m/min cutting speed, 0.5 mm depth of cut, and 0.15 mm/rev feed rate, the lowest surface roughness (1.21 µm) was achieved. The depth of cut had a significant impact on the material removal rate (66.13%), and the optimum material removal rate was 453.57 mm^3/s, which was attained at 90 m/min, 2.5 mm, and 0.35 mm/rev. With an average relative error of 4.85%, the Taguchi prediction and finite element simulation were in fair deal with the experimental finding. Tool temperature and tool wear rate were significantly affected by cutting speed with a contribution of 88.05% and 77.22%, respectively. A lower tool temperature (78.5^{0}C) and a lower tool wear rate (0.01494mm^3/s) were obtained at the lower level of parameters. Predicting and simulation of tool temperature and tool wear rate was closely related to the experimental results, with average relative errors of 5.58% and 6.69%, respectively. Cutting speed has the greatest influence on multiple responses of grey relational analysis, with a significance of 56.85%. The optimum parametric combination of multi-responses is 90 m/min, 0.25 mm, and 0.15 mm/rev.

Keywords: *Dry turning, AISI 1030 steel, FEM simulation, Surface Roughness, Tool wear, Material Removal Rate, Tool Temperature, grey relational analysis*

CHAPTER 1

INTRODUCTION

1.1 Background of the study

Modern industries aim to produce low-cost, high-quality items quickly since these factors impact the degree of satisfaction of the purchaser all through the utilization of the product. It additionally improves the goodwill of the company (Çelik & Kaçal, 2020)

Because a high-quality turned surface improves corrosion resistance, fatigue strength, and creep life. Other practical characteristics of parts, such as light reflection, wear, surface friction, lubricant retaining and dispersing, load-bearing capacity, coating, and fatigue resistance are also influenced by the quality of the surface (Dijmărescu & Tiriplica, 2019; Korkmaz et al., 2020). For that, computerized numerical control (CNC) equipment with high accuracy and quick processing times is used alongside automated and flexible manufacturing systems. Turning is the first and most used method of cutting, particularly for finishing machined parts. (Nalbant et al., 2007). The choice of cutting parameters for a turning operation is crucial to achieving excellent cutting performance. Typically, the required cutting settings are chosen using a handbook or based on experience

Turning metal steel is a significant segment of the manufacturing sector (Lalwani et al., 2008, Gunjal & Patil, 2018). To increase its strength and fracture resistance in comparison to other kinds of iron, steel is an alloy composed primarily of iron with a little amount of carbon. Steels can be divided into low carbon steels (0.05–0.30%), medium carbon steels (0.3-0.5%), and high carbon steels (greater than 0.6%) depending on the quantity of carbon present. AISI 1030 carbon steel is one of the steel types. It has a carbon content of about 0.30 % and is utilized in a variety of applications, including machinery parts, brackets, brakes, clips, clutches, springs, and washers (Bashir et al., 2018, Shihab et al., 2014). Surface quality, surface texture, dimensional deviations, and productivity all depend on the cutting parameters used for these steels. One of the main qualities of a turning product is surface roughness, which is used to assess and determine the quality of a product.

1.2 Turning

In recent years, advancements in machinery and cutting tools have made it possible to cut materials that have already hardened. The benefits of manufacturing components in a hardened condition include lower machining costs, shorter lead times, fewer machine tools required, increased surface quality, fewer finishing operations, and elimination of heat-induced component distortion (Attanasio et al., 2020; Hosseinkhani & Ng, 2018). One method for getting these benefits is turning. The most common method of the metal removal process in the industry is turning. In the largest context, turning refers to the formation of any cylindrically shaped surface using a single-point cutting tool in a lathe, where the direction of the feeding motion is mostly axial concerning the machine spindle. The basic turning procedure is schematically illustrated in Figure 1.1 with the feed rate, f, depth-of-cut, d, and spindle rotational speed, N in rev/min. Cutting speed is the workpiece's surface speed at the tooltip (Dhandapani et al., 2014).

In turning machining operations, the choice of cutting-tool materials for a certain application is one of the most crucial elements (Kam & Şeremet, 2021). The surface quality of products that have been machined during the turning process is affected by the type of tool material used. The cutting tool's strength must be greater than the material being machined. For turning activities, a variety of cutting tools are typically utilized. High-speed steel, coated and uncoated brazed type carbide tools, and ceramic and cubic boron nitride tools are some of them.

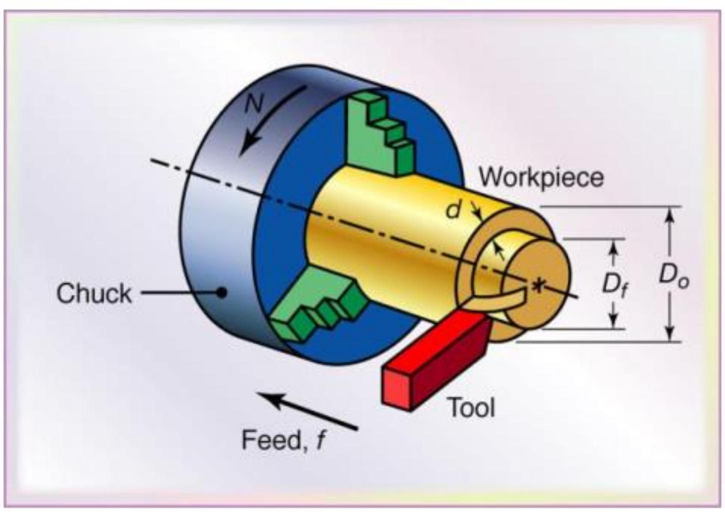

Figure 1. 1 Schematic Representation Of The Turning Process (Dhandapani et al., 2014)

The cutting tool separates chips from the workpiece which means removing material to obtain the desired shape and size. There are many different types of metal cutting tools, each of which is made to do a certain task. On a lathe machine, a single-point cutting tool is used to turn a variety of cylindrical shapes. The choice of the proper tool material is influenced by the material to be machined as well as the machine tool's specifications and the process parameters.

Proper selection of cutting parameters and tool geometry that affect surface roughness are essential factors (Obiko et al., 2021). In general, the preferred surface finish is specified, and the appropriate techniques are chosen to achieve the desired quality. To provide high precision and efficient machining, optimization of cutting parameters is crucial. This provides a foundation for survival in today's dynamic market conditions (Hosseinkhani & Ng, 2018; Zhou et al., 2019). Every manufacturing level must carefully monitor the cost-to-quality product ratio, and if the ratio deviates from the desired trend, quick corrective action must be done (Varghese et al., 2018).

1.3 Surface Roughness

Surface roughness is a measurement of a product's quality and a major determinant of production costs. It describes the geometry of the machined surfaces. As we all know, several machining-related elements might affect surface quality.

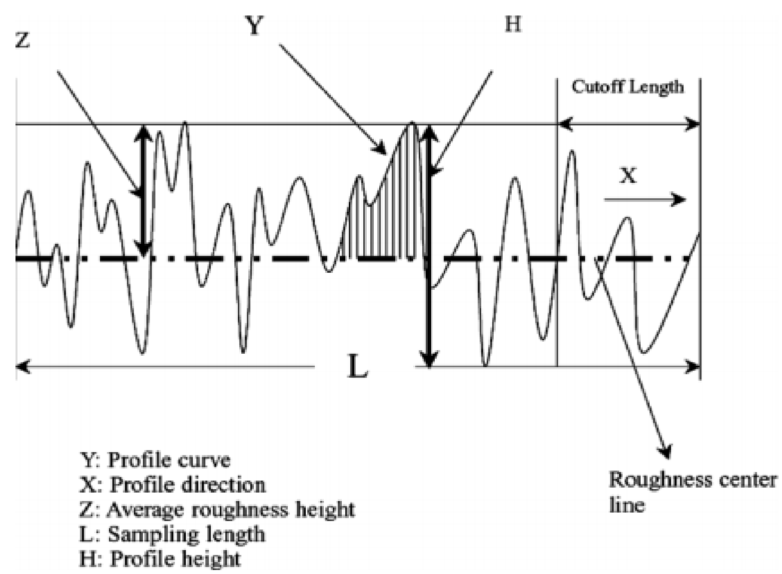

Figure 1. 2 Surface Roughness Profile (Nalbant et al., 2007).

They consist of workpiece variables, cutting conditions, and tool variables. Feed, speed, and depth of cut are examples of cutting conditions. Tool variables include material, nose radius, vibration, rake angle, cutting-edge geometry, etc. Workpiece variables include the material's hardness and the material's mechanical characteristics.

The surface quality of products is normally found in terms of the measured surface roughness (Obiko et al., 2021). To enhance product quality and performance in machining, there has been currently an extensive computation that specializes in surface roughness at a global level. Surface roughness variables are depicted in Figure 1.2. This computation may be observed in turning processes, particularly in the aerospace and car industry by growing the alternative answers for obtaining more proper surface roughness.

1.4 Tool Wear

Change of shape of the tool from its original shape during cutting resulting from the gradual loss of cutting tool dimensions. High temperatures and high normal and shear stresses are the characteristics of the metal-cutting tribological system, which is caused by the interaction between the tool, the workpiece, and the chip (Binder et al., 2015). Metal cutting tools are subject to wear due to the thermomechanical load spectrum, which affects both tool life and product quality. The tool is worn using a variety of techniques. Abrasion, diffusion, and adhesion are the three main mechanisms that lead to cutting tool wear.

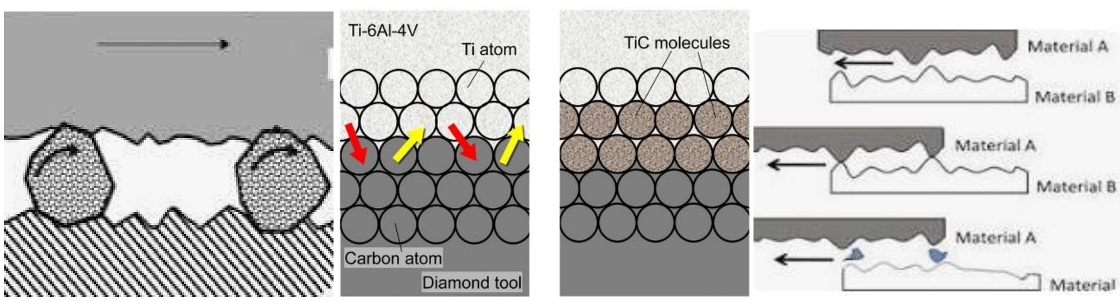

a) b) c)

Figure 1. 3 (a) Abrasive Wear, (b) diffusion, and (c) Adhesive Wear (Kamaruddin et al., 2016)

Abrasive wear is a type of wear mechanism where the hard particle in contact with the surface wears away the material on the surface (Zhou et al., 2022). This is illustrated in Figure 1.3a. In addition, a material loss may come through the sliding or interaction of particles or a hard surface with a soft surface. The deterioration, erosion, or corrosion of a metal's surface brought on by larger surface temperatures is referred to as "diffusive wear" as illustrated in Figure1.3b. The higher surface temperature is brought on by the ongoing frictional contact with two or more metals. Diffusion wear is characterized by a smooth worn surface with no plastic deformation. A crater eventually forms on the tool rake face as a result of material transfer toward the chip (Liu et al., 2020).

The micro-junctions that link the opposing parts on the rubbing surfaces of the parts in contact, as shown in Figure 1.3c, are what cause adhesive wear. When the load on the interacting abrasive particles is sufficiently strong that it causes them to deform, the adhesion bonds are formed. Depending on the process parameters and the combination of cutting and work material, several mechanisms may contribute a small but significant amount to the overall wear. Even if only one or a few of the wear processes were dominant, most of them coexisted at the same time (Zhenyu et al., 2021). Tool wear during the machining process affects tool life, tool replacement strategy, and the final product's quality in terms of roughness, geometrical accuracy, and residual stress state. Researchers found that several factors, such as material adhesion, abrasion, erosion, diffusive wear, corrosion, and fracture, which affect tool wear.

1.5 Need for Simulation

Finite element analysis can offer a comprehensive and sometimes complementary technique to the experimental observation of the machining process (Yadav et al., 2015). As a result, it may be able to design and modify the process input parameters to avoid issues that might occur during actual machining operations (Kuntoğlu et al., 2020). It gives the capacity to predict what might occur during the machining process. To further understand the process, a realistic simulation of chip formation, tool wear, and temperatures are useful. It is possible to accurately describe the material behavior in terms of strain, strain rate, and temperature by incorporating a material model into the finite element simulation (Uhlmann et al., 2007). A Lagrangian finite element-based machining model is used in FEM simulations to predict the tangential cutting force, temperature distribution at the tooltip, and effective strain and stress (Rajesh et al., 2021).

The Lagrangian and the Eulerian finite element formulations are the two methods that are most frequently employed when simulating the cutting process (Zukeri & Zaim, 2010). While the Eulerian approach considers the concentration of particles and calculates the overall diffusion and convection of numerous particles, the Lagrangian approach deals with individual particles and calculates the trajectory of each particle separately.

1.6 Research Motivation

The performance of dry turning is greatly influenced by the surface quality since a well-turned surface enhances corrosion resistance, fatigue strength, and creep life. The surface quality of the machined product is one of the most specific customer requirements in machining as well, and it is essential to the development of manufacturer competition. During the industrial training course, I had the opportunity to visit the Ethio-engineering group factory. Medium carbon steels have several uses in the factory, in particular, to produce shafts, keys, washers, bolts, nuts, gears, and other machine parts. The main difficulty in the factory during the machining of these steels was achieving the required surface finish.

Additionally, there are many functional aspects of parts that are affected by surface roughness including coating, surface friction, wear, the capacity to disperse and hold lubricant, light reflection, load-bearing capacity, and fatigue resistance (Çelik & Kaçal, 2020). Tool wear is yet another element that affects both surface quality and tool life. On the other hand, when machining the actual turning, many problems could arise. Predictive methods are therefore required to minimize or completely avoid issues that may arise during actual machining. Therefore, the above reasons are the primary drivers of this work's motivation.

1.7 Statement of The Problem

Environmental and health issues arise when cutting fluid (coolants) is used during manufacturing. Also, there are additional costs associated with purifying, drying or disposal procedures needed for cooling the lubricant itself in addition to health hazards and environmental harm. As a result, dry machining that is machining without a cutting fluid offers a greater level of surface finish than machining with coolants and is therefore preferable for the cleanest manufacturing. Surface roughness and cutting temperature should be kept as low as possible to avoid defects such as dimensional inaccuracy, load-bearing capacity, tool wear, corrosion, valley development, fatigue strength, coating, and crack formation (Jebaraj et al., 2019). However, achieving a high surface finish while maintaining a low tool temperature is difficult in the machining industry. In dry turning, specifically turning AISI 1030, the optimization of the cutting parameters (cutting speed, depth of cut, and feed) is useful and desired to successfully reduce machining challenges like a good surface finish, improve cutting efficiency (lower tool wear and minimum cutting temperature), and increase productivity (maximum material removal rate). so that product quality demands will rise and market competition will intensify. To reduce or eliminate issues that may arise during actual machining, FEM simulations are thus an alternative approach for experimental studies to improve process parameters with minimum time, cost, and work (Kuntoğlu et al., 2020). The focus of this study is to investigate (experimentally and numerically) and optimize cutting parameters (cutting speed, depth of cut, and feed rate) in dry turning of AISI 1030 steel to reduce surface roughness, tool temperature, tool wear rate, and maximize MRR (Kesavan et al., 2020).

1.8 Research Questions

In addition to the above, the following research questions are raised:

A. How can machining parameters be predicted for the actual machining process?
B. What are the optimum cutting parameters for dry-turning materials made of AISI 1030 Steel?
C. What are the challenges in dry turning using a CNC lathe machine, especially of AISI 1030 steel material, and how can we reduce them?
D. What are the optimal cutting parameters for achieving quality and increased productivity?
E. What impact do the cutting parameters have on the temperature that is generated at the tooltip?
F. What does the AISI 1030 carbon steel chip analysis resemble?

1.9 Objectives

1.9.1 General Objective

The general objective of this research is to experimentally and numerically investigate dry turning operations, particularly with AISI 1030 steel material, and optimize machining parameters using a CNC machining process to achieve a good surface finish.

1.9.2 Specific Objectives

1. To optimize cutting parameters for achieving the best surface finish in the dry turning of AISI 1030 Steel by using the grey relational analysis and analysis of variance (ANOVA);
2. To investigate tool wear and its causes
3. To investigate tool temperature;
4. To investigate and optimize material removal rate;
5. To predict material removal rate, tool temperature, and tool wear using FEM simulation with comparison to experimental findings.

1.10 Significance of the Studies

Dry-turning machining is part of the manufacture of many metallic products. The surface finish is important in this dry-turning process because it influences surface friction, light reflection, fatigue resistance, and creep life. Therefore, to achieve a good surface finish, an optimum material removal rate, a lower tool-chip temperature, and reduced tool wear, it is important to optimize cutting parameters in machining, particularly in dry turning of AISI 1030. Additionally, a cutting tool's performance has a significant impact on the machining economy. When a cutting tool performs properly for a longer time, it permits more machining time. This saves time and the cost of an extra cutting tool. On the other hand, many industries and educational institutions are looking for an alternative that will enable them to understand the metal-cutting process to improve manufacturing quality, create optimum cutting conditions, enhance the effectiveness of the machining process, and decrease costs. Simulation with various software programs, such as finite element analysis software, is one of those choices. Therefore, it is crucial to study the machinability of dry turning and optimize machining parameters that affect surface quality to produce high-quality products, improve productivity and tool life, and improve customer satisfaction while spending less money and time.

1.11 Scope of the Study

The scope of this study is to optimize dry turning cutting parameters, identify the most important process variables that affect the surface quality of AISI 1030 steel, and determine how to increase material removal rate, decrease tool wear, and improve customer satisfaction while also improving product surface roughness. Additionally, predicting the effect of cutting parameters on the responses using a finite element method (FEM) simulation, and comparing it with the results of the actual experiment.

1.12 Limitation of the Study

Without taking into account the impact of cutting force, machine vibration, and tool geometry parameters on surface quality and productivity, this research focuses on the optimal cutting parameters to produce a better surface finish during the dry turning of AISI 1030 steel. Because adding more input parameters makes the study more complicated and makes it more challenging to measure vibration frequencies and force without a dynamometer.

1.13 Structure of the Thesis

This study entitled experimental and numerical investigation of dry turning AISI 1030 carbon steel using CNC lathe machining is organized into five chapters.

- Chapter one of the thesis is an introduction with an overview of the chosen workpiece and cutting tool, machining parameters, the statement's problem, its significance and objectives, and finally its scope and limitations.
- Chapter two provides an overview of previous research work related to this research, and the summary of the literature with the research gap is described.
- Chapter three discusses the materials and methodologies used in this research study. This includes detailed information about the workpiece and cutting tool used, machines and equipment used, and the experimental procedure followed.
- In Chapter four, the main results of experimental studies and predictions are presented together with a detailed discussion. This chapter examines the effects of cutting parameters (spindle speed, depth of cut, and feed rate) on surface roughness, material removal rate, tool temperature, tool wear rate, and machining simulation.
- At the last the whole study's conclusion, recommendations, and future research directions.

CHAPTER 2

LITERATURE REVIEW

2.1 Introduction

The key issues facing the metal-based sector are raising productivity and the quality of machined components. The quality of the surface finish is one of the most crucial production engineering parameters (Tiwari et al., 2018, Suhail et al., 2010). It has an impact on the efficiency of mechanical parts as well as the cost of production. This study focuses on the experimental and numerical investigation of dry-turning AISI 1030 steel using CNC lathe machining. The effect and optimization of machining parameters on material removal rate, surface roughness, temperature, tool wear and chip analysis are considered in this study. Cutting speed, feed rate, and depth of cut are three of the most crucial input parameters in machining that influence production costs and product quality in machining (Vaxevanidis et al., 2018). To achieve the desired surface quality of a machined product and make it simple to assemble for the intended use, those parameters must be optimized. So that, surface roughness, tool wear, and production cost can be reduced.

For years, scientists have worked to identify the optimal collection of input parameters and determine how each parameter affects a given outcome. Various works related to this investigation by earlier scholars were presented in this section, and after reviewing their work, a significant research gap was found.

2.2 Tool Wear

Tool wear is the gradual failure of cutting tools brought on by repetitive use. Poor surface finish, higher cutting temperatures and forces, reduced quality of the produced part, and changes in tool geometry are all consequences of tool wear, which can also lead to tool breakage (Badiger et al., 2018, Yume & Kwon, 2007). Wear on the tool's flanks, craters, nose, or any combination of these limits its performance. Tool wear is influenced by the material of the tool, the material of the workpiece (physical, mechanical, and chemical properties), the tool's geometry, the cutting fluid used, and other factors. Friction between the tool's flank face and the machined surfaces is what causes flank wear (Attanasio et al., 2020).

Adhesion and abrasion are major wear mechanisms for the flanks (Zhou et al., 2022). When small pieces are pulled away from the tool surfaces while sliding, adhesive wear occurs. The cause of flank wear is thought to be the rubbing of the tool against the workpiece at the interface, which, at high temperatures, results in abrasive and/or adhesive wear. The rake face of the tool experiences crater wear. The ability to predict the tools that will be worn during dry turning is crucial for choosing the best cutting variables. Avoiding catastrophic tool failure, which could damage the workpiece surface and affect the functionality of the machine, is also advantageous.

The wear equation was first theoretically derived and then experimentally validated. The hardened high chromium high carbon steel specimen in CNC turning has been investigated for the results of tool wear and surface roughness (Ra) (Bovas Herbert Bejaxhin et al., 2021). Physical vapor deposition coated carbide CNMG turning insert nomenclature was used as the cutting tool, and it was mostly based on the shape, clearance angle, tolerance, and kind of tool inserts. For coatings with a thickness of 3–4 mm, titanium nitrate, aluminum chromium nitrate, and Latina were selected. For this CNC turning operation, the variable input parameters of speed and depth of cut under a constant feed rate had used as the machining parameters. The outcome showed that the main influencing factors on surface roughness were the depth of cut and the hardening effect. The use of covered CNMG tool inserts for high-speed cutting conditions reduced tool wear and machining time, which minimized wear interruption and increased surface quality.

Another study examined tool wear in Inconel 718 drilling under various cooling conditions using a modern numerical method (Attanasio et al., 2020). In DEFORM 3D, an implicit FEA program, a subroutine that can change the tool shape based on a specified tool wear model was created and tested. Using typical metalworking fluids and liquid nitrogen cooling, experimental evaluations were finished to determine tool wear in drilling. To calibrate the tool wear model and validate the drilling models, experimental data was employed. The developed drilling model's applicability to predict tool wear under both MWF and LN2 cooling conditions was proved by a comparison of measured and simulated results. The number of costly and time-consuming tool wear tests can be reduced by using the established model to evaluate how the cutting conditions (together with cooling conditions) affect tool wear.

In another work, the empirical wear rate models were calibrated using a combination of finite element simulations and a small number of experiments. The investigation's cutting tool was uncoated tungsten carbide, which was used to machine AISI 1045 orthogonally. Four distinct wear rate models were assessed during calibration using the following criteria: independence from the proportions of major wear processes and the involvement of the fewest quantitative assumptions. (Hosseinkhani & Ng, 2018). Additionally, research was done to determine how few experiments are necessary to calibrate the empirical models so that, for a given set of cutting parameters, the predicted wear rates and experimental findings agree. Results showed that Usui's wear rate model was the most reliable since there had been no restriction on selecting the size of the process parameter during calibration. Additionally, Usui's model could be calibrated using only cutting experiments.

2.3 Surface Roughness

Measurement of surface roughness is a crucial task in many engineering applications (Singh & Singh, 2018). It is a crucial quality attribute that may dominate the functional requirements of many components. An important factor in determining the quality of a machined surface is surface roughness (Ra). Numerous factors affect it, such as the cutting condition, vibration of the machine tool, cutting tool, and work holding mechanisms (Jebaraj et al., 2019).

A study on the impact of low-quantity lubrication circumstances on machinability has been conducted. To determine the effects of surface roughness and how they relate to the experimental parameters, a range of statistical studies were carried out. In those cases, a good result was obtained (Kaçal2, 2020).

For a CoCrWNi alloy, another paper research was conducted to determine how the cutting parameters affected the turning cutting forces and the quality of the resulting machined surface. The development of prediction models for the cutting forces used in turning as well as the Ra roughness parameter for dry longitudinal turning with TiAlN PVD coated insert cutters was the main objective. The cutting forces and roughness parameters were recorded throughout thirteen processing experiments. The feed rate, followed by the depth of cut, had the greatest impact on the cutting forces and Ra roughness values, whilst the cutting speed had little effect. Ra is negatively impacted by cutting speed (Dijmărescu & Tiriplica, 2019).

Using (Cubic Boron Nitride) CBN inserts, Karthik et al. (2020) optimize cutting settings for surface roughness during dry hard turning of EN 31 bearing steel. For EN31 steel-bearing bush hard-turning tests, CBN inserts were used. To achieve the best cutting conditions, the impact of the cutting parameters on surface roughness was explored. The Taguchi design of trials and ANOVA served as the foundation for the conclusions. For all possible combinations of cutting speed and depth of cut, the surface roughness of EN31 steel rises as the feed rate increases. To improve surface roughness, feed is the parameter that has the greatest influence and dominance. The Taguchi L9 Orthogonal array and main effect plots were used to determine the ideal cutting parameters, which are cutting speed(v) = 100 m/min, feed(f) = 0.04 mm/rev, and depth of cut(d) = 0.2 mm.

Gray relational analysis was used by Siva Surya et al. (2017) to perform multi-response optimization on EN19 steel through dry and wet machining. Using gray relational analysis, the paper seeks to maximize the multi-response objectives (material removal rate and surface roughness) during the machining of EN19 steel. The process parameters impacting material removal rate (MRR) and surface finish are cutting speed, feed rate, and depth of cut. The design of experiments with the L9 orthogonal array is created using the Minitab program. Rankings are used to determine how the cutting parameters affect wet and dry machining. By using the analytical process, the ranks are determined. Spindle speed, which is considered the most influential characteristic of dry machining, is followed in importance by feed rate and depth of cut. The depth of cut is determined to have the most influence during wet machining, coming in at number one; spindle speed came in second, and feed rate came in third.

An experimental examination by Venkata Vishnu et al. (2018) compares the machining of EN353 steel alloys under dry, flooded, and MQL environments. The turning of EN 353 steel alloy under varied lubrication circumstances, such as dry machining, flooding, and MQL conditions, is the subject of this paper. The optimal and best combination for reducing the cutting temperature from the current investigations is determined by the testing results to be a cutting speed of 1100 rpm, a feed rate of 0.2 mm/rev, a depth of cut of 0.5 mm, and a PVD coated tool. There are relatively few changes in the findings between MQL and Flooded settings, therefore it can be said that MQL is preferable to Flooded as it reduces the flow of lubricant in terms of millilitres (ml) to litres. Machining under flooded conditions is determined to be better than in dry and MQL conditions.

Assessment of machining parameters on EN 24 steel utilizing multi-coated inserts in dry, wet, and MQL conditions was done by Gupta et al. (2019). In this experiment, a turning machine's minimum quantity lubrication setup was created and built for comparison between dry and wet circumstances, and its impacts are taken into account under various parameters. On Taguchi's orthogonal array L9, the experiment's design was put into practice to optimize the chosen process parameters during the turning of EN-24 under various circumstances. The Grey relational approach was used for optimizing as well. The ideal parameters include a cut that is 0.6 mm deep, a nose radius of 0.8 mm, and a cutting speed of 575 rpm. It was discovered that the depth of cut is the most important factor. MQL performs better than dry and wet situations in terms of surface roughness.

Syed Irfan et al. (2019) used Taguchi's orthogonal array tests to optimize the CNC turning of en45's machining parameters. In this work, a simple carbide-cutting tool was used to CNC turn EN-45 spring steel, and the Taguchi method and regression analysis were utilized to optimize the machining parameters. L18- orthogonal array conceived and carried out the experiments. Cutting speed, feed rate, and depth of cut were taken into account as machining factors to maximize the surface roughness and material removal rate. Statistical software called Minitab 17 was used to generate the ANOVA. Following the ANOVA and regression analysis, a comparison between dry and wet machining is conducted. Speed and feed were directly proportional to surface roughness, whereas DOC was inversely proportional. i.e., Ra drops as DOC increases. All three parameters were discovered to be proportional in the case of MRR, meaning that as speed, feed, and DOC increased, so did MRR.

Shahid (2020) Process parameters for spinning heat-treated steel are optimized. The process variables that affect the productivity and machining quality of plain turning are examined in the current work using an experimental turning methodology. Taguchi's L9 orthogonal array served as the foundation for the experiment design. When turning heat-treated steel, the machining parameters Speed, Feed Rate, and Depth of Cut are optimized for maximum material removal rate (MRR) and minimal surface roughness (EN-9). It demonstrates that feed, with a contribution of 40.99%, is the most significant element for the material removal rate, followed by the depth of cut, with a contribution of 36.90%. Additionally, cutting speed, which influences MRR just a little (11.40%), is ineffective. It shows that speed, which contributes 54.87 percent, is the main turning parameter that determines how rough a surface is machined. Depth of cut comes in second, contributing 35.80% of the total. The least significant factor, contributing only 5.38 per cent to surface roughness, is found to be the feed rate.

2.4 Temperature

Due to the relative movement between the tool and workpiece, cutting temperature is an important factor that directly affects cutting tool wear, quality, and machining precision. The type of material being machined and the cutting parameters, particularly cutting velocity, which has the greatest effect on temperature, affect how much heat is produced (Bhemuni et al., 2014, Suhail et al., 2010).

On carbon steel AISI 1020, an experimental examination was conducted to determine the best cutting parameters based on the workpiece surface temperature, performance indicators, and surface roughness. A CNMG 432 TT5100 insert with a Sandvik device holder and a PCLNR 2525M/12 universal turning machine device were the cutting tools utilized in the experiments. Through Taguchi methodology, the optimum cutting parameters for each performance measure have been determined. The experimental results proved that it is possible to sense and use the workpiece surface temperature as a reliable indicator to control cutting performance and enhance the optimization process. In an automated production process, it is therefore possible to increase equipment utilization and lower manufacturing costs (Suhail et al., 2010).

2.5 Material Removal Rate (MRR)

The rate at which material is removed from a part during machining is known as the material removal rate (MRR) (Yanda H et.al., 2010). Material Removal Rate in Turning is determined using the following equation:

$$\text{MRR} = \text{Depth of Cut} \times \text{Cutting Speed (SFM)} \times \text{Feed Rate (Dist./Rev)} \qquad (2.1)$$

The effects of various machining parameters on the material removal rate (MRR) have been researched. When turning AISI 4340 steel with an uncoated carbide cutting tool, the cutting speed, feed rate, and depth of cut were all optimized. The output responses to flank wear, surface roughness, and material removal rate (MRR) have been measured using the Taguchi Orthogonal Array DOE. Using linear regression models, empirical models that represent the output responses were developed. The optimal set of machining parameters for minimizing wear and maximizing MRR while taking into account surface roughness values within a chosen limit was determined (Dhandapani et al., 2014).

2.6 Studies on Chip Analysis

The chip morphology is the result of the chip formation mechanism occurring during machining.

Because chips significantly influence the surface finish produced, cutting forces, and overall cutting operation, it is crucial to analyze. Continuous chips imply a good surface finish and steady cutting forces. Built-up edge chips show a poor surface finish. Discontinuous chips result in poor surface finish and dimensional accuracy and involve cutting forces that fluctuate. The type of chip indicates the overall quality of the cutting operation. Numerical simulation using the finite element approach can help evaluation of chip formation and tool design in a very effective and cost-effective manner (Parida et al., 2020).

To better understand how undeformed chip thickness affects tool wear and chip morphology during dry milling of titanium alloy, research was conducted. For trochoid milling, a tool wear model based on the volume of material removed was constructed. To improve machining performance through reduced tool wear, optimized cutting parameters in terms of cutting speed and axial depth of cut have been chosen. The discovery enables Ti-6Al-4V to be rough-machined in an eco-friendly manner (Liu et al., 2019).

2.7 Finite Element Analysis (FEA)

The finite element method (FEM) has been developed recently as a useful technique for simulating and modeling manufacturing processes. The fundamental benefit of the FEM is that it allows for the investigation of thermomechanical parameters as well as the estimation of some surface integrity-related variables without the need for time-consuming and expensive tests (Jafarian et al., 2018). However, proving the FE model's reliability successfully through experiments is a crucial challenge (Liu et al., 2016). The controllable input parameters have an impact on how accurate the FE model is. These variables include the flow stress on the workpiece, the temperature, and friction at the chip/tool interface, etc. (Jafarian et al., 2016, Laakso & Niemi, 2015)

The Lagrangian and the Eulerian finite element formulations are the two that are most frequently employed when simulating the cutting process (Zukeri & Zaim, 2010). The Lagrangian technique requires that the material elements in the finite element precisely cover the region of study. These components are joined to the material and change shape together with the workpiece. The Eulerian method calculates the material properties at constant spatial positions while the material flows through the mesh, and the mesh includes elements that are constant in space and cover the control volume.

Different industrial FEM software for simulation systems, such as DEFORM 3D, ABAQUS, ANSYS, advantAGE, etc., are developed to study the flow of various metal-forming processes. For instance, DEFORM 3D is offered in Eulerian modeling as well as two Lagrangian (Transient) modeling and arbitrary Lagrangian options. The use of the finite element approach to analyze chip, tool wear, cutting forces, temperature, and residual stresses to improve the machining environment has been extensively researched. The Hastelloy nickel-based superalloy has been turned to better understand how cryogenic coolant affects cutting temperature, cutting force, thrust force, and feed force. Additionally, in dry conditions, the effect of cutting speed on the machinability properties of Hastelloy was evaluated using coated and uncoated inserts. It was determined that the coated insert has improved the surface roughness and machinability of Hastelloy.

Calculating the amount of heat produced during the machining process involves adding up the heat produced during chip production and the friction that occurs between the workpiece, the tool, and the chips. The plastic deformation that took place throughout the machining process was accelerated by these heat sources.

The Deform 3D analytical tool was used to do a numerical simulation of the machining process under optimum cutting parameters. Additionally, experiments with various cutting parameters have been done using CNC turning. The findings from the simulation had been compared to the results of experimental investigations and were accurately in agreement with those findings. The findings suggested that machining under cryogenic settings could reduce the cutting temperature by up to 57%. From all of the simulation and test studies, it was found that machining under cryogenic conditions effectively lowers the cutting temperature and machining forces as compared to those under dry conditions (Kesavan et al., 2020).

Modern CNC turning plays a significant role in production industries. There are a lot of alloys on the market that are very challenging to machine, so choosing a great tool, optimal machining parameters, tool geometry, and cutting condition are essential. It is a challenging, expensive, and time-consuming activity for industries to offer the highest quality products to clients at the lowest price. On AISI 304 with various inserts, an experimental and numerical study was conducted, and the effects of the CNC turning process parameters were investigated experimentally. CNC turning operations were simulated using finite elements (Verma & Pradhan, 2020). DEFORM 3D was the simulation software utilized. Using CNC turning on stainless steel with various inserts, Taguchi orthogonal arrays are used to verify the parameters, including temperature, forces, and strain, predicted by the simulated environment. The simulation result of temperature at the tool-workpiece interface of AISI 304 with various inserts, such as cubic boron nitride, is shown in Figure 2.1.

Cutting Speed, Feed, and Cut Depth are the parameters used as inputs for CNC turning processes. Any associated analysis starting with ANOVA can be performed in the approved simulated environment. In the instance of the carbide tool insert, the following findings were reached:

- for strain equivalent to cutting strain, the main significant factor is the depth of cut and the second significant factor is spindle speed;
- the depth of cut is the most important significant element for material removal rate, while the feed is the second-most important significant factor;
- the depth of cut and spindle speed are the two most important significant factors for the temperature at the tooltip;
- the depth of cut most important major factor for the strain and the second significant factor is feed**.**

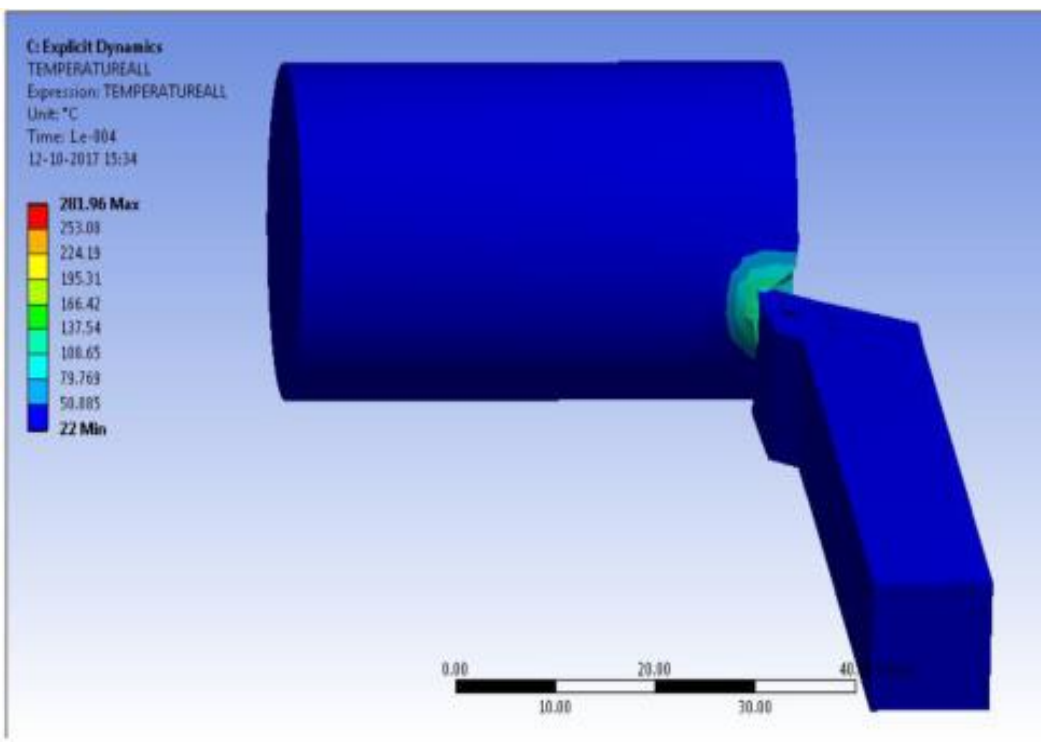

Figure 2. 1 Temperature at The Tool-Workpiece Interface (Verma & Pradhan, 2020).

2.8 Cutting tool geometry

Cutting tools come in a variety of shapes, which are distinguished by their angles or geometries. The right type of cutting tool geometry is critical for completing a specific job. A cutting tool's geometry is defined by seven parameters. The back rake angle, side rake angle, end relief angle, side relief angle, end cutting edge angle, side cutting edge angle, and nose radius are the parameters.

Singh et al. (2018) found that tool nose radius has an impact on the finish turning of hardened AISI 52100 sheets of steel. The white layer, tool wear, cutting forces, and surface quality were all evaluated at various machining settings. The findings showed that as compared to tools with a narrow nose radius, bigger nose radii give a smoother surface quality. The instrument causes a modest increase in the cutting energy. The nose's radius Only new tools with aggressive feeds (0.3 mm/rev) and small bit sizes exhibit white layers. The depth of the white layers increases with increasing nose radius. On used instruments, white coatings appear even with light feeding. On the other side, a wide nose radius results in deeper white layers (0.05 mm/rev). The greater the radius, the greater the shear plane heat source and, thus, the greater the uncut chip thickness, which may lead to induction for deeper white layers. Temperature analysis at machined surfaces shows that, particularly for worn tools where wear-land sliding is the main heat source, the higher the tool nose radius, the deeper the temperature penetration because of a shorter transition-material zone from the cutting edge to the final machined surface

Senthilkumar and Tamizharasan (2014) investigated how tool geometry affected surface roughness when AISI 1045 steel was turned. The Brinell hardness of AISI 1045, a low-cast alloy with good strength and toughness, is 181 BHN. It is a medium-carbon steel that is frequently employed in building and engineering. An uncoated cemented carbide tool with a Brinell hardness of 1433 BHN was chosen as a cutting tool for general machining operations. This study examined cutting insert geometrical parameters while maintaining constant other machining parameters, including insert shape (including cutting edge angle), nose radius, and relief angle. Taguchi's experimental design analyzes output properties such as surface roughness, flank wear, and material removal rate utilizing analysis of variance and signal-to-noise ratio. The L9 orthogonal array was chosen. It was appropriate for the experiment because it used nine different cutting tool inserts with various forms, nose radiuses, and relief angles. According to the experimental findings, the cutting insert is the most important element. It is determined that the nose radius contributes 36.37%, and the cutting insert contributes 45.27%. The relief angle, which accounts for 5.28% of the reaction, is the least important element.

Karim et al. (2013) investigated surface finishing and tool wear during the machining of Al6061 aluminum alloy using positive and negative rake angles. The experiment was carried out on a traditional lathe with a workpiece made of Al6061 aluminum alloy. While the machining parameters remained constant, the rake angles were adjusted from positive to negative values. Surface roughness and flank wear were measured with a Handysurf surface roughness tester and a Motic Images Plus microscope at every 200-mm tool travel distance. The tool wear results showed that flank wear increases as the positive or negative rake angle increases. The flank wear was greatest when the rake angle was equal to 15. The plot of flank wear versus cutting length shows a linear relationship with the same slope, indicating that the cutting tool wears at the same rate. As a result, during the turning process, both negative and positive rake angles have the same effect on flank wear. The rake angle is inversely proportional to the surface roughness value. Surface roughness decreases as the rake angle increases.

Shetty et al. (2014) examined surface roughness while turning Ti-6Al-4V under near-dry conditions and came to the conclusion that lubrication had the biggest physical impact on surface roughness, with a 95.1 percent significance level while using PCBN tools.

2.9 Summary of Literature

Numerous researchers have determined the optimum cutting parameter values for a variety of materials, but the same work has not yet been done on several materials.

According to the literature reviewed above and summarized in Table 2.1, the majority of researchers concentrated on determining how cutting speed, feed rate, tool geometry, and depth of cut affect surface roughness, material removal rate, tool temperature, and tool wear when turning various materials under various circumstances. Also, some researchers studied how to predict machining using FEM simulation.

Table 2. 1 Summary of Literature Work

No	Author(s) & Year	Operation and Material	Cutting parameters/ Working Conditions and Response(s)	Method
1	Bovas Herbert Bejaxhin et al., 2020	Turning OF hardened high chromium high carbon steel (HCHCR-D3) using PVD coated carbide (CNMG) turning insert	The effect of Cutting speed, depth of cut and constant feed on Tool wear and Surface Roughness	Deform 3D
2	Attanasio et al., 2020	drilling Inconel 718 using coated (TiAlN coating) cemented carbide tool	The effect of Fluid Pressure, Cutting speed, (m/min) Feed, on Tool wear	Deform 3D
3	Hosseinkhani & Ng, 2018	Turning of AISI 1045 steel using uncoated tungsten carbide	The effect of feed rate, cutting speed, and then Depth of cut and rake angle was held constant on Tool wear	FEM simulation
4	Kaçal2, 2020	Milling of EN-GSJ 700-02 spherical graphite cast iron using multi-layer TiN coated tool in the machining of hardened	The effect of minimum quantity lubrication (MQL) type Pressure (bar) Flow rate (ml/h) on Surface roughness and tool wear	Investigation
5	Dijmărescu & Tiriplica, 2019	Turning of CoCrWNi alloy using TiAlN PVD coated insert	The effect of cutting speed, feed rate and depth of cut on the cutting forces and surface roughness	Investigation
6	D. Liu et al., 2019	milling titanium alloy Ti 6Al–4V using Coated (TiAlN)	The effect of cutting speed, feed rate and depth of cut on Chip morphology and tool wear	Taguchi optimization
7	M. Necpal1 et al., 2017)	Turning C45 non-alloy steel using carbide insert	The effect of Cutting speed, feed rate, and depth of cut on cutting forces, stresses, and temperature	FEM, DEFORM 3D
8	M. Agmell, et al., 2011)	Dry Turning AISI 4140 steel using CNMG120408 MF4 TP2500	The effect of feed rate on cutting forces, chip thickness ratio and Deformation widths	FEM, ABAQUS /Explicit v6.9

2.10 Research Gap

The turning parameters for lathe machines have been the subject of extensive investigation in the past. Numerous researchers have focused their work on the effects of cutting parameters, such as cutting speed, feed, depth of cut, tool geometry, tool, and workpiece material, workpiece hardness, and cutting fluid, on the surface quality of the machined part, which affects the desired output, including surface finish, tool wear, tool life, and overall performance on different materials, as noted in the literature.

However, there is no research on experimental and numerical investigation and optimization of the effect of machining conditions on the responses, such as surface finish, cutting temperature, tool wear, material removal rate, and chip analysis, for AISI 1030 steel.

This work attempts to fill the gap in these studies. Therefore, this study intends to add a new contribution to;

- reducing the challenges associated with dry turning AISI 1030 steel on CNC lathe machines;
- predicting machining conditions through numerical simulation software and comparing the result with the experimental;
- the quality and productivity gaps observed in dry turning of AISI 1030 steel are then filled by determining the optimum cutting parameters to obtain a better surface finish, reduced tool wear, and optimal material removal, lower tool temperature.

CHAPTER 3

MATERIALS AND METHODOLOGY

3.1 Introduction

Through experimental investigation and numerical simulation, this study examined the dry turning of AISI 1030 steel using a CNC lathe and optimize cutting parameters that affect the surface finish, tool wear, tool temperature, material removal rate (MRR), and chip.

3.2 Machine and Equipment

The machine and equipment used for the study are;

- CNC lathe machine
- Coated (TiCN-Al_2O_3) tungsten carbide tools insert
- Digital thermometer
- Optical microscopy
- Profilometer, etc.

3.3 CNC Lathe Machine

CNC lathes are machine tools that are controlled by CNC systems and given exact design instructions.

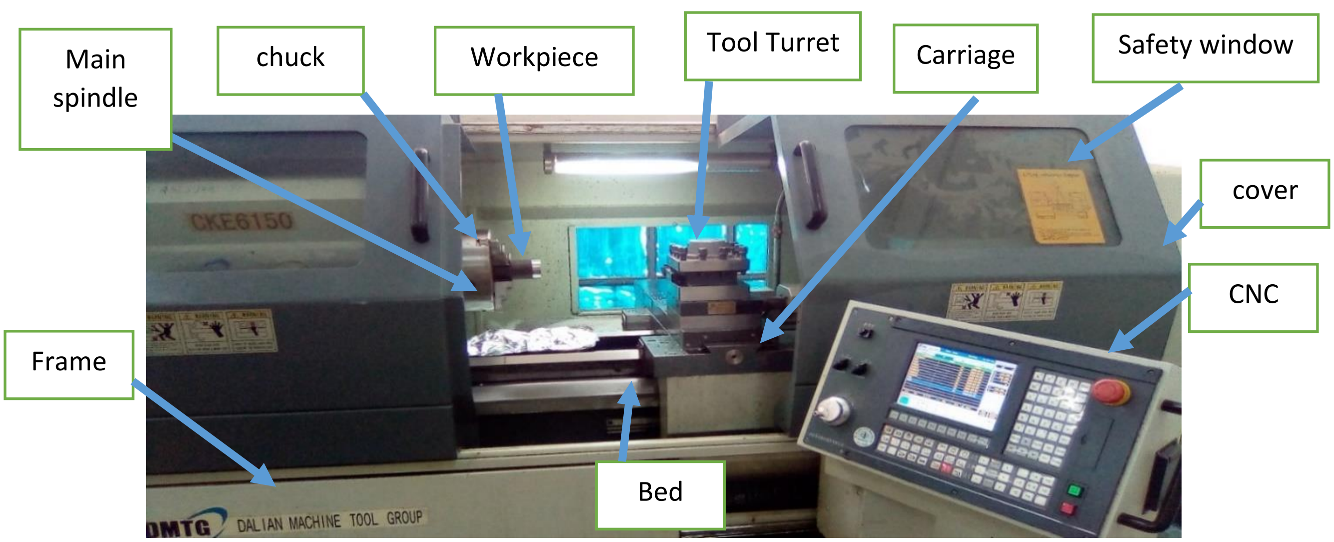

Figure 3. 1 CNC lathe machine tool

The main spindle of a CNC lathe is used to clamp and rotate the material or part as the cutting tool works on it while mounted and moved in various axes. Figure 3.1 depicts the CKE6150 type CNC lathe used in this investigation, which is available at Ethiopian Technical University.

3.4 Workpiece Material

The work-piece material used for this study is AISI 1030 carbon steel as shown in Figure 3.2. The typical standard for AISI 1030 steel is ASTM A684. 1030 steel bar is a grade that has moderate strength and hardness, fair machinability and ductility, and good weldability. This grade of steel is frequently used for machinery parts, hooks, brackets, brakes, clips, clutches, springs, washers, and other items.

Figure 3. 2 AISI 1030 Steel Before Machining

3.4.1 Chemical Composition

The chemical composition of AISI 1030 carbon steel was tested using spectrometry Figure 3.3 which is known as Oxford Instruments PMI-MASTER Smart (Available at Ethio Technical University). the result is outlined in the following Table 3.1.

Figure 3. 3 Spectrometry for Chemical Composition

Table 3. 1 Property of AISI 1030 Plain Carbon steel (Engineering Toolbox, AISI/SAE Steel and Alloys - Designation System*, n.d.)*

Chemical Composition		Physical Properties		Thermal Properties	
Element	Content (%)	Properties	Metric	Properties	Metric
Iron, Fe	98.67-99.13	Density	7.85 g/cc	Thermal expansion	11.7 µm/m°C
Manganese, Mn	0.60-0.90	Melting	1510°C	Thermal Conductivity	51.9 W/mK
Carbon, C	0.270-0.340				
Phosphorous, P	≤ 0.040				
Sulfur, S	≤ 0.050				

3.4.2 Mechanical Properties

The following Table 3.2 shows the mechanical properties of the AISI 1030 carbon steel.

Table 3. 2 Mechanical Properties of AISI 1030 Plain Carbon Steel (Engineering Toolbox, AISI/SAE Steel and Alloys - Designation System*, n.d.)*

Properties	Metric	Imperial
Tensile strength, ultimate	525 MPa	76100 psi
Tensile strength, yield	440 MPa	63800 psi
Modulus of elasticity	190-210 GPa	29700-30458 ksi
Shear modulus (typical for steel)	80 GPa	11600 ksi
Poissons ratio	0.27-0.30	0.27-0.30
Hardness, Brinell	149	149
Hardness, Rockwell B (converted from Brinell hardness)	80	80

3.5 Cutting Tool Materials

Among other considerations when selecting the cutting tool are: the material of the cutting tool should be harder than the material of the workpiece to be cut; the cutting tool should be designed such that its cutting edge can easily penetrate the material, and the tool must be strong and rigid enough to resist cutting pressures.

The cutting tools selected for turning AISI 1030 steel bar are tungsten carbide tools coated with TiCN and Al_2O_3. Due to its significantly higher wear resistance than high-speed steel, ability to withstand higher working temperatures, and excellent optimization capabilities to satisfy the demands of varied processes, tungsten carbide plays an exceptional role in the machining process. It is characterized by high hardness and high strength at high temperatures since it has a high melting point (2870 ^{0}c), high corrosion resistance, high wear resistance, and high elastic modulus, as well as good impact toughness and corrosion resistance.

Figure 3. 4 Tungsten Carbide Tools

3.5.1 Physical properties

The ultimate tensile strength of tungsten carbide is 344 MPa, the ultimate compression strength is around 2.7 GPa, and the Poisson's ratio is 0.31. Tools made of tungsten carbide have a density of 15.63 g/cm^3 (0.01563 g/mm^3). The designations of the inserts used in this investigation are 0.4 nose radius CNMG160404 and TNMG160404-MA for CNC which is shown in Figure 3.4. The designation of cutting tool inserts is shown in Table 3.3.

3.6 Tool Holder

A tool holder is a short steel bar with a clamp on one end to hold small interchangeable cutting bits and a shank on the other end to clamp it to a machine.

Figure 3. 5 MTXNL 2020 K16 WIDAX Tool Holder

When working on a lathe, they are used to hold cutting tools or inserts in place while performing a variety of tasks, such as facing, threading, and boring. Typically, tool posts on lathes are used to attach tool holders. The experiment was carried out using an MTXNL 2020 K16 WIDAX tool holder as shown in Figure 3.5.

Table 3. 3 The Designation of Cutting Tool Inserts (Tools united)

<table>
<tr><th colspan="4">Description</th><th colspan="3">Value</th></tr>
<tr><td colspan="4">Tool style code</td><td colspan="3">1</td></tr>
<tr><td colspan="4">Insert included angle</td><td colspan="3">60 Degree</td></tr>
<tr><td colspan="4">Clearance angle</td><td colspan="3">0 Degree</td></tr>
<tr><td colspan="4">Cutting edge length</td><td colspan="3">16.49 mm</td></tr>
<tr><td colspan="4">Inscribed circle diameter</td><td colspan="3">9.525 mm</td></tr>
<tr><td colspan="4">Insert thickness</td><td colspan="3">4.76 mm</td></tr>
<tr><td colspan="4">Corner radius</td><td colspan="3">0.4 mm</td></tr>
<tr><td colspan="4">Insert rake angle</td><td colspan="3">22 Degree</td></tr>
<tr><td colspan="4">Cutting-edge condition code</td><td colspan="3">T - Chamfered</td></tr>
<tr><td colspan="4">Face land width</td><td colspan="3">0.2 mm</td></tr>
<tr><td colspan="4">Face land angle</td><td colspan="3">6 Degree</td></tr>
<tr><td colspan="4">Chip breaker manufacturer's designation</td><td colspan="3">MA</td></tr>
<tr><td colspan="4">Insert hand</td><td colspan="3">N - Neutral</td></tr>
<tr><td colspan="4">Tolerance class insert</td><td colspan="3">M</td></tr>
<tr><td colspan="4">Fixing hole diameter</td><td colspan="3">3.81 mm</td></tr>
<tr><td colspan="4">Coolant supply property</td><td colspan="3">0 - Without a coolant supply</td></tr>
<tr><td colspan="4">Coating</td><td colspan="3">$TiCN-Al_2O_3$</td></tr>
<tr><td colspan="7">General Turning Insert Nomenclature</td></tr>
<tr><td>T</td><td>N</td><td>M</td><td>G</td><td>16</td><td>04</td><td>04</td></tr>
<tr><td>C</td><td>N</td><td>M</td><td>G</td><td>16</td><td>04</td><td>04</td></tr>
<tr><td>Turning Insert Shape Triangle and C shape</td><td>Turning Insert clearance angle 0°</td><td>Turning Insert Tolerances Which is M</td><td>Turning Insert Type which is a cylindrical hole and Double-Sided Chip breaker</td><td>Turning Insert Size length of the turning insert 16.49 mm</td><td>Turning Insert Thickness 4.76 mm</td><td>turning Insert Nose Radius 0.4</td></tr>
</table>

3.7 Experimental Procedure

The overall general procedures of the experimental and numerical investigations to optimize the cutting parameters of the dry-turning process of AISI 1030 steel is shown in Figure 3.6.

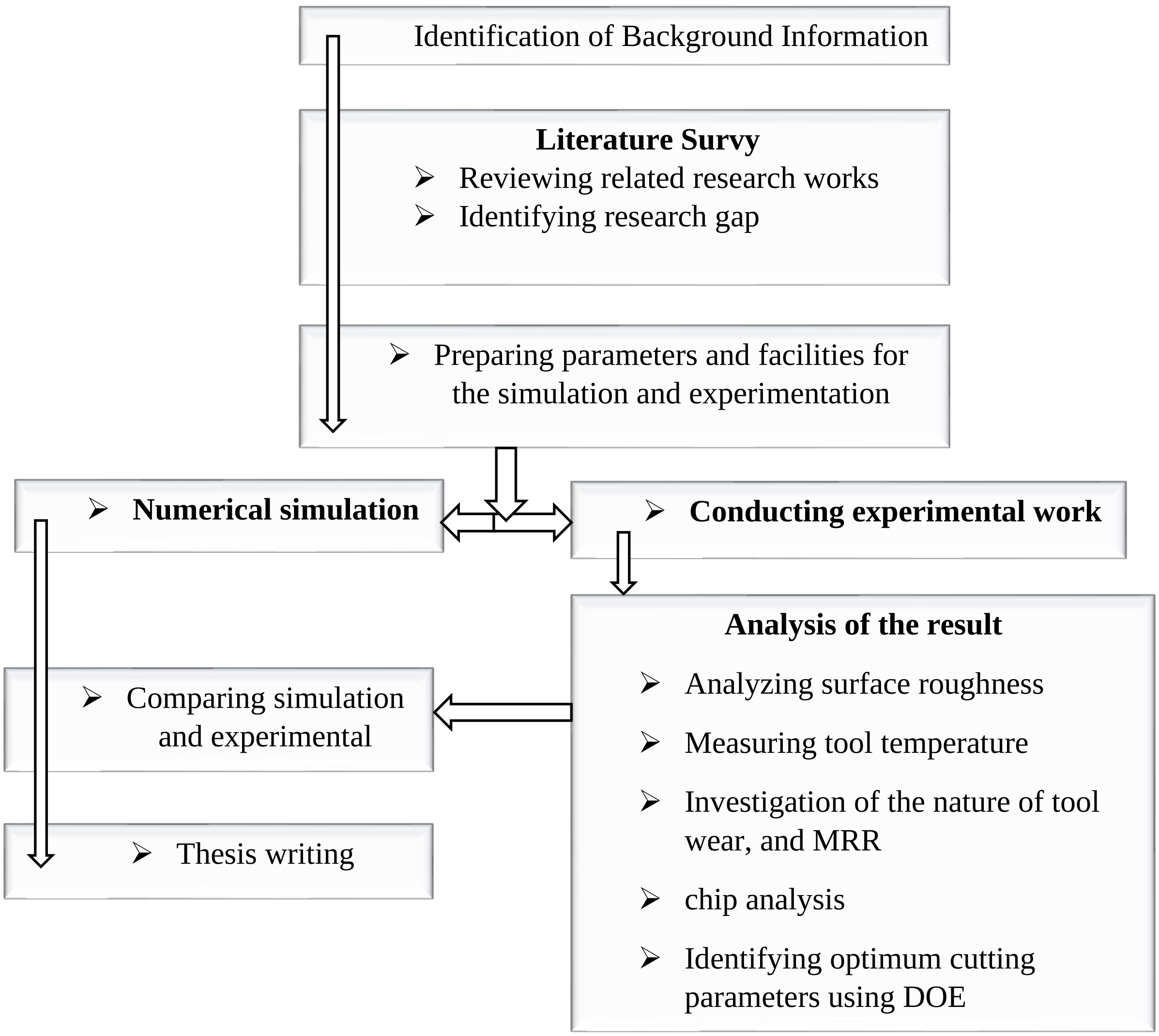

Figure 3. 6 Experimental Procedure

3.8 Research Methodology

The experimental work and simulation were done using the materials and equipment mentioned above through the methods described in this section. Under research methodology, the way of Sample (workpiece) material preparation, design of experiments (DOE) procedures such as Taguchi orthogonal array selection, Finite element simulation, and analysis of variance (ANOVA) are explained. Also, the methods for measuring surface roughness, tool wear, tool temperature, material removal rate (MRR), and chip analysis are described.

3.9 Sample Material Preparation

The work part has a diameter of 60 mm and a length of 300 mm. To prevent chattering, which is self-excited vibration that can happen during machining operations and frequently limits productivity and part quality, the selection is based on a small length-to-diameter ratio. The cut lengths of the nine trials that were chosen using an orthogonal array are each 20 mm**.**

3.10 Design of Experiment (DOE)

Speed, feed rate, and depth of cut were the cutting parameters used in both the simulation and experiment. The Taguchi technique was typically used in the design of the experiment (DOE) for machining parameter optimization because it is a problem-solving tool that can enhance product performance, and process design, shorten experimentation times, lower costs, and identify significant elements more quickly (Kuntoğlu et al., 2021). Taguchi technique uses a signal-to-noise (S/N) ratio to determine the performance characteristic (response) deviating from the desired value (ÖZSOY, 2019). It uses a special design of orthogonal arrays to examine the full parameter space with a limited number of experiments only. In the analysis of the S/N ratio, there are typically three types of performance characteristics: the lower-the-better, the higher-the-better, and the nominal-the-better. Based on the S/N analysis, the S/N ratio is calculated for each level of the process parameters. The bigger S/N ratio refers to the better performance characteristic, regardless of the category of the performance characteristic (Kannan et al., 2020). As a result, the level of the process parameters that has the largest S/N ratio is the optimum amount.

Nominal is the best: $$S/N_T = 10\log\left(\frac{\bar{y}}{s_y^2}\right) \tag{3.1}$$

Larger-is-the better (maximize); $$S/N_L = -10\log\left(\frac{1}{n}\sum_{i=1}^{n}\frac{1}{y_i^2}\right) \tag{3.2}$$

Smaller-is-the better (minimize); $$S/N_s = -10\log\left(\frac{1}{n}\sum_{i=1}^{n} y_i^2\right) \tag{3.3}$$

where $\bar{y}$, is the average of observed data, s_y^2 is the variance of y, n is the number of observations and y is the observed data (Karazi et al., 2019).

Taguchi's design procedures are;

- Identifying and selecting cutting parameters (control factors) and their levels;
- Select proper orthogonal array (OA);
- Analyze data;
- Identify optimum conditions;
- Confirmation test.

3.10.1. Selection of cutting parameters and their levels

The depth of cut, feed, and cutting speed has been chosen as the cutting conditions for this investigation. Following the recommendations of a tool manufacturer and machinery handbook, and also based on knowledge from the literature and experience these level values of control factors were chosen (Oberg, 2020). As a result, the cutting parameters were divided into three levels, as indicated in Table 3.4.

Table 3. 4 List of Parameters and Their Levels

Symbol	Cutting parameter	Level 1	Level 2	Level 3
A	Cutting speed (m/min)	90	170	250
B	Depth of cut (mm)	0.5	1.5	2.5
C	Feed rate (mm/rev)	0.15	0.25	0.35

3.10.2 Selection of Orthogonal Array

Using the Taguchi approach, a particular orthogonal array was chosen based on the number of levels of various factors. The entire number of experiments in the orthogonal array (OA) should exceed or be equal to the total number of degrees of freedom (DOF) needed for the experiment. The Degree of Freedom can now be calculated using Equation (3.4).

$$DOF = P * (L - 1) \tag{3.4}$$

where DOF is the degree of freedom, P is the number of factors, and L is the number of levels

According to this L9, as stated in Table 3.5, has been chosen as the orthogonal array, and Minitab 16 was used to conduct the experiments using the following step:

- Selection of factors to be evaluated;
- Selection of the number of levels;
- Selection of appropriate orthogonal array;

- Experiment and analyze the results.

Table 3. 5 Experimental Layouts Using L9 Orthogonal Array

Exp. No.	A Cutting speed (m/min)	B Depth of cut (mm)	C Feed (mm/rev)
1	90	0.5	0.15
2	90	1.5	0.25
3	90	2.5	0.35
4	170	0.5	0.25
5	170	1.5	0.35
6	170	2.5	0.15
7	250	0.5	0.35
8	250	1.5	0.15
9	250	2.5	0.25

3.10.3 Analysis of Variance (ANOVA)

Finding the variables that have a substantial impact on the quality characteristic is the goal of the analysis of variance (ANOVA). The percentage contributions of each control factor are utilized in the analysis of variance to calculate the corresponding effects on the performance characteristics. Equation 3.5 determines this. In this analysis, the significance level of 5%, or for a degree of confidence of 95%, is taken into account.

$$\text{contribution P } (\%) = \frac{SSTR}{SST} \times 100 \tag{3.5}$$

Where SSTR is the sum of the square of treatments and SST is the total sum of squares (Larson, 2008).

3.11 Multi-Objective Optimization

Although the Taguchi technique is simple and effective for parameter optimization, one of its main drawbacks is that it can only be applied to single-objective optimization (Prakash et al., 2020). Grey Relational Analysis (Uhlmann et al.) linked with Taguchi DOE has gained popularity as a way to overcome this issue by making it easier to handle multi-objective optimization problems. Through GRA method reduces multi-objective issues to single objectives**.**

3.11.1 Optimization steps using grey relational analysis (GRA)

Step 1

The GRA approach consists of several steps to improve the response parameters, but the first step is to normalize the response data to prevent using different units and reduce variability. Since the variation of one data differs from that of the other data, it is essentially necessary. To create an array between 0 and 1, an appropriate value is deduced from the original value (Panda et al., 2016). Generally speaking, it is a technique for transforming the original data into equivalent data. Smaller is better and larger is better normalization was applied appropriately because the goal is to reduce surface roughness, tool wear, and tool temperature and raise the MRR. The equation for the smaller, better normalizing technique is shown in equation 3.6.

$$x_i{}^*(k) = \frac{max\ x_i(k) - x_i(k)}{max\ x_i(k) - min\ x_i(k)} \tag{3.6}$$

The formulae for the larger the better normalization method concerning MRR are shown in equation 3.7. (Kuram & Ozcelik, 2013)**.**

$$x_i{}^*(k) = \frac{x_i(k) - min\ \ x_i(k)}{max\ x_i(k) - min\ x_i(k)} \tag{3.7}$$

where, i = 1,…, m; k = 1…, n., m is the number of experimental data and n is the number of responses. $x_i(k)$ denotes the original sequence, $x_i{}^*(k)$ denotes the sequence after the data preprocessing, $max\ x_i(k)$ denotes the largest value of $x_i(k)$, $min\ x_i(k)$ denotes the smallest value of $x_i(k)$, and x is the desired value.

Step-2

calculate grey relational coefficient, $\zeta_i(k)$ from the normalized values by the following equations 3.8 and 3.9

$$\zeta_i(k) = \frac{\Delta_{min} + \zeta\Delta_{max}}{\Delta_{oi}(K) + \zeta\Delta_{max}} \tag{3.8}$$

where, $\Delta_{oi}(K)$ is the deviation sequence of the reference sequence and the comparability sequence and

$$\Delta_{oi} = \|x_o(k) - x_i(k)\| \tag{3.9}$$

where Δ min and Δ max are the minimum and maximum values of the absolute differences (Δ_{oi}) of all comparing sequences (Kuo et al., 2008). $x_o(k)$ implies the reference sequence and $x_i(k)$ termed as comparability sequence. ζ is the distinguishing or identification coefficient and the range is between 0 to 1. Usually, the value of ζ is taken as 0.5.

Step-3

calculating grey relational grade (GRG):

$$y_i = \frac{1}{n}\sum_{k=1}^{n} \zeta_i(k) \tag{3.10}$$

where, y_i is the required grey relational grade for i_{th} experiment and n = the number of responses characteristics (Achuthamenon et al., 2018). The correlation between the reference sequence and the comparability sequence is represented by the grey relational grade, which is an overall representation of all the quality features (Prakash et al., 2020). Thus, using grey relational analysis, the multi-response optimization problem is changed into a single-response optimization problem.

Step-4

Then, using a higher grey relational grade, which denotes a higher level of product quality, an optimal level of process parameters is established. This can be accomplished by determining the average grade values for each level of the process parameter, which can then be displayed as a mean response table. Higher average grade values are selected as the optimum parametric combination for multiple responses from the mean response table.

Step-5

After the optimal combination is identified, the analysis of variance (ANOVA) is carried out to determine the parameters that significantly affect the multi-responses at a 95% confidence level, providing crucial information about the experimental data. The Taguchi technique cannot be used to determine the impact of each parameter on multi-response; thus, the ANOVA analysis will be useful to determine the percentage of contribution to identifying the effects (Varghese et al., 2018).

Step-6

The improvement of the grey relational grade by confirmatory experimentation comes next after the optimal combination of process parameters has been identified. Following are the steps to achieve the predicted value of the grey relational grade for the optimal level:

$$y_i = y_m + \sum_{k=1}^{b}(y_i{}^* - y_m) \tag{3.11}$$

Where y_m is the total mean grey relational grade, y_i is the mean grey relational grade at the optimal level of each parameter, and b is the number of significant process parameters (Younas et al., 2019)

3.12 Experimental Investigation

The behavior of the machining parameters (cutting speed, feed rate, and depth of cut) on the surface roughness, tool temperature, rate of material removal, tool wear, and chip of AISI 1030 steel was evaluated through a series of experiments in a CNC lathe.

3.12.1 Measurement of Surface Roughness

As previously said, surface roughness is the foundation of product quality. It is a good pointer to the potential functioning of a mechanical element, since irregularities on the surface may form nucleation sites for cracks or corrosion.

Figure 3. 7 Surface Roughness Tester

In this study, Surface roughness is determined by taking the average of all surface heights and depths which is average roughness (Ra). In most cases, surface roughness is expressed in microns (µm). The VOGEL surface contact profilometer roughness tester, which is depicted in Figure 3.7, was used to measure the surface roughness parameters (available at Ethio-Technical University). Nine trials with three tests each were conducted using this roughness measurement apparatus, and the average roughness value was calculated.

3.12.2 Measurement of Material Removal Rate (MRR)

This is the volume of material removed during machining per unit time. The material removal rate (MRR) has a significant impact on the machining operations' economics. To preserve both quality and productivity when cutting metal, estimation of this machining response is crucial and required. The rate of material removal must be increased during machining. The MRR can be determined using equation 3.12 during the experiment.

$$MRR = \frac{(V_i - V_f)}{t_m} \tag{3.12}$$

where, V_i = initial volume of work-piece, V_f = final volume of work-piece and t_m= machining time (Gohil & Puri, 2016).

3.12.3 Measurement of Tool Temperature

The heat produced during cutting in machining impacts surface quality, and tool wear, and produces hot chips which lead to safety hazards to the machine operator, and dimensional accuracy due to thermal expansion (Pervaiz et al., 2017, Yu et al., 2019). As a result, it's critical to keep the cutting temperature low while machining. The tool utilized in this work to measure cutting temperatures is a digital thermometer, as depicted in Figure 3.8. the device can measure T° up to 800 °C.

Figure 3. 8 Digital Thermometer

3.12.4 Measurement of Tool Wear

Tool wear is caused by relative motion between the workpiece and the cutting tool or the cutting tool and chip in the machining area during turning. Like MRR, tool wear has a significant impact on the cost-effectiveness of machining processes. To maintain both productivity and quality in metal cutting, estimation of this response is also crucial.

Both wear quantity and morphology are taken into account in this work. Using an optical microscope at 20X magnification, it experimentally measured wear morphology as shown in Figure 3.9. At various cutting parameters, photographs of the tooltip of the inserts for cutting tools were taken.

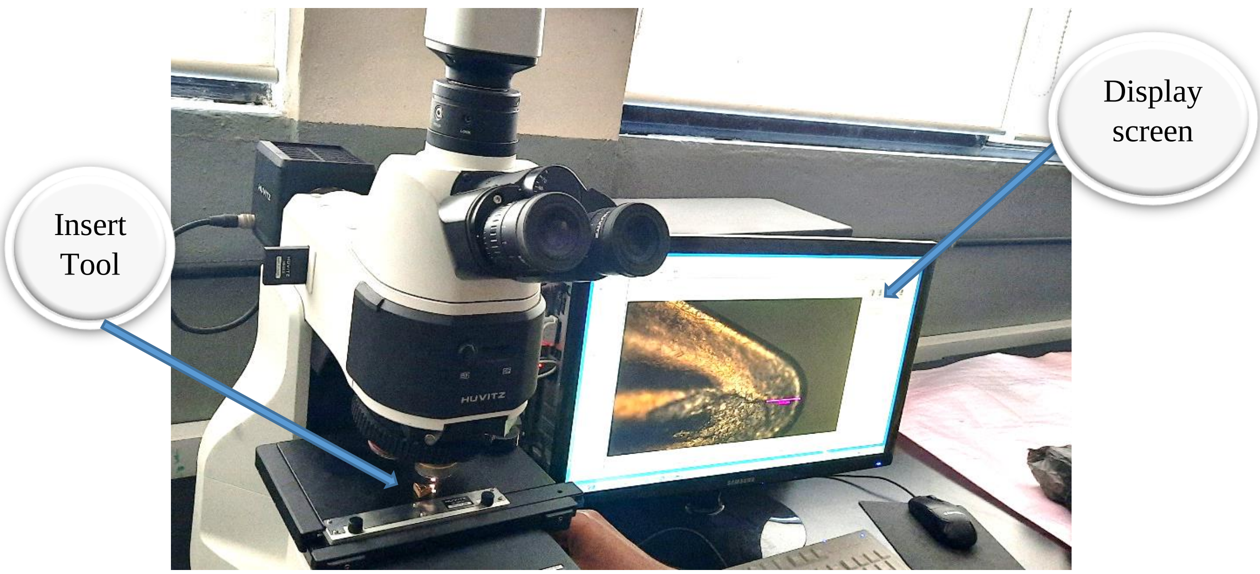

Figure 3. 9 Optical Microscope

The flank wear and crater wear are observed in the wear morphology using the optical microscope. As a result of friction between the machined surface of the workpiece and the tool flank, flank wear develops on the tool flank, gradually chipping the cutting edge. By raising the cutting forces, flank wear has a significant impact on the cutting process. The crater wear occurs on the rake face of the tool.

Equation 3.13 can be used experimentally to determine the wear amount, which is also known as the wear rate. The weight losses are measured using digital balance as shown in Figure 3.10.

$$\text{Tool wear rate} = \frac{w_i - w_f}{t_m \rho} \ (mm^3/s) \qquad (3.13)$$

Where: W_i= Initial Weight of the cutting tool insert (g); W_f = Final Weight measured of the cutting tool insert (g); t_m= Machining time in a sec; ρ = Density of the cutting tool materials (g/mm^3) (Yousuf and Salim, 2018).

Figure 3. 10 Digital Balance to Measure Weight Loss of Cutting Tool Insert

3.12.5 Chip Analysis

The characteristics of the material, cutting speed, feed, depth of cut, tool geometry, and the machining environment, such as temperature and cutting fluid type, all affect the kind of chip production during the metal cutting process. The cutting tool's surface quality and coefficient of friction are other, less important parameters that influence chip formation.

The machining state can be determined by evaluating chip morphology, making it crucial to examine the chip in machining. In this experiment, chips will be collected at the end of each experimental run for the subsequent analyses. For each experimental run, the type of chips will be determined.

3.13 Finite element method (FEM) for Numerical approach

Experimental evaluation of the metal machining process is usually expensive and time-consuming. An alternative technique to get insight into the machining process is computational techniques such as boundary element, finite difference, finite element, and analytical techniques. Amongst these methods, finite element modelling (FEM) is famous among researchers (Pervaiz et al., 2017).

The present work attempts to observe the impact of machining parameters such as spindle speed, feed rate, and depth of cut on performance characteristics such as material removal rate and tool wear in dry turning of AISI 1030 steel. The work aims at developing a 3-dimensional machining model for the simulation of material removal rate, tool temperature, and tool wear using DEFORM 3D. The machining simulation is accomplished using a Lagrangian technique to predict the flank wear, tool temperature, and material removal rate (Afrasiabi, 2021).

3.13.1 Modelling

For analyzing the process of chip formation and predicting machining performance characteristics like temperatures, forces, stresses, wear rate, material removal rate, and others, a finite element approach is a successful tool (Liu et al., 2020; Özel et al., 2010). In this study, the turning of AISI 1030 steel using coated tungsten carbide tool was simulated using the finite element method. Finite element analysis is performed using DEFORM 3D software.

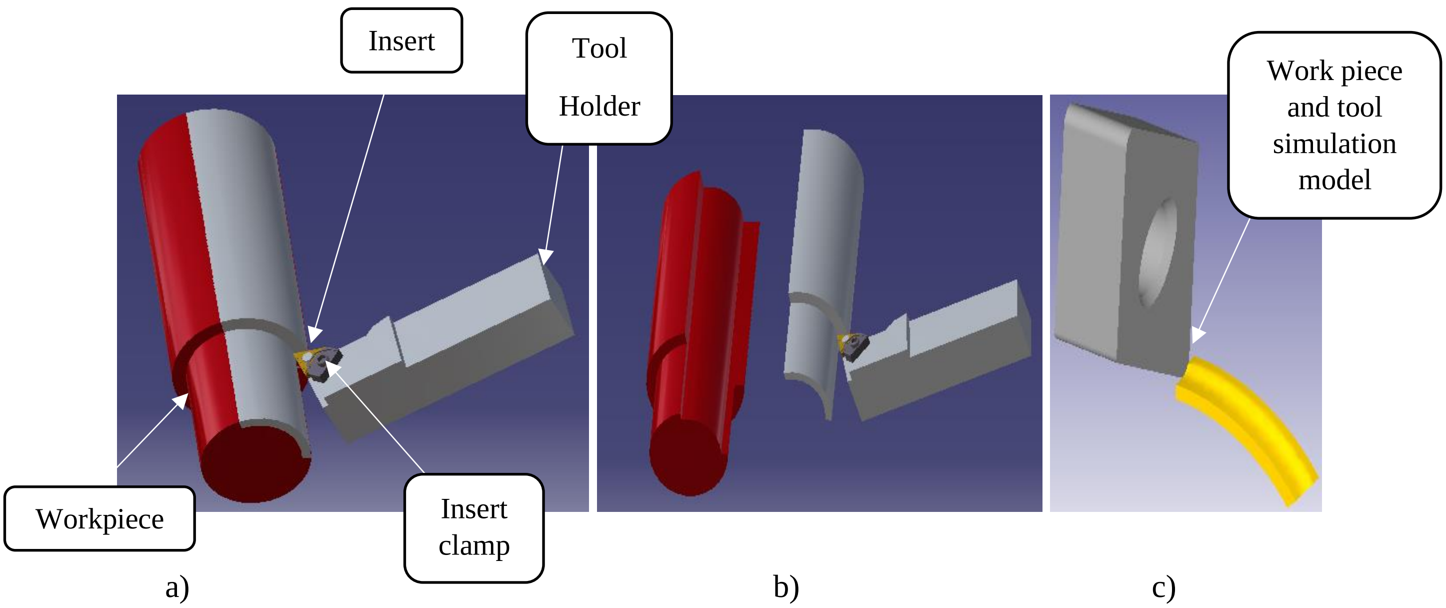

Figure 3. 11 Catia and Simulation Model

During simulation, an initial temperature of 20°C, a shear friction factor of 0.6, a convection coefficient of 0.02 N/sec/mm/°C and no coolant are set. The size ratio for the tool insert is considered 4. Similarly, the size ratio for the workpiece is 7. Tetrahedral element type for both work and tool inserts with the relative mesh size of 25000 is considered. Here, the workpiece is considered a plastic material whereas the tool insert is treated as a rigid material.

The CATIA model of turning is shown in Figure 3.11a. In the simulation process, an arc portion of the whole 60mm diameter is considered for the modelling purpose, as shown in Figure 3.11b. In the workpiece modelling, the arc angle is taken as 25^0 and a diameter of 60 mm has been taken. The numbers of simulation steps are 2000. This work material is AISI 1030 steel, which is included in the software library. Figure 3.11c shows the simulation model of the workpiece and tool using DEFORM 3D. The cutting direction is on the +y-axis, the feed direction is on the -x-axis and the depth of the cut direction is on the -z-axis.

Material model

The material model and mesh describe the flow stress of a certain material under the challenging conditions of machining. In machining applications high temperature, strain and

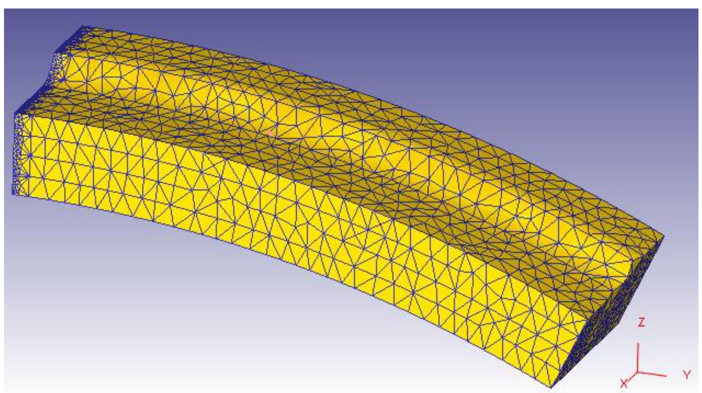

Figure 3. 12 Workpiece Model and Mesh

strain rates act at the same time affecting the flow stress of the work material (Alabi et al., 2010). A well-established constitutive equation used in metal cutting is the Johnson Cook Material model, taking strain hardening, strain rate hardening, and thermal softening into account, as shown in equation (3.14):

$$\sigma = [A + B\bar{\varepsilon}^n]\left[1 + c\ln(\frac{\dot{\varepsilon}}{\dot{\varepsilon}_0})\right]\left[1 - (\frac{T-T_r}{T_m-T_r})^m\right] \tag{3.14}$$

where σ is the flow stress, $\dot{\varepsilon}$ is the strain rate, $\dot{\varepsilon}_0$ is the reference strain rate, $\tilde{\varepsilon}$ is the equivalent strain, T is the temperature of the work material, T_m is the melting temperature, T_0 is the room temperature and A; B; n; C, and m are material constants. A is yield strength (MPa). it is the initial yield strength of the material, B represents the hardening modulus (MPa), C is the strain rate sensitivity coefficient, n is the hardening coefficient, and m is the thermal softening exponent (Akram et al., 2018). The Johnson-Cook equation can be applied by determining a set of parameters, usually obtained by experimental material testing. Material modelling and its meshing are shown in Figure 3.12 and the values of the constants are given in Table 3.6.

Table 3. 6 Johnson–Cook Parameters for AISI 1030 (Alabi et al., 2010)

A (MPa)	B (MPa)	n	C	m	T_r(^{0}C)	T_m (^{0}C)
409	608	0.0439	0.0083	1.1144	20	1450

Cutting tool modelling

A two-layered CVD-coated (Al2O3 and TiCN) tungsten carbide tool is used as shown in Figure 3.13 from the library of the tool. This material is selected due to its excellent buildup edge resistance, high hardness capable of cutting hard materials, high stability at high speeds and temperatures, and good wear resistance characteristics.

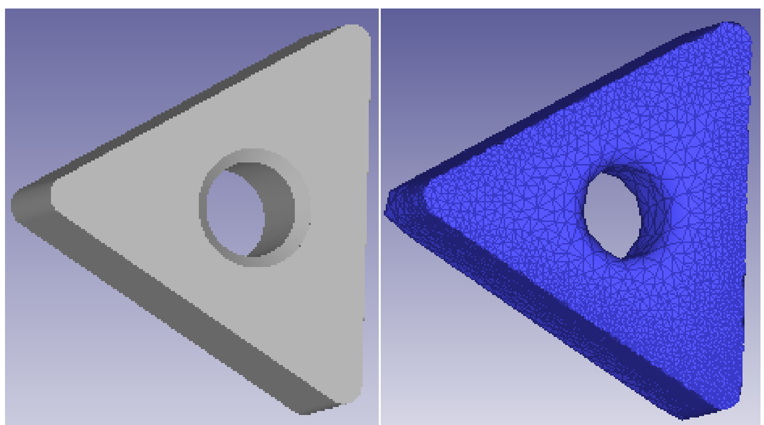

Figure 3. 13 Tool model and mesh

3.13.2 Material Removal Rate MRR Simulation

It is defined as the volume of workpiece material that can be removed per time unit. For the simulation MRR can be determined using equation (3.15);

Material removal rate (MRR)= (initial volume of work piece-final volume of the workpiece)/machining time

$$MRR = \frac{(V_0 - V_f)}{t_m} \tag{3.15}$$

Where, V_0=initial volume, V_f =final volume of the workpiece after machining and t_m=machining time (Gohil & Puri, 2016).

Volume change and machining time were taken from the outcome of the deform 3d simulation result.

3.13.3 Temperature Simulation

During machining, energy is transformed into heat due to the plastic deformation of the workpiece surface and friction between the tool and the workpiece. High temperatures are generated in the region of the cutting edge, which has a very important influence on the wear rate of the cutting tool and tool life. Simulation of maximum tool temperature is considered in this work as maximum tool wear has occurred at this point. The FEA simulation of temperature in the turning process was done with the help of DEFORM 3D.

3.13.4 Tool Wear Simulation

The chip formation simulation provides resolved information about the thermo-mechanical load spectrum in the contact between the workpiece and tool. This information is transformed into local wear rates via a tool wear model which is implemented in a tool wear subroutine. In this work, the Usui wear rate model is used to transform the thermomechanical load spectrum into a local wear rate. The Usui model is used for the calculation of the wear rate (equation 3.16). The parameters such as interface pressure, interface temperature and sliding velocity are noted down from each simulation run.

$$\frac{dw}{dt} = A\, \sigma\, V \exp\left(\frac{-B}{T}\right) \tag{3.16}$$

where $\frac{dw}{dt}$ = wear rate, σ = Interface pressure, V = Sliding velocity, T =Interface temperature (Usui et al., 1984).

A and B are constants that are calibrated experimentally. According to the Usui model, the values of A and B are;

$$\mathrm{A} = 7.8 \times 10^{-9} \quad \mathrm{B} = 5.302 \times 10^{3} \quad if\ temperature < 1150^{0}C$$

$$\mathrm{A} = 1.198 \times 10^{-2} \quad \mathrm{B} = 2.195 \times 10^{4} \quad if\ temperature > 1150^{0}C$$

But for the accuracy of results, these constants are recommended to calibrate depending on the combination of the workpiece and tool since these constants are dependent on both tool and workpiece. Therefore, in this work, these constants were calibrated by combining experimental and simulation results using regression. The calibration was done using successive machining experiments at different times and the same cutting parameters for all.

In addition to the experimental tools utilized, additional tools are used for the calibration of wear constants A and B as illustrated in Figure 3.14.

This is done to avoid overusing tools during experimentation and to get an accurate result using a new tool. However, the specifications of the tools are all equal to the tools used in the experiment.

Figure 3.14 Tungsten Carbide Cutting Tool for Wear Calibration

CHAPTER 4

RESULTS AND DISCUSSION

4.1 Introduction

Experimental work was conducted to evaluate the effect of cutting parameters (cutting speed, depth cut, and feed) on the surface roughness, tool wear, material removal rate, tool temperature, and chip analysis of AISI 1030 Steel material during the dry-turning process.

The experiment was carried out on a CNC lathe machine using a tungsten carbide insert cutting tool. Nine experiments were performed to identify the optimum condition. During and after the machining operation, measurements were taken for each of the end responses, statistical analysis was made to get the optimum parameters according to the requirement and the main effects are identified. The values of responses that are conducted by orthogonal array were analyzed using the Taguchi optimization technique. Statistical work was performed using Minitab 17 software. The overall (multi-optimization) was done using grey relational analysis.

Simulation modelling was also done on material removal rate, tool temperature, and tool wear using the same input parameters Then compared with the experimental.

4.2 Samples After Turning Process

All nine experiments with different cutting parameters but with the same length of cut of 20mm after the turning process of AISI 1030 Steel are given in Figure 4.1. The diameter of the workpiece prepared for experimental work is 60mm.

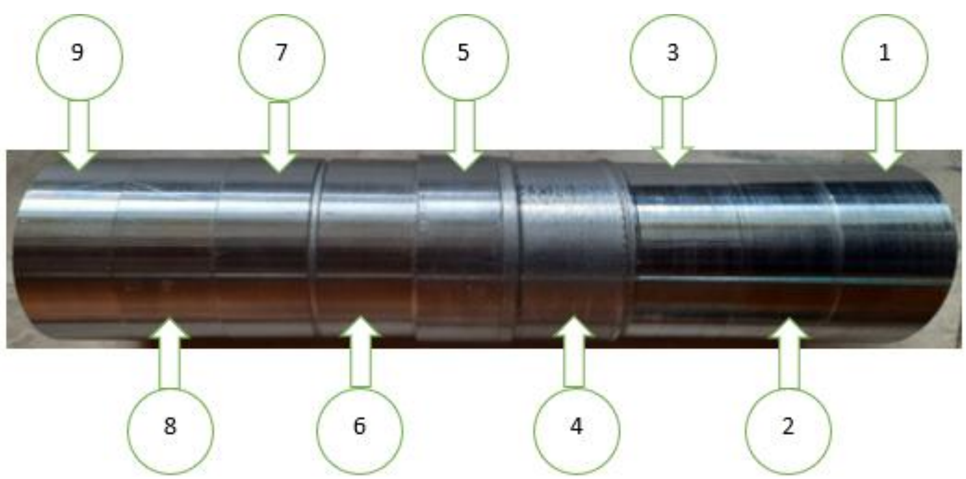

Figure 4. 1 AISI 1030 steel after machining

Experiment numbers 1, 2, and 3 were operated by a similar cutting speed of 90m/min but, with different depths of cuts (0.5mm, 1.5mm, and 2.5mm) respectively and feeds (0.15mm/rev, 0.25mm/rev, and 0.35mm/rev respectively). In a similar manner experiments numbers 4,5 and 6 were operated by a similar cutting speed of 170m/min but with different depths of cuts (0.5mm, 1.5mm, and 2.5mm) and feeds (0.25mm/rev, 0.35mm/rev, and 0.15mm/rev) respectively. Lastly, experiments numbers 7,8, and 9 were also operated by a similar cutting speed of 250m/min, but with different depths of cut (0.5mm, 1.5mm, and 2.5mm) respectively and feeds (0.35mm, 0.15mm, and 0.25mm) respectively.

4.3 Analysis of Material Removal Rate (MRR)

The amount of material removed per unit of time is known as the material removal rate (MRR). In this investigation, a higher rate of material removal was attained compared to cylindrical grinding. Equation 3.12 was utilized to compute the MRR.

Table 4. 1 Experimental Result of Material Removal Rate (MRR)

Experimental result					
Exp. No.	**A** Cutting speed (m/min)	**B** Depth of cut (mm)	**C** Feed (mm/rev)	MRR (mm^3/sec)	$^{S}/_{N_L}$
1	90	0.5	0.15	43.94	32.86
2	90	1.5	0.25	161.47	44.16
3	90	2.5	0.35	453.57	53.13
4	170	0.5	0.25	54.29	34.69
5	170	1.5	0.35	274.45	48.77
6	170	2.5	0.15	215.95	46.68
7	250	0.5	0.35	92.28	39.30
8	250	1.5	0.15	130.71	42.33
9	250	2.5	0.25	251.71	48.0180
Average				186.49	43.33

Using Taguchi techniques and signal-to-noise (S/N) ratios, which were employed for the optimization of the measured control variables, MRR was measured through the experimental design for each combination of the control factors. The highest MRR number is crucial for the product's quality development. For this reason, the S/N ratio was calculated using the "larger-the-better" equation 3.2.

4.3.1 Experimental Result

The findings in Table 4.1 are the result of an experimental material removal rate study and are shown in graphical form as shown in Figure 4.2. The material removal rate was calculated by using the volume change and machining time. The design of experiments was used to calculate the means and S/N ratios for each experiment listed in the table. From the figure, the maximum material removal rate was observed in experiment number three (453.57 mm^3/s) because of the higher cutting depth and feed rate. The minimum material removal rate was also observed in experiment number one (453.57 mm^3/s) because of the lower cutting depth and feed rate. The mean and S/N ratios have average values of 186.49 mm^3/s, and 43.33, respectively.

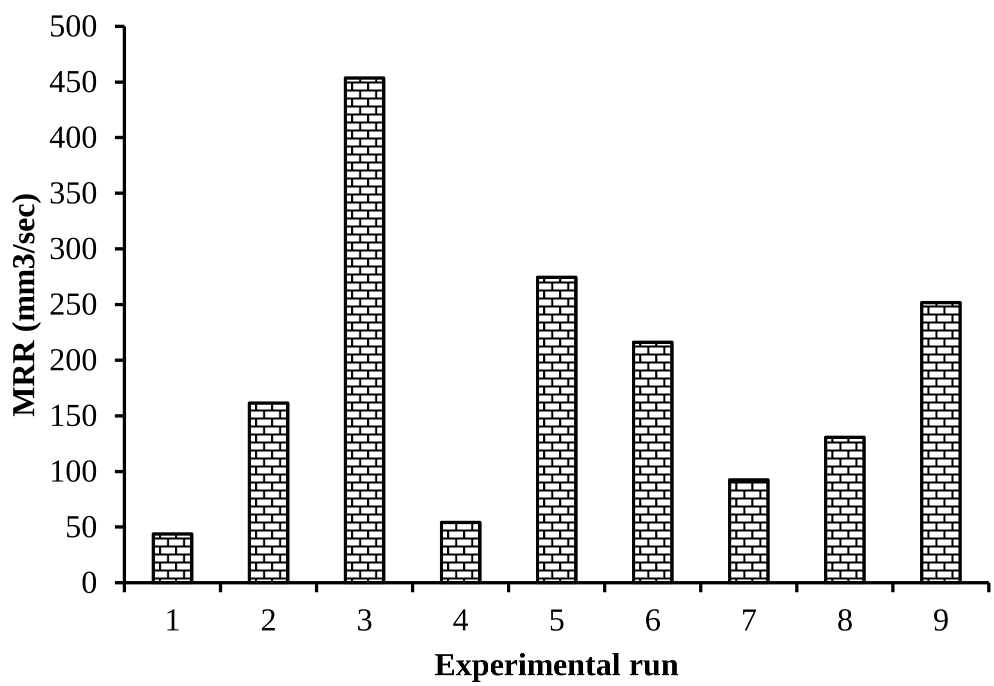

Figure 4. 2 Experimental Result of MRR

4.3.2. ANOVA for Material Removal Rate (MRR)

To identify the key variables affecting the cutting process, an ANOVA is performed. The effects of cutting speed, depth of cut, and feed rates on material removal rate were examined in this study using ANOVA (Parthiban et al., 2017). This was done with a 95 % confidence level and a significance level of 0.05. Table 4.2 displays the statistical ANOVA tables for all variances. It can be seen from the table data that the depth of cut has the greatest influence on the MRR. The second most important component that has an impact on MRR is the feed rate. the percent of the contribution of the cutting parameters on MRR was determined using equation 3.5.

According to Figure 4.3, the contributions of the A, B, and C factors on the MRR were found to be 4.29%, 66.13% and 26.01% respectively. Thus, the most important factor affecting the MRR was the depth of cut (factor B, 66.13%) followed by feed at 26.01%. The percent of error was considerably low at 3.57%.

Table 4. 2 Analysis of Variance for Means of MRR

Source	DF	SST	SSTR	MSE	F	P	Percent contribution P (%)	Significance e (α=0.05)
Cutting speed	2	5769	5769	2884	1.20	0.455	4.29	Less Significant
Depth of cut	2	89016	89016	44508	18.51	0.051	66.13	Highly Significant
Feed	2	35005	35005	17502	7.28	0.121	26.01	Significant
Residual Error	2	4809	4809	2404			3.57	
Total	8	134598					100%	

Where; DF is the degree of freedom, SST is the total sum of squares, SSTR is a treatment Sum of squares, MSE is mean square error, and F is the F- Ratio calculated by using Minitab 16 software.

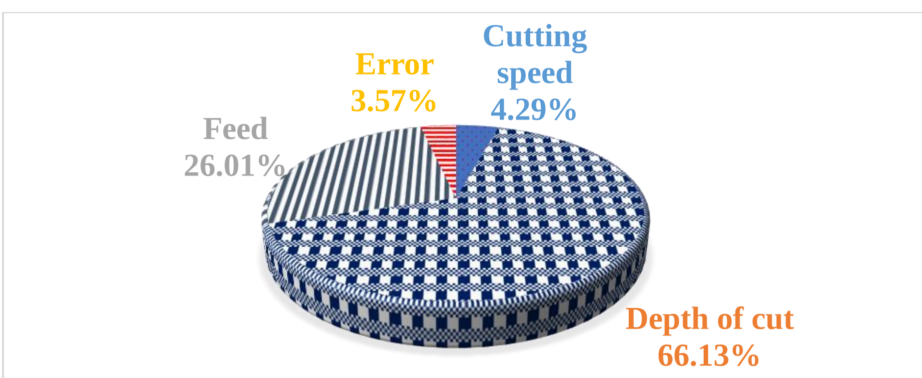

Figure 4. 3 Contribution of cutting parameters on MRR

4.3.3 Optimization of Cutting Parameters

The effect of cutting parameters on the Material removal rate (MRR) of the machined product and the optimum parameters combination is described as follows.

4.3.3.1 Analysis of mean

The mean value of MRR for each factor i.e., Cutting speed (A), Depth of cut (B), and Feed (C) at each level was obtained and the result was listed in response to Table 4.3, taking the mean value from Table 4.1. mean is calculated based on the equation below with an example for factor B (Depth of cut).

$$S/N_1 = \frac{43.944 + 54.285 + 92.285}{3} = 63.5$$

$$S/N_2 = \frac{161.468 + 274.45 + 130.71}{3} = 188.88$$

$$S/N_3 = \frac{453.567 + 215.95 + 251.71}{3} = 307.08$$

The range (delta) is then calculated using a "mean response table" to analyze the impact of each control factor (cutting speed, feed rate, and depth of cut) on MRR.

Where delta is determined by;

$$Delta = (MaximumS\ /N\ ratio - Minimum\ S/\ N\ ratio) \qquad (4.1)$$

This table shows the optimal levels of control factors for the optimal MRR value. The main effect plot for MRR is also shown in Figure 4.4.

Table 4. 3 Response Table for Means of MRR

Level	Cutting speed	Depth of cut	Feed
1	**219.66**	63.50	130.20
2	181.56	188.88	155.82
3	158.23	**307.08**	**273.43**
Delta	61.42	243.57	143.23
Rank	3	1	2

From the Figure 4.4, it is observed that, as feed and depth of cut increased, MRR increased. This is because an increase in feed rate and depth of cut increases chip load and shear force, and thus material removal becomes higher, resulting in higher cutting forces (Varghese et al., 2018). Optimal levels of the control factors for maximizing the MRR can be easily determined from this graph. The optimum level for each control factor was found according to the highest mean point in the main effect plot. Factor A (Level 1, mean = 219.66), Factor B (Level 3, mean = 307.08), and Factor C (Level 3, mean = 273.43), or a lower cutting speed, higher depth of cut, and higher feed A1B3C3 combination, were the factors with the levels and means that produced the best MRR value. The optimum parameter setting levels and their values are displayed in Table 4.4.

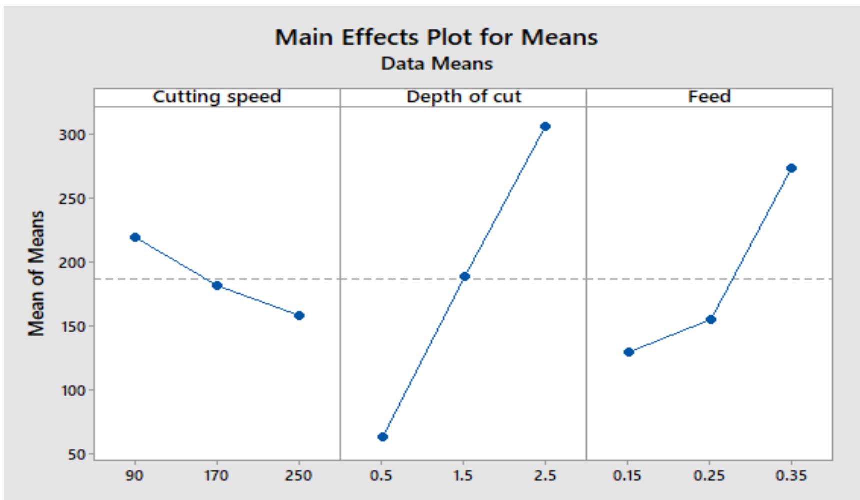

Figure 4. 4 Main Effect Plot for Mean

This indicates that the best MRR value was obtained at cutting speed (A_1) at 90 m/min, Depth of cut (B_3) at 2.5 mm, and feed rate (C_3) at 0.35 mm/rev (Figure 4.4). Results of the main effect of cutting parameters on material removal rate are in agreement with (Krishankant et al., 2012) results. From the main effect plot for the mean, the depth of cut has the greatest effect on MRR with (Delta = 243.57, Rank = 1).

Table 4. 4 Optimum Parameters Setting Levels and Their Values of MRR

Factors	Level selected	Value of level	Rank
Cutting speed	2	90 m/min	3
Depth of cut	3	2.5 mm	1
feed	3	0.35 mm/rev	2

The factor with the least effect on the MRR was the cutting speed (Delta = 61.42, Rank = 3). The optimum parameter combinations obtained by (Krishankant et al., 2012) for EN-24 steel were also similar to this.

4.3.3.2 Interaction Effect

The impact of interactions of cutting speed and depth of cut on MRR is shown in Figure 4.5. According to the interaction plot in Figure 4.5 when the cutting speed is set at a lower level, the MRR was raised from 43.944 mm^3/s to 161.47 mm^3/s by increasing the depth of cut from 0.5 mm to 1.5 mm. Then, as the depth of cut increased to 0.35 mm, it increased to 453.57 mm^3/s with a somewhat steeper slope. When the cutting speed rises to a medium level as the depth of cut increases from 0.5 mm to 1.5 mm, MRR was increased from 54.29 mm^3/s to 274.45 mm^3/s but decreased to 215.95 mm^3/s as the depth of cut increased to 2.5 mm. similarly, as the cutting speed rises to the higher level of 250 m/min the MRR was decreased. In this when the depth of cut increased from 0.5 mm to 1.5 mm, MRR decreased from 92.28 mm^3/s to 130.71 mm^3/s but as the depth of cut increased to 2.5 mm, MRR was increased to 251.71 mm^3/s.

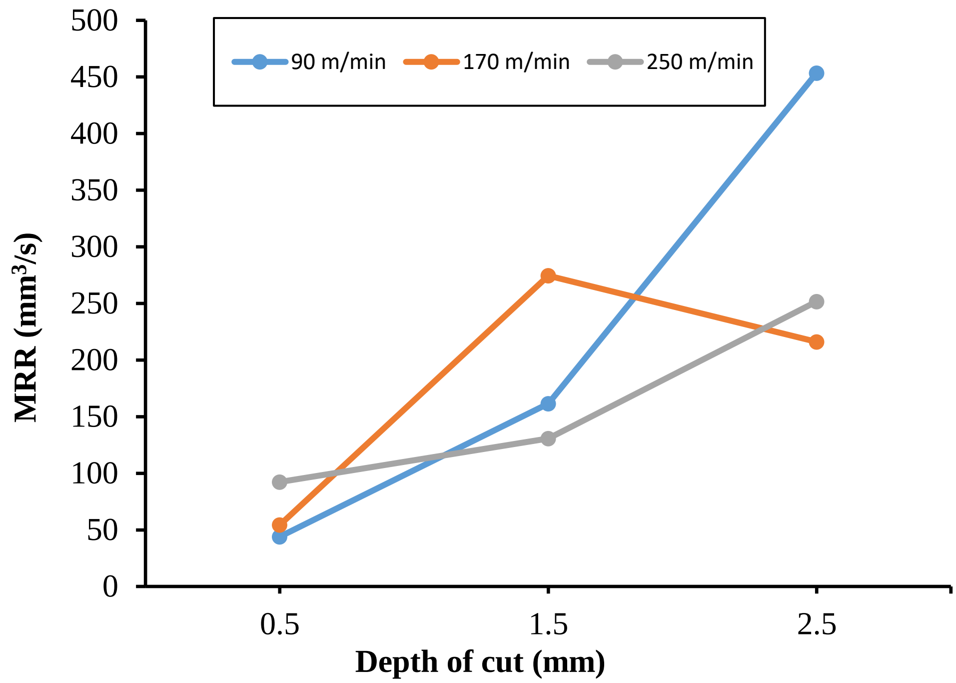

Figure 4. 5 Effect of depth of cut on MRR at different cutting speeds

The influence of feed and depth of cut on MRR Figure 4.6 indicates that at the depth of cut of 0.5 mm, increasing feed from the lowest to the highest level, MRR was increased from 43.944 mm^3/s to 92.284 mm^3/s. Similarly, when the depth of cut is 1.5 mm, increasing feed from 0.15 to 0.25 mm/rev, MRR was increased from 130.71 mm3/s to 161.468 mm^3/s and also increased to 274.45 mm^3/s as feed was increased to 0.35 mm/rev. MRR rose with a reduced slope from 215.95 mm^3/s to 251.71 mm^3/s at a 2.5 mm depth of cut as feed increased from 0.15 to 0.25 mm/rev. However, the MRR rose to 453.567 mm^3/s with a sharp slope when the feed was raised to 0.35 mm/rev.

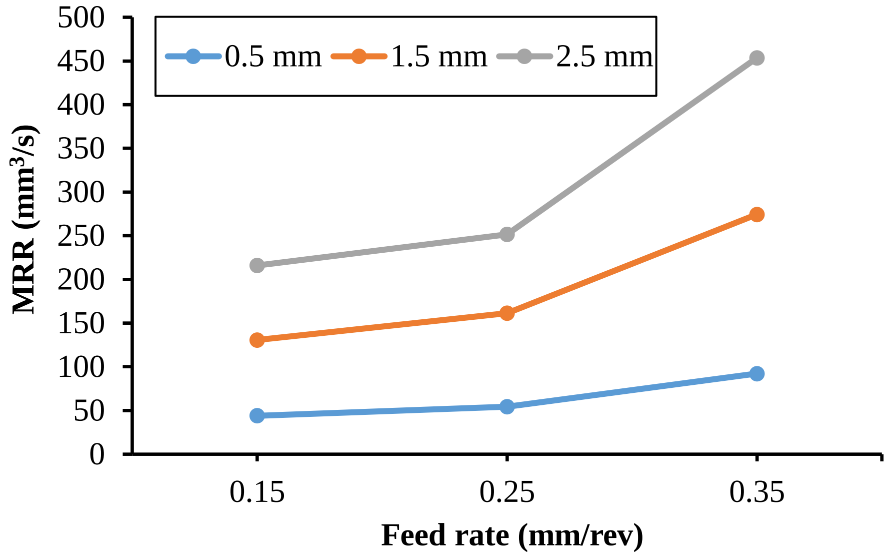

Figure 4. 6 Effect of feed rate on MRR at different depth of cuts

4.3.3.3 Analysis of S/N ratio for MRR

Similar to mean analysis, we may use the S/N approach to determine the optimal parameter combinations and determine how various factors affect the answer. This S/N is applied in the Taguchi approach.

Table 4. 5 Response Table for Signal-to-Noise Ratios Larger Is Better For MRR

Level	Cutting speed	Depth of cut	Feed
1	**43.38**	35.62	40.62
2	43.38	45.09	42.29
3	43.22	**49.28**	**47.07**
Delta	0.17	13.66	6.44
Rank	3	1	2

The Response Table for Signal to Noise Ratio is displayed in Table 4.5, and larger-the-better characteristics were used to maximize MRR.

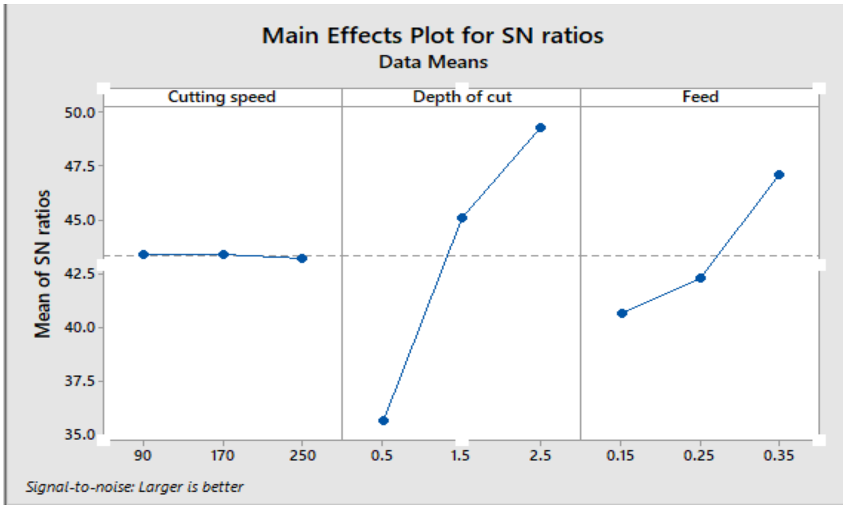

Figure 4. 7 Main Effects Plot for SN Ratios

The main effect plot is depicted in Figure 4.7. From this graph, one can readily identify the control factor values that will maximize the MRR. The highest S/N ratio point on the main effect plot served as the benchmark for determining the optimal level for each control factor. According to the graph, factor A (Level 1, S/N = 43.38), factor B (Level 3, S/N = 49.28), and factor C (Level 3, S/N = 47.07) represent the optimum cutting speed, depth of cut, and feed ratios, respectively. that is the **A1B3C3** combination.

4.3.3.4 Prediction of Performance at Optimal Levels of Mean and S/N Result

For predicting the optimum response using Taguchi, linear regression equation 4.2 was used: **A1B3C3** is the optimum levels combination of the factors for MRR value.

$$y_{opt} = \mathrm{m} + (\mathrm{m}A_3 - \mathrm{m}) + (\mathrm{m}B_1 - \mathrm{m}) + (\mathrm{m}C_1 - \mathrm{m}) \quad (4.2)$$

$$y_{opt} = \mathrm{m}A_3 + \mathrm{m}B_1 + \mathrm{m}C_1 - 2\mathrm{m}$$

Where, (mA1, mB3, mC3) represent the optimum level average values of Mean and S/N of MRR and m is the average of all of the MRR values obtained from Table 4.1.

$$y_{opt} = 219.66 + 307.08 + 273.43 - 2(186.49)$$

y_{opt}= 427.19 mm^3/s (predicted mean value for MRR)

Then S/N was also obtained; $y_{opt} = 43.38 + 49.28 + 47.07 - 2(43.33)$

y_{opt}= 53.0763 (predicted S/N value for MRR)

Predicted Optimum Mean and S/N For MRR are shown in Table 4.6.

Table 4. 6 Predicted Optimum Mean and S/N For MRR

Response	Optimal parameter	Predicted value	
		Mean	S/N
MRR (mm^3/s)	**A1B3C3**	427.19 mm^3/se	53.076

4.3.4 Simulation Result of MRR

The simulated MRR was calculated using Equation 3.15. Figure 4.8 illustrates a simulation result of volume change for the first experimental run with parameters of 90 m/min cutting speed, 0.5 depth of cut, and 0.15 mm/rev feed. MRR is calculated using the machining time and volume change from the simulation results in Figure 4.8. The remaining simulation runs are listed similarly in Table 4.7.

V_0=30.4mm^3, V_f=30.1mm^3, t_m=0.00727sec

$$MRR = \frac{(30.4mm^3 - 30.1mm^3)}{0.00727\text{sec}} = 41.27\, {}^{mm^3}/_{sec}$$

Table 4. 7 Simulation Results of Material Removal Rate (MRR)

Simulation result					
Exp. No.	A Cutting speed (m/min)	B Depth of cut (mm)	C Feed (mm/rev)	MRR (mm^3/sec)	${}^{S}/_{N_L}$
1	90	0.5	0.15	41.27	32.31
2	90	1.5	0.25	171.92	44.71
3	90	2.5	0.35	412.66	52.31
4	170	0.5	0.25	51.95	34.31
5	170	1.5	0.35	300	49.54
6	170	2.5	0.15	225.47	47.06
7	250	0.5	0.35	90.91	39.17
8	250	1.5	0.15	127.79	42.13
9	250	2.5	0.25	234.36	47.39
Average				184.0367	43.22

Table 4.7 shows the simulation results of MRR for each measurement and their S/N ratios. From the table, the average values of the MRR for mean and S/N ratio were calculated to be 184.0367 mm^3/s and 43.22, respectively.

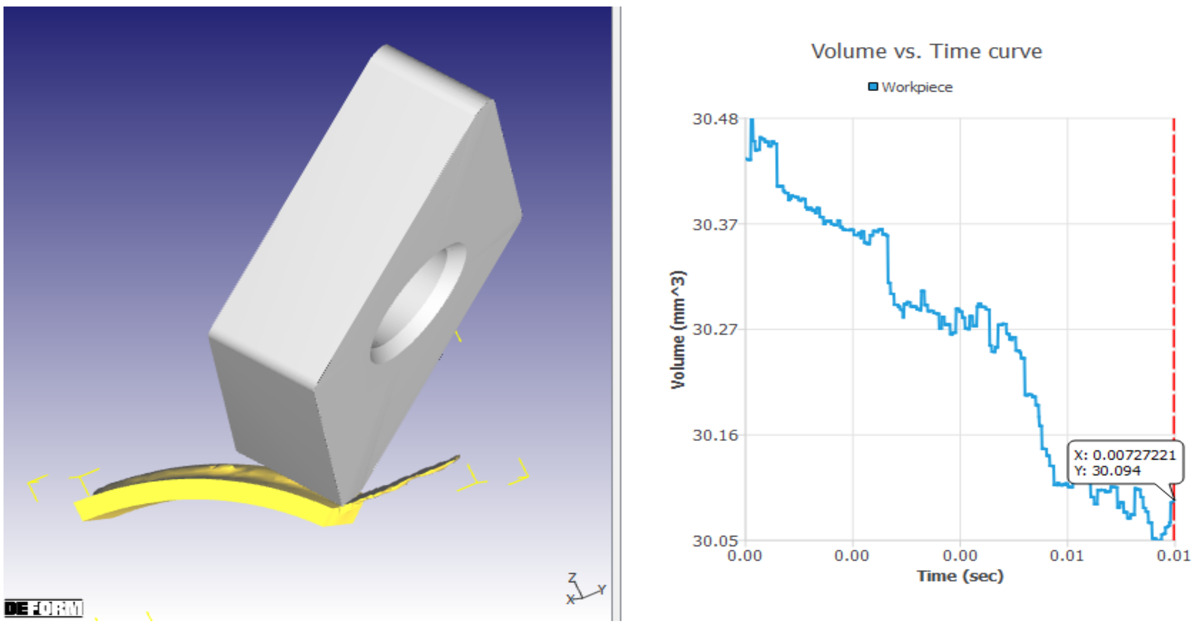

Figure 4. 8 simulations of MRR At 90 m/min, 0.5 mm, And 0.15 mm/rev

4.3.5 Comparison

The simulation and Taguchi-predicted results of the material removal rate were compared with the experimental results in this section. Comparisons were done separately for the optimum result and all experimental runs.

4.3.5.1 Confirmation tests of optimum result

A confirmation experiment was needed to verify the optimal condition when using the Taguchi optimization technique (Parthiban et al., 2017). This means that the final stage is to compare the experimental result to the expected outcome after obtaining the optimum combination of process parameters and their levels. There is no need for a confirmation test if the optimum set of parameters and their values coincides with one of the trials in the orthogonal array. A confirmatory test is required if not. Based on this, Table 4.8 then shows the findings of the confirmation experiment. The optimal mean of confirmation experimental data is compared to simulation and predicted results for MRR. The predicted and simulation results are very close to the experimental. With smaller errors, the error value was within acceptable limits.

Table 4. 8 Confirmation Result of The Optimum Mean For MRR

Material removal rate (MRR) (mm^3/sec)						
Level	Confirmation Experimental Result (mm^3/s)		Taguchi method		Simulation	
			Pred	Error (%)	Sim.	Error (%)
A1B3C3 (optimum)	Mean	453.57	427.19	5.81	412.66	9.01
	S/N	53.13	53.08	0.10	52.31	1.54
A3B2C1 (Random)	Mean	161.47	191.39	18.52	171.92	6.47
	S/N	44.16	44.11	0.11	44.71	1.25

4.3.5.2 Comparison of predicted, numerical and experimental results

Error-values must be under 20% for statistical analysis to be considered reliable (Kıvak, 2014). Despite being larger than the average of all relative errors of the S/N result, the average of all error percentages determined in the mean value is still within acceptable bounds. Therefore, the results obtained from the confirmation tests reflect successful optimization. To compare the simulation and experimental findings and assess the model's accuracy, the relative percentage error must be calculated using equation (4.3).

$$\text{Relative Error (\%)} = \frac{|M_i - Y_i|}{Y_i} \times 100 \tag{4.3}$$

Where; M_i and Y_i are the simulation and experimental response values for the run number i.

The average relative error of experimental, simulation and predicted results are displayed in Table 4.9. The comparison of the material removal rate findings from simulation, experiment, and predicted methods is also shown in Figure 4.9. For MRR, the average of all relative errors is discovered to be 4.85 %. MRR values in experiments range from 43.94 to 453.57 mm^3/sec, but in simulations, MRR ranges from 41.27 to 412.66 mm^3/sec. Additionally, the predicted MRR ranges from 27.92 to 427.20 mm^3/sec. As a result, it can be said that the turning AISI 1030 experimental produces findings that are in good agreement with both simulation and the expected outcome. Thus, it can be inferred that DEFORM 3D simulation of the machining process can quickly and accurately predict the MRR and saves time for running additional sets of experiments (Yadav, Abhishek, & Mahapatra, 2015).

Table 4. 9 Comparisons of Simulation, Experimental and Predicted Result

Material removal rate (mm^3/sec)						
Exp. No.	Comparison of the experimental and predicted value of MRR (mm^3/sec)			Comparison of experimental and simulation		Average Relative Error
	Experimental	predicted	Error (%)	simulation	Error (%)	
1	43.94	40.40	8.08	41.27	6.09	7.08
2	161.47	191.39	18.52	171.92	6.47	12.50
3	453.57	427.20	5.81	412.66	9.02	7.42
4	54.29	27.92	48.57	51.95	4.30	26.44
5	274.45	270.90	1.29	300	9.31	5.30
6	215.95	245.87	13.85	225.47	4.41	9.13
7	92.28	122.20	32.42	90.91	1.49	16.95
8	130.71	104.34	20.17	127.79	2.23	11.20
9	251.71	248.16	1.41	234.36	6.90	4.15

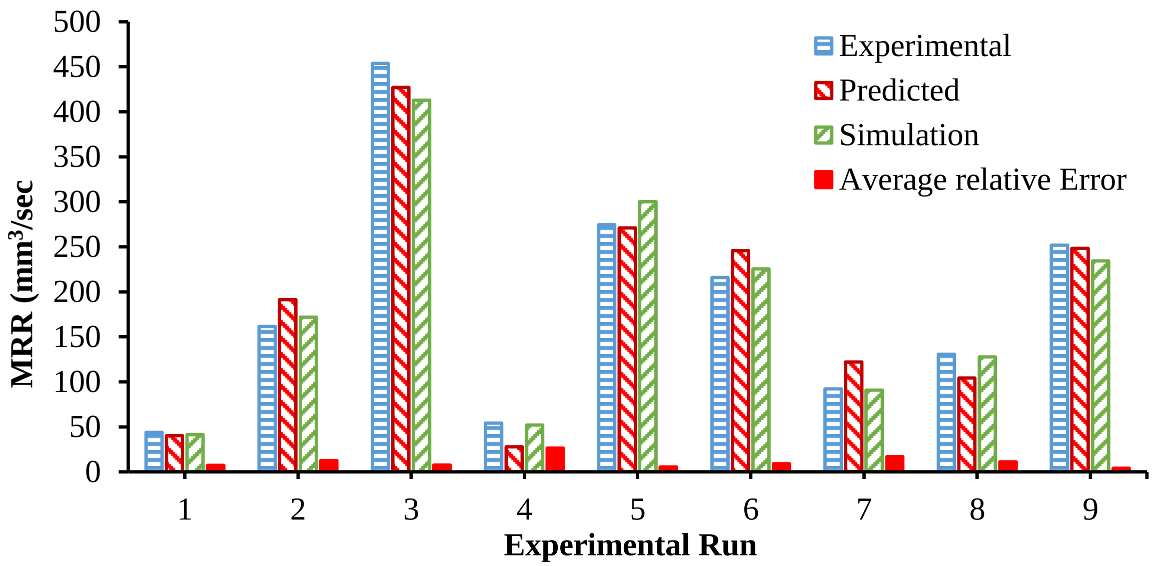

Figure 4. 9 Comparison of simulation, experimental and predicted result

4.4 Analysis of Surface Roughness

Using tungsten carbide cutting tools and the L9 orthogonal array of the Taguchi experimental design approach with three levels of spindle speeds, depths of cut, and feed rates for each, AISI 1030 steel is turned under dry turning conditions.

Figure 4. 10 Surface Roughness At 90 m/min, 0.5 mm, And 0.15 mm/rev.

Three measurements of surface roughness were made for each experimental run, and the average value of the results was examined. According to Taguchi's "smaller-the-better" characteristic equation 3.3, the S/N of the surface roughness was calculated using Minitab17. Figure 4.10 displays the measurement of experiment one's surface roughness at 90 m/min cutting speed, 0.5 depth of cut, and 0.15 mm/rev feed.

Table 4.10 lists the surface roughness values for each measurement along with their S/N ratios using. The table's average surface roughness values for mean and S/N ratio were determined to be 2.73 µm and -8.12, respectively. The results of experimental surface roughness are also shown in graphical form as shown in Figure 4.11

Table 4. 10 Experimental Results of Surface Roughness

Experimental result								
Exp. No.	A Cutting speed (m/min)	B Depth of cut (mm)	C Feed (mm/rev)	Surface Roughness Ra (μm)			Mean	S/N_L
				Meas.1	Meas.2	Meas.3		
1	90	0.5	0.15	3.24	3.21	3.26	3.24	-10.20
2	90	1.5	0.25	3.82	3.86	3.86	3.85	-11.70
3	90	2.5	0.35	4.67	4.38	4.55	4.53	-13.13
4	170	0.5	0.25	1.82	1.79	1.84	1.82	-5.19
5	170	1.5	0.35	3.54	3.56	3.49	3.53	-10.96
6	170	2.5	0.15	1.89	1.87	1.9	1.89	-5.51
7	250	0.5	0.35	2.13	2.45	2.31	2.30	-7.24
8	250	1.5	0.15	1.63	1.65	1.67	1.65	-4.35
9	250	2.5	0.25	1.78	1.72	1.69	1.73	-4.76
average							2.73	-8.12

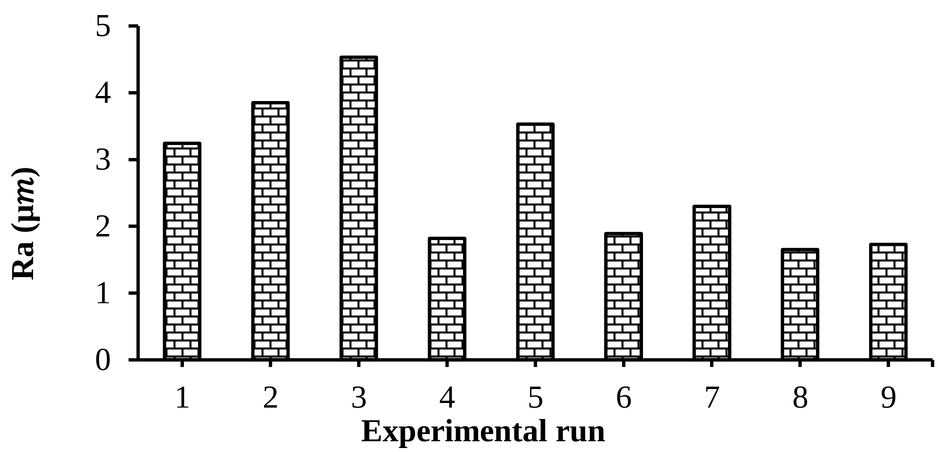

Figure 4. 11 Experimental Results of Surface Roughness

4.4.1 ANOVA For Surface Roughness

ANOVA was used to evaluate how cutting speed, depth of cut, and feed rates affected surface roughness. This was done with a 95 % confidence level and a significance level of 0.05. Table 4.11 displays the statistical ANOVA result for surface roughness.

Table 4. 11 Analysis of Variance for SN Ratios

Source	DF	SST	SSTR	MSE	F	P	Percent contribution P (%)	Significance e (α=0.05)
Cutting speed	2	61.816	61.816	30.9078	34.93	0.028	67.21	Highly Significant
Depth of cut	2	3.643	3.643	1.8214	2.06	0.327	3.96	Less Significant
Feed	2	24.754	24.754	12.3768	13.99	0.067	26.91	Significant
Residual Error	2	1.770	1.770	0.8848			1.92	
Total	8	91.982					100%	

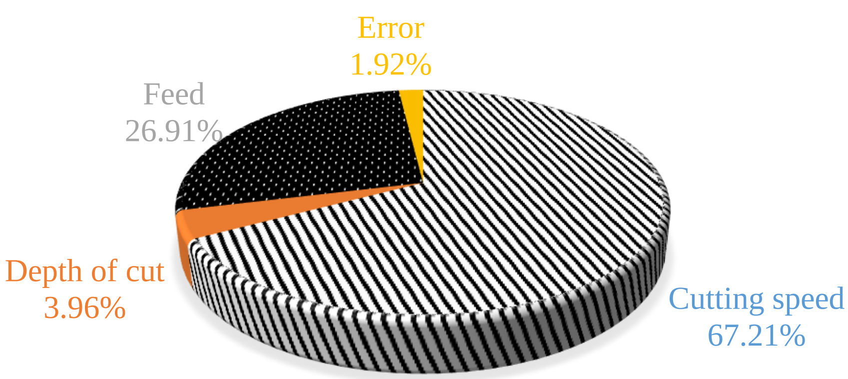

Figure 4. 12 Contribution of cutting parameters on surface roughness

The cutting speed was found to be the most important element affecting the surface roughness based on the table data. As Varghese et al., (2018) described, at lower cutting speeds, there is the highest surface roughness. The second most important component that influences surface roughness is feed rate. According to the metal-cutting principle, every increase in feed rate causes the cross-section and deforming volume to rise, which deteriorates the surface and increases surface roughness (Kumar et al., 2017). According to Figure 4.12, the A, B, and C factors contributed 67.21 %, 3.96 %, and 26.91 %, respectively, to the surface roughness. Cutting speed had the greatest impact on surface roughness, followed by feed. At 1.92 %, the error percentage was significantly reduced. The surface roughness is not statistically significantly impacted by the depth of cut. A qualitative comparison can be made, nevertheless. For instance, (Feng & Wang, 2003) discovered that the surface roughness of turned surfaces is unaffected by the depth of cut.

However, utilizing the fractional factorial experimental method, the measured surface roughness is significantly influenced by the feed rate, work material, and speeds.

4.4.2 Optimization of Cutting Parameters

This study's ultimate objective was to use the Taguchi process to optimize the cutting settings for AISI 1030 steel. The following describes the impact of cutting parameters on the surface quality (surface roughness) of the machined product and the optimum parameter combination.

4.4.2.1Analysis of Mean for Surface Roughness

According to Table 4.12, compared to other parameters, cutting speed has the biggest impact on surface roughness, followed by feed and depth of cut. The A3B1C1 combination for smaller-the-better characteristics is the optimum set of parameters that results in the best surface quality. Figure 4.13 depicts the main effect plot for the means of surface roughness.

Table 4. 12 Response Table for Means of Surface Roughness

Level	Cutting speed	Depth of cut	Feed
1	3.872	**2.450**	**2.258**
2	2.411	3.009	2.464
3	**1.892**	2.717	3.453
Delta	1.980	0.559	1.196
Rank	1	3	2

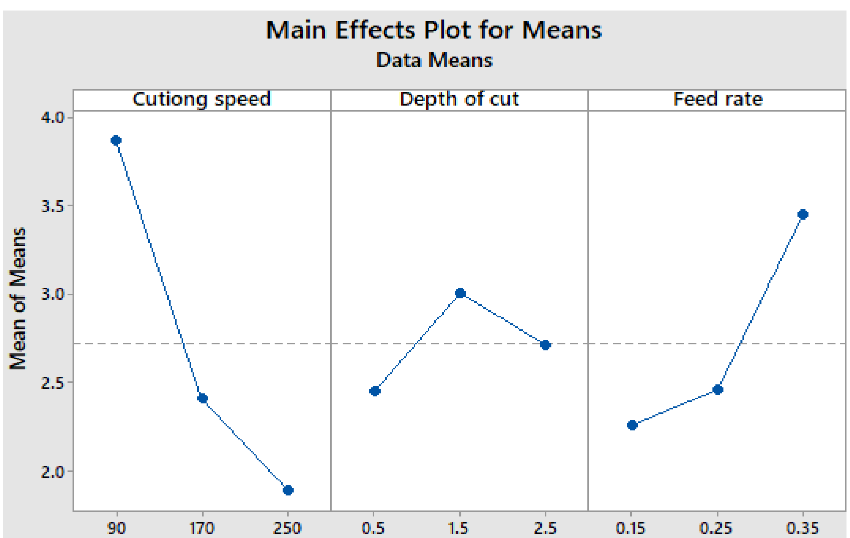

Figure 4. 13 Main Effects Plot for Means

Low cutting speeds produce a rough surface because they increase built-up edges and make chips more brittle. By raising the cutting speed, it is possible to eliminate the built-up edges, which reduces chip fracture and produces a better finish (Kıvak, 2014). Surface roughness measurements demonstrated a tendency to decrease with increasing cutting speed. Cutting more quickly reduced the amount of tool-chip contact, which in turn reduced friction and improved surface quality. The best value of the surface finish can be seen at the lowest position on the plot. this also shows the optimum conditions within the constraints of the experiment.

The graph shows the optimum parameters that are cutting speed at level three (250 m/min), depth of cut at level one (0.5 mm), and feed rate at level one (0.15 mm/rev) which is an $A_3B_1C_1$ combination which is summarized in Table 4.13.

Table 4. 13 Optimum Parameters Setting Levels and Their Values

Factors	Level selected	Value of level	Rank
Cutting speed	3	250 m/min	1
Depth of cut	1	0.5 mm	3
feed	1	0.15 mm/rev	2

4.4.2.2 Interaction Effect

Figure 4.14 shows the interaction effect of feed and cutting speed. A lower feed (0.15mm/rev) gives the best surface finish. when the cutting speed was 90 m/min then increasing feed from 0.15 mm/rev to 0.25 mm/rev resulted in increasing (decreased surface finish) the surface roughness from 3.24µm to 3.85µm and further increased to 4.53 µm as feed increased to 0.35 mm/rev.

The graph shows that surface roughness rises with rising feed rates because higher feed rates induce helicoid grooves. With an increase in feed rate, these furrows grow wider and deeper (Aouici et al., 2013). when cutting speed was increased from 170 m/min. as feed increased from 0.15 mm/rev to 0.25 mm/rev, surface roughness decreased from 1.89µm to 1.82 µm, but surface roughness increased (decreased surface finish) to 3.53 µm as feed increased to 0.35.

Similarly, as the cutting speed was increased to 250 m/min surface finish improved due to increased cutting temperatures and plastic deformation at the tool-chip contact, surface (Agrawal & Patil, 2018). In this, as feed increased from 0.15 mm/rev to 0.25 mm/rev, surface roughness increased from 1.65 µm to 1.73µm and increase also to 2.3 µm as feed increased to 0.35 mm/rev. From this interaction plot, it can be seen that the best surface finish was obtained at a lower level of feed rate with all given cutting speeds. In addition, surface roughness decreased as the cutting speed increased.

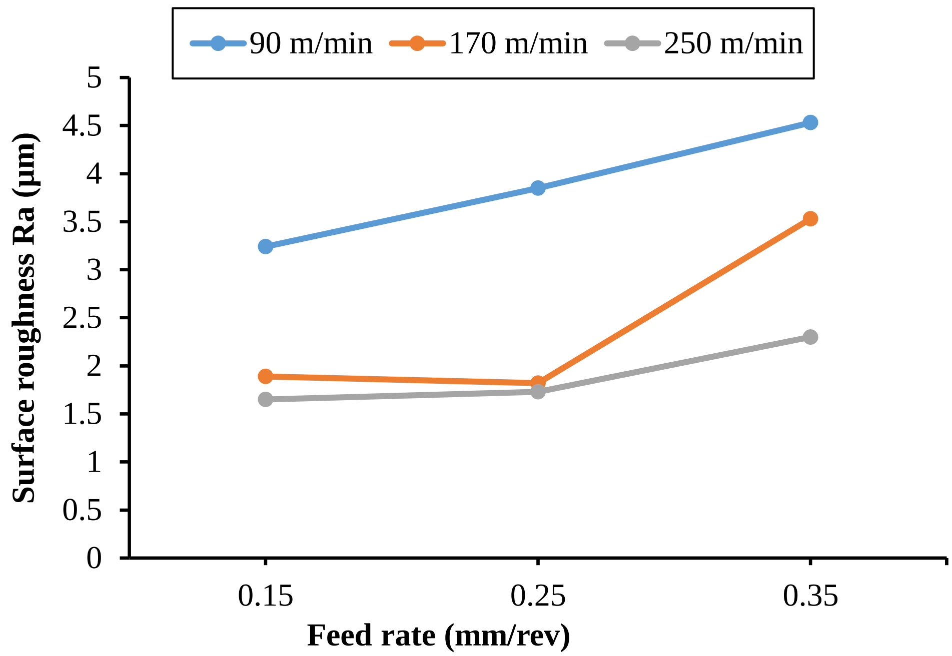

Figure 4. 14 Effect of feed rate on surface roughness at different cutting speeds

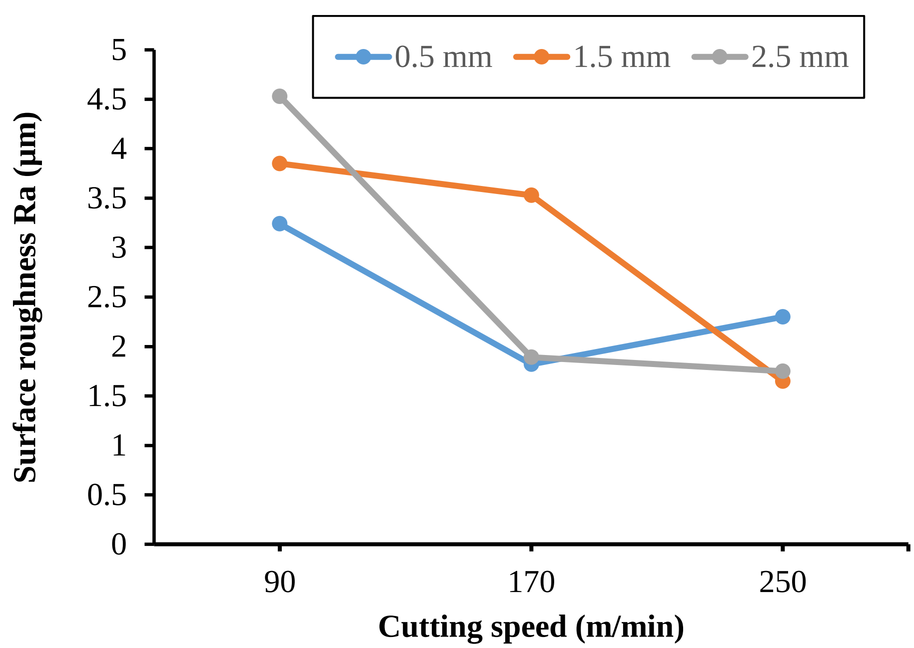

Figure 4. 15 Effect of cutting speed on surface roughness at different depth of cuts

The interaction effect of depth of cut and cutting speed on surface roughness is indicated in Figure 4.15. At 0.5 mm depth of cut, when the cutting speed increases from lower to medium level, surface roughness was decreased from 3.24 µm to 1.82 µm. Then increased to 2.3 µm as the cutting speed increased to a higher level. When the depth of cut is 1.5 mm, as the cutting speed increases from 90 m/min to 170 m/min, surface roughness was decreased from 3.85 µm to 3.53 µm, also decreased to 1.65 µm as the cutting speed increases to 250 m/min. At 2.5 mm depth of cut as the cutting speed increases from 90 m/min to 170 m/min, surface roughness was decreased from 4.53 µm to 1.89 µm which is in this cutting speed good surface finish was obtained when the depth of cut increases. Also surface roughness was further decreased to 1.75µm as the cutting speed further increased to 250 m/min.

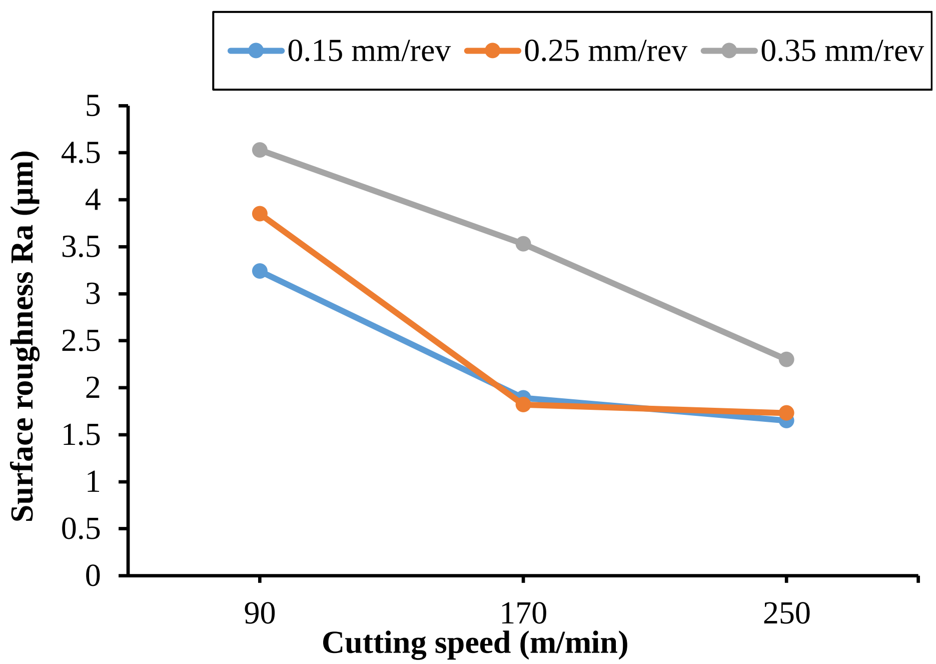

Figure 4. 16 Effect of cutting speed on surface roughness at different feed rates

The effect of cutting speed on surface roughness at a given feed is shown in Figure 4.16. The surface roughness decreased from 3.24 µm to 1.89 µm when the feed was 0.15 mm/rev and increasing cutting speed to the medium level. This condition is consistent with the result obtained by (Valera & Bhavsar, 2014). This means a better surface finish was obtained as the cutting speed increased. As the cutting speed increased to a higher level (250 m/min), the surface finish (surface roughness) was improved to 1.65 µm.

As the feed is increased from 0.15 mm/rev to 0.25 mm/rev the surface roughness was also increased. In this when the cutting speed increased from 90 m/min to 170 m/min, surface roughness decreased from 3.85 µm to 1.82µm and further decreased to 1.73 µm as the cutting speed increased to 250 m/min. when feed is 0.35 mm/rev then as the cutting speed increased from 90 m/min to 170 m/min, surface roughness decreased from 4.53 µm to 3.53 µm and further decreased to 2.3 µm as the cutting speed increased to 250 m/min. The factor most affecting surface roughness is the cutting speed followed by feed rate. depth of cut has the least effect on the surface roughness.

4.4.2.3 Analysis of Signal-to-noise ratio (S/N)

The S/N approach, like the mean, can be used to identify the factors which influence the response effectively as well as the optimum set of parameters. This S/N has been applied in the Taguchi approach The Response Table for S/N Ratios with Smaller-the-Better Control Factor Characteristics is shown in Table 4.14. The main effect plot for the response table is depicted in Figure 4.17.

Table 4. 14 Response Table For S/N Smaller is Better for Surface Roughness

Level	Cutting speed	Depth of cut	Feed
1	-11.678	**-7.541**	**-6.689**
2	-7.219	-9.003	-7.217
3	**-5.450**	-7.803	-10.441
Delta	6.229	1.461	3.752
Rank	1	3	2

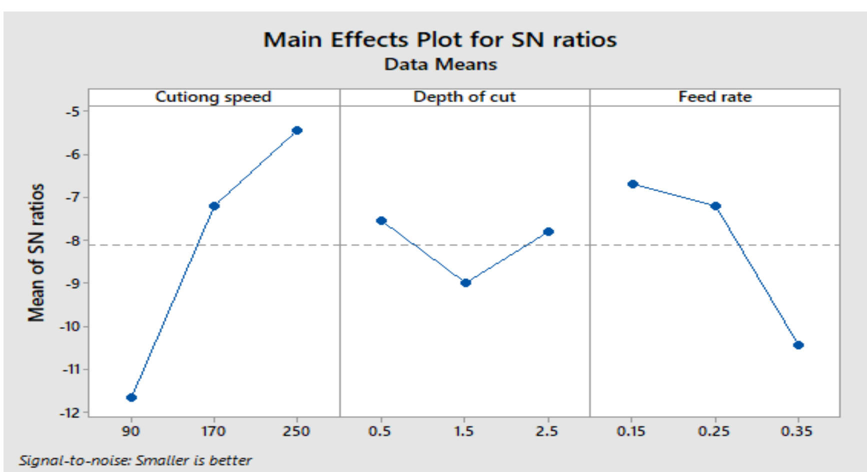

Figure 4. 17 Main Effects Plot for SN Ratios

The best control factor settings for reducing surface roughness can be easily identified from this graph. The highest S/N ratio point on the main effect plot served as the benchmark for determining the optimal level for each control factor. According to the graph, the optimum surface roughness value is given by factors A (Level 3, S/N = -5.450), B (Level 1, S/N = -7.541), and C (Level 1, S/N = -6.689), which correspond to a combination of a higher cutting speed, a lower cut, and a lower feed. Cutting speed has a greater impact on surface roughness than any other factor, as shown by the main effect plot for signal-to-noise (S/N) ratios (Delta = 6.229, Rank = 1). The depth of cut (Delta = 1.461, Rank = 3) had the least impact on the surface roughness of the material.

4.4.2.4 Prediction of Performance at Optimal Levels of Mean and S/N Result

Equation 4.4 of the linear regression model was used to predict the optimum response using Taguchi: The optimum level of the factor combinations for surface roughness value is **A3B1C1**.

$$y_{opt} = \mathrm{m} + (\mathrm{m}A_3 - \mathrm{m}) + (\mathrm{m}B_1 - \mathrm{m}) + (\mathrm{m}C_1 - \mathrm{m}) \tag{4.4}$$

$$y_{opt} = \mathrm{m}A_3 + \mathrm{m}B_1 + \mathrm{m}C_1 - 2\mathrm{m}$$

Where, (mA3, mB1, mC1) represent the optimum level average values of Mean and S/N of surface roughness and m is the average of all of the surface roughness values obtained from Table 4.10.

$$y_{opt} = 2.73 + (1.892 - 2.73) + (2.45 - 2.73) + (2.258 - 2.73)$$

y_{opt}= 1.1496 µm (predicted mean value for surface roughness)

Then S/N was also obtained;

y_{opt}= -1.21 (predicted S/N value for surface roughness)

Predicted Optimum Mean and S/N For Surface Roughness are shown in Table 4.15

Table 4. 15 Predicted Optimum Mean and S/N For Surface Roughness

Response	Optimal parameter	Predicted value	
Surface Roughness (µm)	**A3B1C1**	Mean	S/N
		1.150 µm	-1.21

4.4.3 Comparison

In this part, the predicted and experimental outcome for each parameter combination in the orthogonal array and the optimal result will be compared.

4.4.3.1 Confirmation tests

Verifying the predicted outcome versus the experimental result is the last step after obtaining the optimum combination of process parameters and their levels.

Table 4. 16 Predicted Values and Confirmation Test Results

Response	Level	Experimental				Pred.	Error (%)
		Meas.1	Meas.2	Meas.3	mean		
Surface roughness Ra (μm)	A3B1C1 (optimum)	1.19	1.23	1.22	1.21	1.15	4.96
	A3B2C1 (Random)	1.63	1.65	1.67	1.65	1.71	3.55

There is no need for a confirmation test if the optimum set of parameters and their values coincides with one of the trials in the orthogonal array. If not, a confirmatory test is required. Therefore, a confirmation test was needed in this study since the orthogonal array design experiment did not correspond to the best set of parameters and their levels (A3B1C1).

Table 4. 17 Comparison of all Predicted Results and Experimental Results

Exp. No.	A Cutting speed (m/min)	B Depth of cut (mm)	C Feed (mm/rev)	Comparison of the experimental predicted value of surface roughness		
				Experimental Mean value (μm)	predicted	Error (%)
1	90	0.5	0.15	3.24	3.13	3.41
2	90	1.5	0.25	3.85	3.89	1.17
3	90	2.5	0.35	4.53	4.59	1.37
4	170	0.5	0.25	1.82	1.87	3.03
5	170	1.5	0.35	3.53	3.42	3.03
6	170	2.5	0.15	1.89	1.93	2.39
7	250	0.5	0.35	2.30	2.34	1.96
8	250	1.5	0.15	1.65	1.71	3.55
9	250	2.5	0.25	1.73	1.62	6.19

Table 4.16 compares results from the confirmation experiment and prediction. The relative error between the predicted and confirmed experiment at the optimum condition is found to be 4.96 %.

This implies the predicted result is in good agreement with the experimental result. The results obtained from all experimental runs and predicted values were compared in Table 4.17. Relative percentage error was calculated using equation 4.3.

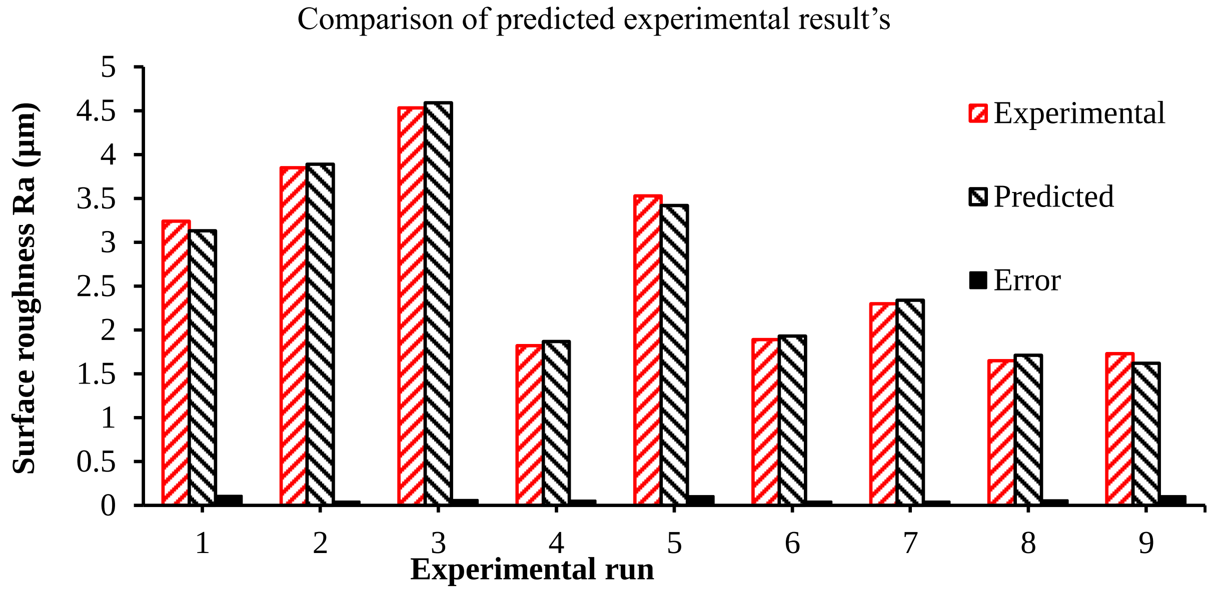

Figure 4. 18 Comparison of the Experimental and Predicted Results

The average relative error of the experimental and predicted results for surface roughness is displayed in the Table. The graphical comparison of the surface roughness results from the experimental and predicted methodologies is shown in Figure 4.18. From the figure, the average of all relative errors is found to be 2.9 % for surface roughness. Therefore, it can be concluded that the predicted results are in good agreement with the experimental result.

4.5 Analysis of Tool Temperature

The heat was produced during dry machining as a result of friction during the tool-to-work interaction (Kumar et al., 2017). The kind of material being machined and the cutting parameters employed affect how much heat is produced. Cutting tools experience friction throughout the cutting process, which causes a temperature increase then leads to decreased precision and poor surface roughness (San-Juan et al., 2015). In addition to this, the consequences of allowing temperatures to rise to high levels in cutting leads tool wear to accelerate, causing dimensional changes in the workpiece (reducing dimensional accuracy), and inducing thermal damage and metallurgical changes to the machined surface. Thus, the machining temperature must be reduced.

The heat was produced by friction forces at the tool to workpiece interface during the dry turning of AISI 1030 steel using a tungsten tool, according to observations and measurements made during the process. Figure 4.19 displays the measurement of tool temperature at 170 m/min cutting speed, 0.5 depth of cut, and 0.25 mm/rev feed Using a digital thermometer.

Figure 4. 19 Tool Temperature at 170 m/min, 0.5 mm, And 0.25 mm/rev.

Table 4. 18 Experimental Results of Tool Temperature

Experimental result					
Exp. No.	A Cutting speed (m/min)	B Depth of cut (mm)	C Feed (mm/rev)	Max. Temp. (^{0}C)	$^S/_{N_L}$
1	90	0.5	0.15	78.5	-37.89
2	90	1.5	0.25	83.0	-38.38
3	90	2.5	0.35	102.0	-40.17
4	170	0.5	0.25	104.5	-40.38
5	170	1.5	0.35	115.9	-41.28
6	170	2.5	0.15	121.3	-41.67
7	250	0.5	0.35	134.7	-42.58
8	250	1.5	0.15	139.1	-42.86
9	250	2.5	0.25	148.7	-43.44
Average				114.19	-41.19

Table 4.18 records the value of tool temperature for various cutting parameters during the dry-turning operation and is shown in Figure 4.20. The tool temperature readings were taken at maximum values, as shown in Table 4.18. The highest temperature 148.7^{0}C occurs at a high cutting speed of (250 m/min), a medium feed rate of 0.05mm/rev, and a high depth of cut. The minimal cutting temperature of 78.5^{0}C was attained at a low cutting speed. (90 m/min). Consequently, the increase in cutting speed causes the tool temperature to grow.

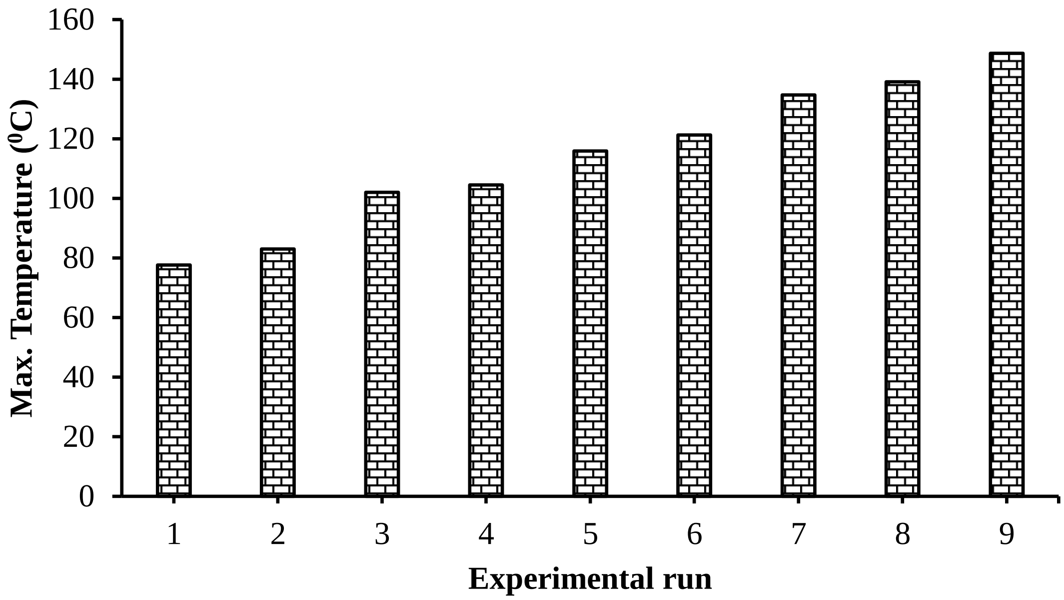

Figure 4. 20 Experimental Results of Tool Temperature

4.5.1 ANOVA For Tool Temperature

The statistical ANOVA tables for tool temperature are shown in Table 4.19. From the ANOVA tables, it is noted that the cutting speed is the most dominant factor which affects the tool temperature. Depth of cut is the next most dominant factor. As shown in Figure 4.21, the contributions of the A, B, and C factors to the tool temperature were found to be 88.05%, 10.68%, and 1.11%, respectively.

Thus, the most important factor affecting the tool temperature was cutting speed (factor A, 88.05%), followed by the depth of cut (Factor B, 10.68%). The contribution of error was considerably lower at 0.15%. Based on the relative motion between the tool and workpiece, the tool, workpiece surface integrity, and machining precision are all directly impacted by the cutting temperature (Ming et al., 2003). On the other hand, cutting forces, tool-to-chip contact length, and friction between the tool and the work material all have an impact on the temperature in the cutting zone (Ejieji et al., 2018). The combination of the tool and the work material, the cutting tool's geometry, chip control, and the magnitude and direction of the cutting force all affect the quality of the machined surface and the optimum cutting temperature.

Table 4. 19 Analysis of Variance for Means of Tool Temperature

Source	DF	SST	SSTR	MSE	F	P	Percent contribution P (%)	Significance (α=0.05)
Cutting speed	2	4261.50	4261.50	2130.75	586.8	0.002	88.05	Highly Significant
Depth of cut	2	516.94	516.94	258.47	71.18	0.014	10.68	Significant
Feed	2	53.93	53.93	26.96	7.43	0.119	1.11	Less Significant
Residual Error	2	7.26	7.26	3.63			0.15	
Total	8	4839.63					100%	

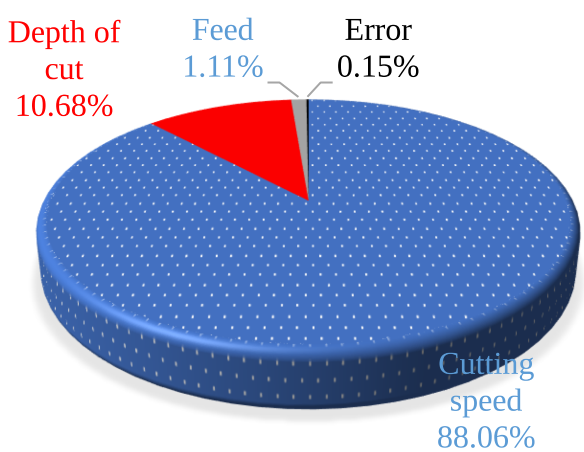

Figure 4. 21 Contribution of Cutting Parameters on Tool Temperature

4.5.2 Optimization of Cutting Parameters

The effect of cutting parameters on the tool temperature of the machined product and the optimum parameter combination was described as follows.

4.5.2.1 Analysis of mean

For each factor, such as cutting speed, depth of cut, and feed rate, average mean values of tool temperature generated on the tool during dry turning of AISI 1030 steel were calculated using

Minitab 18 software, and the results are shown in Table 4.20. As shown in the table, cutting speed with a delta of 53.30, was a significant difference from other factors in determining the average tool temperature generated throughout the turning process. Tool temperature increases significantly as cutting speed is increased.

Table 4. 20 Response Table for Means of Tool Temperature

Level	Cutting speed	Depth of cut	Feed
1	**87.83**	**105.90**	112.97
2	113.90	112.67	**112.07**
3	140.83	124.00	117.53
Delta	53.00	18.40	5.47
Rank	1	2	3

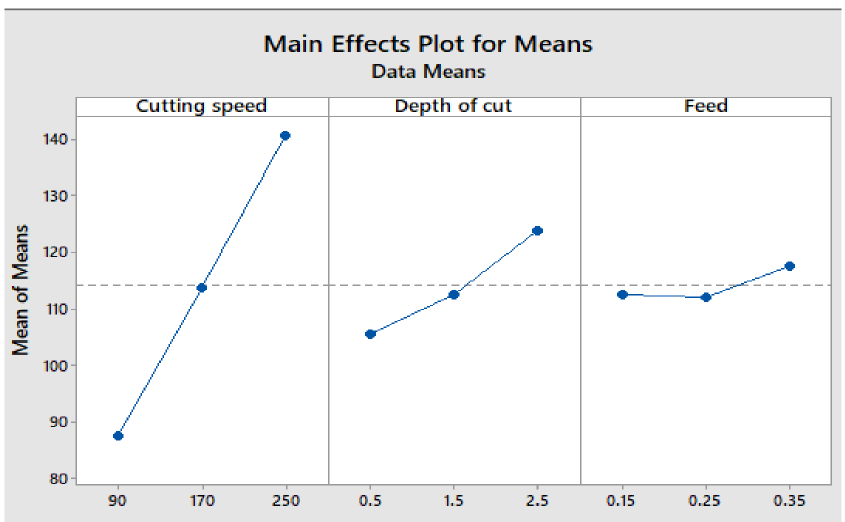

Figure 4. 22 Main Effects Plot for Means of Tool Temperature

The rate at which energy is lost through plastic deformation and friction increases as the cutting speed is increased (Gopal, 2021). Consequently, a high cutting temperature is the result of an increase in the rate of heat generation in the cutting zone. Increasing cutting speed accelerates tool wear by raising the cutting temperature to a point where automatic material diffusion between the tool and workpiece material occurs. The ANOVA Table 4.19 findings confirmed this. With a delta of 18.40, the depth of cut is ranked second in part of its impact on the temperature produced at the tool. Reduced cutting zone temperature is one of the most important factors in achieving optimized outputs in machining processes (Masoudi et al., 2017). When cutting speed and depth of cut are at their lowest point, a minimal temperature was reached. The main effect plot for means of tool temperature is shown in Figure 4.22 In this situation, smaller values of temperature are preferable, and these values are obtained at lower levels of cutting speed, depth of cut, and medium feed rate. The Figure shows that the tool temperature steadily rises as cutting speed rises.

Factor A (Level 1, mean = **87.83**), Factor B (Level 1, mean **105.90**), and Factor C (Level 2, mean = **112.07**), or a lower cutting speed, lower depth of cut, and medium feed **A1B1C2** combination, were the factors with the levels and means that produced the optimum value. The optimum parameter setting and their values are displayed in Table 4.21. This indicates that the best tool temperature value was found at 90 m/min for the cutting speed (A1), 0.5 mm for the depth of cut (B1), and 0.25 mm/rev for the feed rate (C2).

Table 4. 21 Optimum Parameters Setting Levels and Their Values

Factors	Level selected	Value of level	Rank
Cutting speed	1	90 m/min	1
Depth of cut	1	0.5 mm	2
feed	2	0.25 mm/rev	3

4.5.2.2 Interaction Effect

In this section, the interaction effects of cutting parameters on tool temperature are presented. At different cutting speeds increasing the depth of cut results in an increase in the temperature of the cutting tool as shown in Figure 4.23. Keeping the cutting speed at 90 m/min and increasing the depth of cut from 0.5 to 1.5 mm causes the tool temperature to rise from 78.5 ^{0}C to 83.0 ^{0}C, reaching 102.0 ^{0}C when the depth of cut is 2.5 mm. The amount of workpiece material removed rises with cut depth. In turn, this causes the cutting temperature to rise. Less workpiece material sticks to the tool's flank at lesser depths of cut than at deeper depths of cut. Due to the workpiece material adhering to the tool flank, the temperature rises (Gopal, 2021). ANOVA Table 4.19 confirms the findings.

When the cutting speed is set to 170 m/min, the tool temperature gradually rises from 104.5 ^{0}C to 115.9 ^{0}C and 121.3 ^{0}C as the depth of cut rises from 0.5 mm to 1.5 mm and 2.5 mm, respectively.

Maintaining cutting speed at 250 m/min and increasing the depth of cut results in an increase in tool tip temperature from 134.7 ^{0}C to 139.1 ^{0}C and then to 148.7 ^{0}C. It can be concluded that increasing the cutting speed and depth of cut results in an increase in tool temperature.

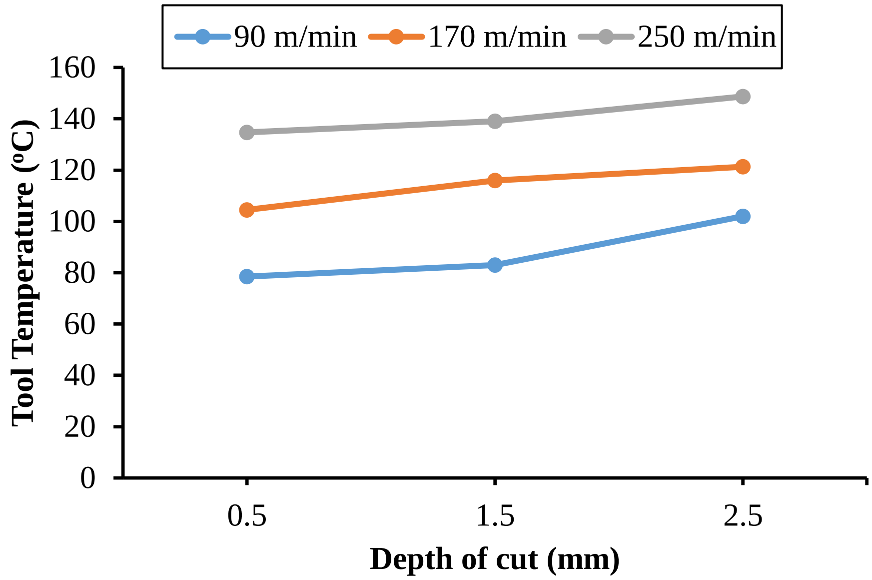

Figure 4. 23 Effect of depth of cut on tool temperature at different cutting speeds.

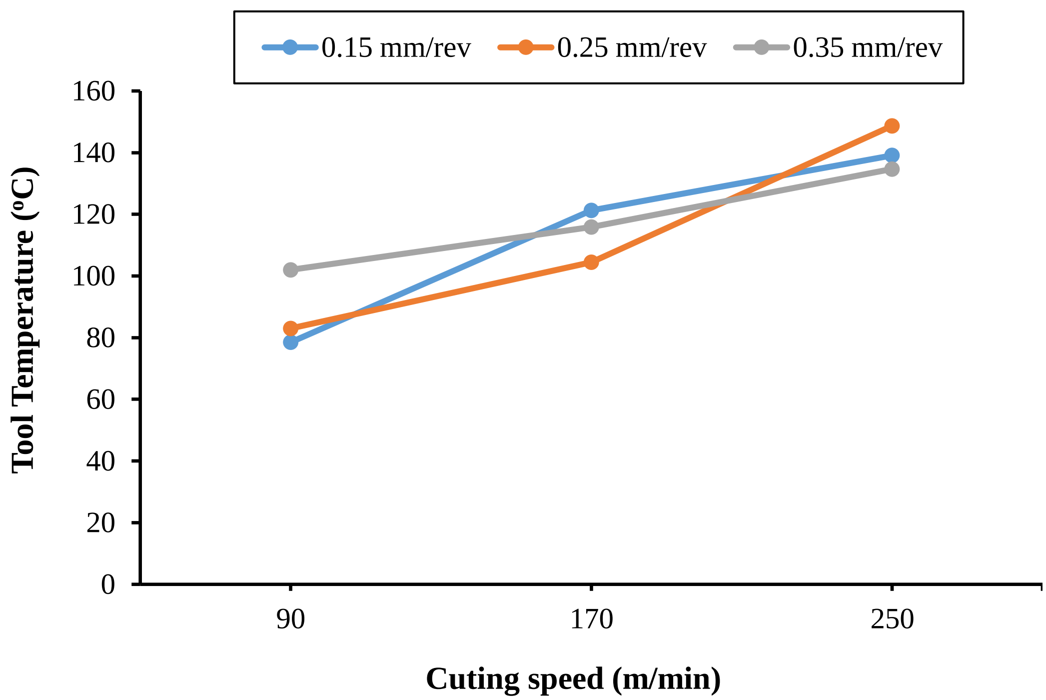

Figure 4. 24 Effect of cutting speed on tool temperature at different feed rates.

The impact of cutting speeds on the temperature of the cutting tool at various feed rates is also shown in Figure. 4.24. Keeping the feed rate at 0.15 mm/rev, the tool temperature rises from 78.5 ^{0}C to 121.3 ^{0}C when the cutting speed was increased from 90 m/min to 170 m/min, and it reached 139.1 ^{0}C when the cutting speed was increased to 250 m/min. The tool temperature increased from 83 °C to 104.5 °C when the feed rate was set to 0.25 mm/rev, then rises to 148.7 °C as the cutting speed increases from 90 to170m/min and then to 250 m/min, respectively. The tool temperature rises from 102 ^{0}C to 115.9^{0}C when the feed was at 0.35 mm/rev while increasing cutting speed from 90 m/min to 170 m/min. When the cutting speed was increased to 250 m/min, the temperature increased to 134.7 ^{0}C.

From the interaction effect of cutting speed and depth of cut Figure 4.25, it can be noted that lower tool temperature was obtained at lower cutting speeds for all given depths of cuts. It can be concluded that increasing cutting speed results in an increase in tool temperature. Figure 4.25's interaction plots make it clear that regardless of low level or high level when speed is combined with the depth of cut, the tool temperature rises. This agrees with the result obtained by Bhemuni et al., 2014.

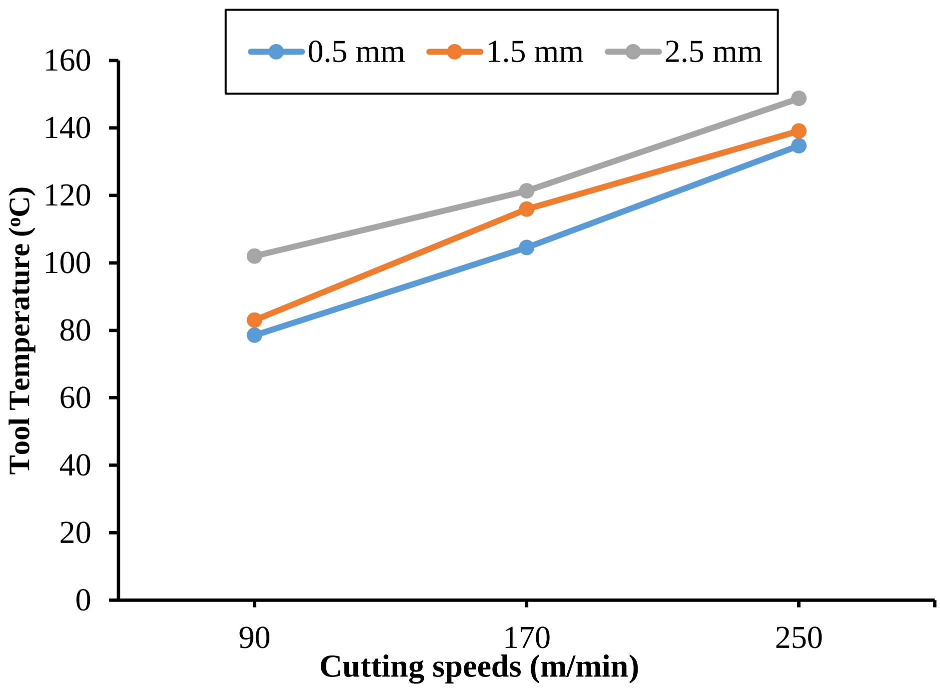

Figure 4. 25 Effect of cutting speed on tool temperature at different depth of cuts.

4.5.2.3 Analysis of S/N ratio for tool temperature

When comparing the level of the desired signal to the level of background noise, a signal-to-noise ratio is used. As a result, Taguchi S/N, which are log functions of the desired output, act as objective functions for optimization, helping in data analysis and predicting the optimal results. In the Taguchi method, response variation is studied with the help of S/N. Table 4.22 contains the S/N of tool temperature for each run of the experiment.

The highest S/N ratio point on the main effect plot Figure 4.26 served as the benchmark for determining the optimal level for each control factor. The graph revealed that factor A (Level 1, S/N = -38.78), factor B (Level 1, S/N = **-40.26**), and factor C (Level 2, S/N = **-40.74**), or a lower cutting speed, lower depth of cut, and medium feed **A1B1C2** combination, were the best combinations to minimize tool Temperature which is the optimum combination.

Table 4. 22 Response Table For S/N Smaller is Better for Tool Temperature

Level	Cutting speed	Depth of cut	Feed
1	**-38.78**	**-40.26**	-40.78
2	-41.11	-40.84	**-40.74**
3	-42.97	-41.77	-41.35
Delta	4.18	1.15	0.61
Rank	1	2	3

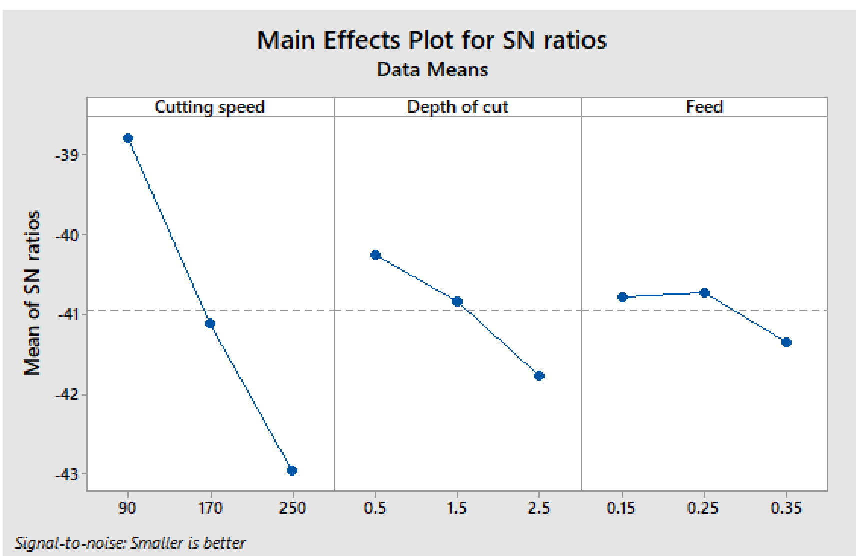

Figure 4. 26 Main effect plot for signal-to-noise ratio

4.5.2.4 Prediction of Performance at Optimal Levels of Mean and S/N Result

For predicting the optimum response using Taguchi, linear regression equation 4.5 was used: **A1B1C2** is the optimum levels combination of the factors for tool temperature value.

$$y_{opt} = \mathrm{m} + (\mathrm{m}A_1 - \mathrm{m}) + (\mathrm{m}B_1 - \mathrm{m}) + (\mathrm{m}C_2 - \mathrm{m}) \tag{4.5}$$

$$y_{opt} = \mathrm{m}A_1 + \mathrm{m}B_1 + \mathrm{m}C_2 - 2\mathrm{m}$$

Where, (mA1, mB1, mC2) represent the optimum level average values of Mean and S/N of tool temperature and m is the average of all of the tool temperature values obtained from the study (Table 4.18).

$$y_{opt} = 87.83 + 105.9 + 112.07 - 2(114.19)$$

y_{opt}= 77.42 ^{0}C (predict the mean value for tool temperature)

Then S/N was also obtained;

$$y_{opt} = (-38.78 - 40.26 - 40.76) - 2(-41.19)$$

y_{opt}= -37.4 (predict S/N value for tool temperature)

Predicted Optimum Mean and S/N For Tool Temperature are shown in Table 4.23

Table 4. 23 Predicted Optimum Mean and S/N For Tool Temperature

Response	Optimal parameter	Predicted value	
Tool Temperature (^{0}C)	**A1B1C2**	Mean	S/N
		77.42^{0}C	-37.4

4.5.3 Simulation Result of Tool Temperature

Due to significant cost savings and insights into the process that are not easily measured in experiments, modelling the 3D cutting process using finite element techniques is an area of ongoing research. In particular, heat transfer and the modelling of the cutting process require careful consideration in any modelling activity.

Finite element analysis software Deform 3D is used to simulate the turning process for all of the experimental runs presented in Table 3.5 that demonstrate the impacts of cutting speed, depth of cut, and feed rate on the temperature behaviour of the AISI 1030 type of steel. The workpiece is modelled as an elastic-plastic material to simulate the thermal, elastic, and plastic effects. The short material length was chosen to save computational time without compromising the model integrity as heat generation in machining is confined to small areas around the cutting zone. The FEA simulation of the temperature of the turning process for experiment number 4 at 170 m/min cutting speed, 0.5 mm depth of cut, and 0.25 mm/rev feed with the help of DEFORM 3D is shown in Figure 4.27. Table 4.24 shows the values of tool temperature for each measurement and their S/N ratios. Theaverage values of the tool temperature for mean and S/N ratio were calculated to be 121.16 ^{0}C and -41.33 ^{0}C respectively.

Table 4. 24 Simulation Results of Tool Temperature

Simulation result					
Exp. No.	A Cutting speed (m/min)	B Depth of cut (mm)	C Feed (mm/rev)	Max. Temp. (^{0}C)	S/N_L
1	90	0.5	0.15	67.77	-36.62
2	90	1.5	0.25	81.50	-38.22
3	90	2.5	0.35	92.10	-39.29
4	170	0.5	0.25	127.49	-42.02
5	170	1.5	0.35	130.24	-42.29
6	170	2.5	0.15	134.98	-42.61
7	250	0.5	0.35	136.36	-42.69
8	250	1.5	0.15	155.65	-43.84
9	250	2.5	0.25	165.67	-44.38
Average				121.16	-41.33

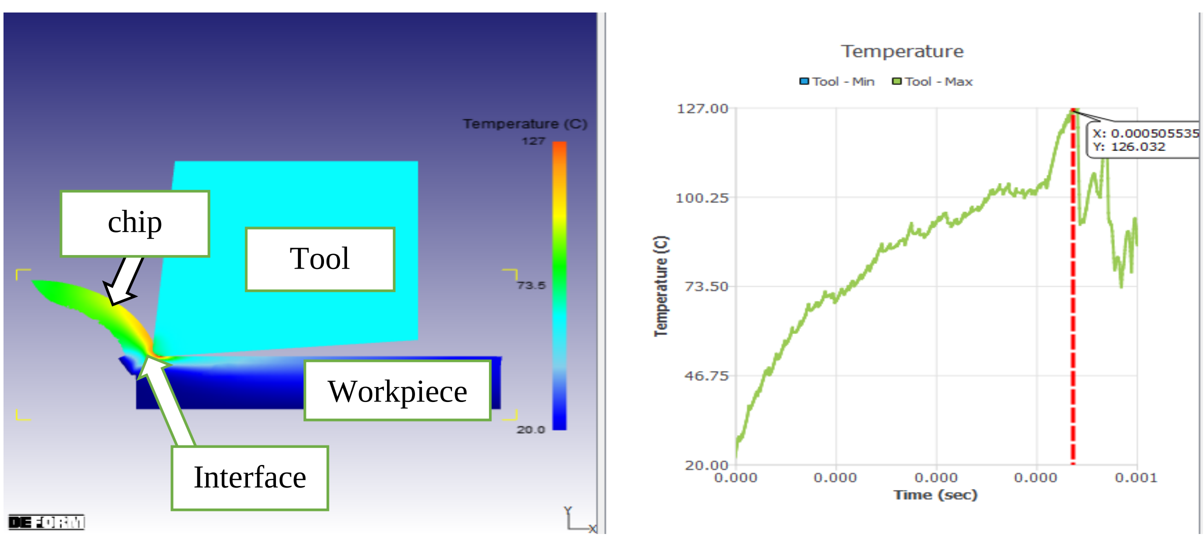

Figure 4. 27 Simulation Tool Temperature At 170 m/min, 0.5 mm, and 0.25 mm/rev

4.5.4 Comparison

A comparison of the tool temperature results obtained from the experiment, simulation, and prediction was done at its optimum and all its experimental runs.

4.5.4.1 Confirmation tests of optimum result

A confirmation experiment was conducted to validate the optimum result. Table 4.25 then presents the confirmation experiment for the optimum result and its comparison with the predicted and simulated result. In this comparison of optimum mean and S/N of confirmation experimental results with simulation, Taguchi, and regression results for tool temperature are shown.

Table 4. 25 Confirmation Result and its Comparison

Comparison						
Level	Confirmation Experimental Result of temp (^{0}C)		Taguchi method		Simulation	
			Pred.	Error (%)	Sim.	Error (%)
A1B1C2 (optimum)	Mean	77.6	77.42	0.23	80.31	3.49
	S/N	-37.79	-37.40	0.49	-38.09	0.79
A1B2C2 (Random)	Mean	83.00	84.10	1.33	81.50	1.81
	S/N	-38.38	-38.45	0.18	-38.22	0.42

The results of the simulation and predictions closely match the experiment. The error value was within acceptable bounds. As a result, the results of the validation tests show that optimization was successful.

4.5.4.2 Comparison of predicted, numerical and experimental results

The results obtained from simulation and prediction were compared with experimental results for all experimental runs and the relative percentage error was determined using equation (4.3).

Table 4.26 shows the comparison of experimental results with simulation and predicted results. The table displays the typical relative error between experimental data, simulation and predicted data on tool temperature. The comparison of the tool temperature findings from simulation, experiment, and predicted approaches is shown in Figure 4.28.

Table 4. 26 Comparison of Experimental Tool Temperature with Simulation and Predicted

Comparison of temperature (^{0}C)						
Exp. No.	Predicted			Simulation		Average Relative Error
	Experimental	predicted	Error (%)	simulation	Error (%)	
1	78.5	77.42	1.38	67.77	13.67	7.52
2	83.0	84.09	1.31	81.50	1.81	1.56
3	102.0	100.89	1.09	92.10	9.71	5.40
4	104.5	103.38	1.06	127.49	22.0	11.53
5	115.9	115.92	0.02	130.24	12.37	6.20
6	121.3	122.38	0.90	134.98	11.28	6.09
7	134.7	135.78	0.81	136.36	1.23	1.02
8	139.1	137.98	0.80	155.65	11.90	6.35
9	148.7	148.72	0.01	165.67	11.41	5.71

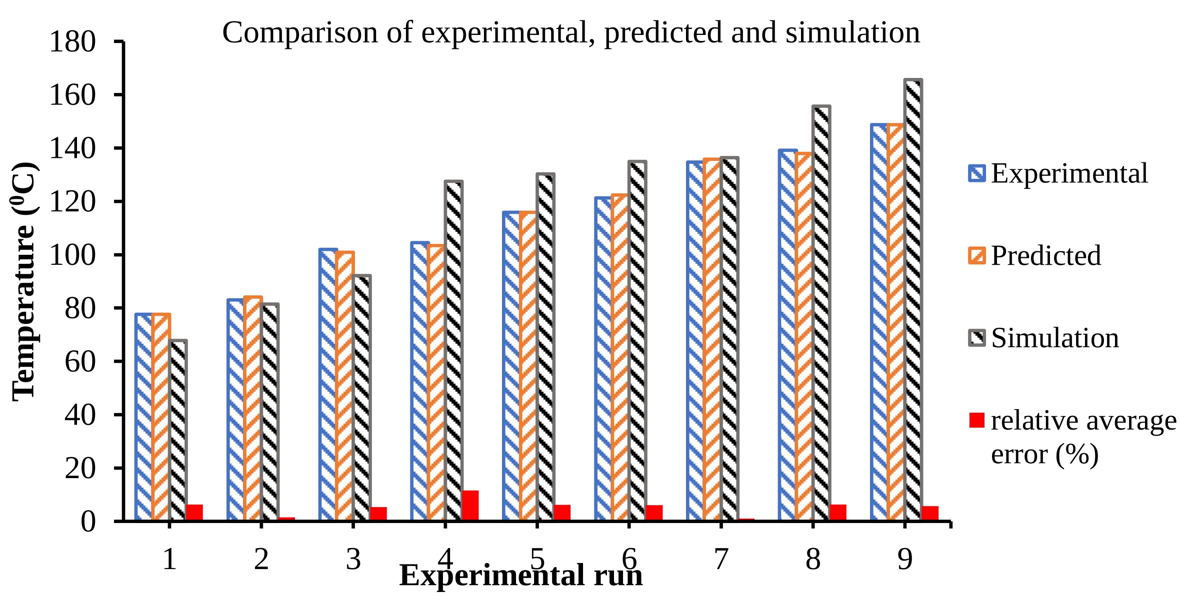

Figure 4. 28 Comparison of Simulation, Experimental and Predicted Results

For tool temperature, the average of all relative errors is found to be 5.71 %. As a result, it can be said that the temperature simulation of the turning process yields findings that are in a fair deal of agreement with the outputs of experiments, and that the predicted result was also quite near to the experimental.

4.6 Analysis of Tool Wear

In this part, the type of tool wear that occurs when dry-turning AISI 1030 steel has been researched and presented.

4.6.1 Experimental Result

Tool wear happens during the machining of materials as a result of the heat and friction produced between the cutting tool and the workpiece (Li et al., 2017). The two significant types of wear often experienced with the cutting tool are observed in this study, which is crater and flank wear.

The wear on the rake face brought on the friction between the tool's rake face and the workpiece or chip is known as crater wear. The tool's flank face and the machined surfaces come into contact and rub against one another, causing flank wear (Teng et al., 2018). The high temperature that is produced over the rake face as a result of the chip and tool insert movement starts to gradually wear away at the flank and rake faces (Jhodkar et al., 2018). As cutting temperature and force increase, the cutting tool softens which leads to the mechanisms that cause tool wear. The frictional force at the tool-work interface causes the cutting tool to endure significant mechanical stress as well as heat stress, which can lead to tool wear. Both tool wear morphology and tool wear amount are considered in this study.

4.6.1.1 Tool wear morphology

The wear of the coated tungsten carbide cutting tool insert that occurred in turning AISI 1030 steel was observed. The image of the cutting tool insert at the crater and flank face was observed and captured using an optical microscope at 20x magnifications.

At various cutting parameters and their combinations, the pattern of tool wear varies. This is because, depending on the parameter values, cutting speed, feed rate, and depth of cut produce variable wear patterns. Figure 4.29 depicts an optical image of the tool wear for experimental run number one at a cutting speed of 90 m/min, a cut depth of 0.5 mm, and a feed rate of 0.15 mm/rev. On the tool rake face and the flank face, abrasive and adhesive wear were the predominant wear mechanisms seen. The cutting tooltip has ridges, lines, or groove traces, as seen in Figure 4.29. These ridges or grooves are the characteristics of the abrasive wear mechanism and are caused by the movement of the hard materials in the workpiece against the cutting tool and impurities within the workpiece material.

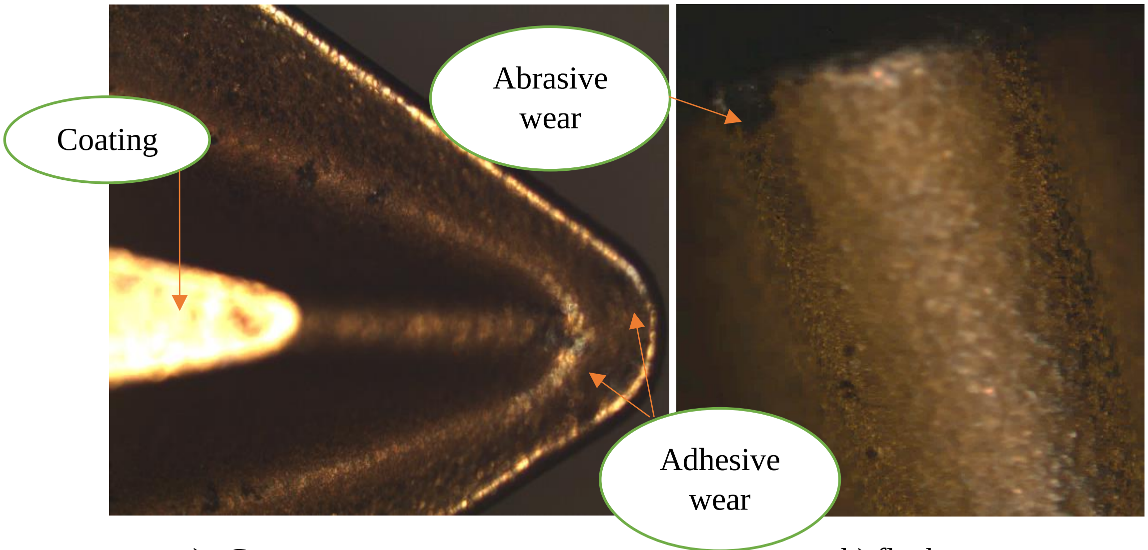

a) Crater wear b) flank wear

Figure 4. 29 Crater and Flank Wear at 90 m/min, 0.5 mm, and 0.15 mm/rev of (Exp.1)

The adhesive wear is due to the high temperature and pressure during cutting, which causes welding to occur between the clean fresh surface of the chip and the rake face.

Experiment 1 optical microscope image of tool wear showed that the tool experienced the lowest wear reported in this investigation. This lowest tool wear resulted in the lowest cutting temperature (78.5°C) which is the result of the lowest cutting speed. Thus, it is possible to conclude that low cutting temperatures increase the life of tools. Lower cutting forces and friction caused by cutting at a slower speed will result in less heat being produced.

An optical microscope view of the cutting tool from experiment number seven is shown in Figure 4.30. This indicates the wear micrographs at 250 m/min cutting speed, 0.5 depth of cut, and 0.35 mm/rev feed. The tool experienced the highest wear reported in this investigation during this run, which was produced due to the high temperature. The temperature for this experiment was 134.7 °C. The use of a high cutting speed has a significant negative impact on this wear. Due to the extreme heat created during machining, the crater and flank's face developed dark areas as shown in the images. Figure 4.30 depicts the formation of lines or groove markings in the cutting tooltip under an optical microscope at a 20X magnification. These groove markings are characteristics of the abrasive wear mechanism and are caused by the movement of the hard workpiece materials against the cutting tool. Additionally, significant mechanical and thermal stress is placed on the cutting tooltip as a result of friction at the tool-work interface, which can lead to tool wear.

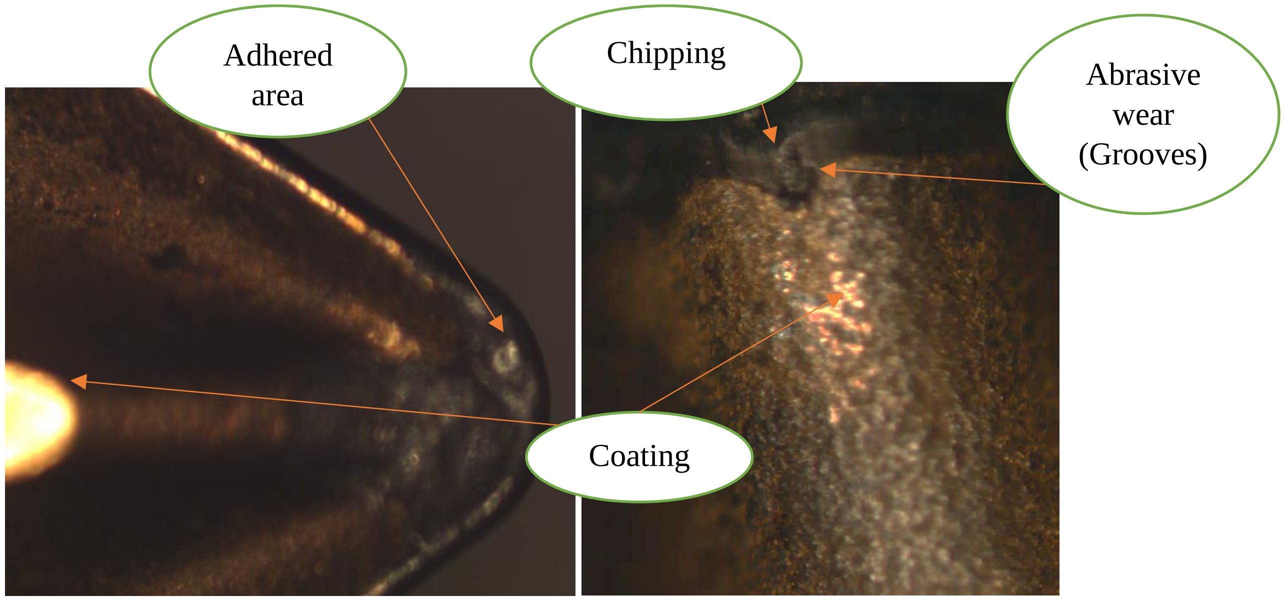

a) Crater wear   b) flank wear

Figure 4. 30 Crater and Flank Wear at 250 m/min, 0.5 mm, and 0.35 mm/rev (Exp. 7)

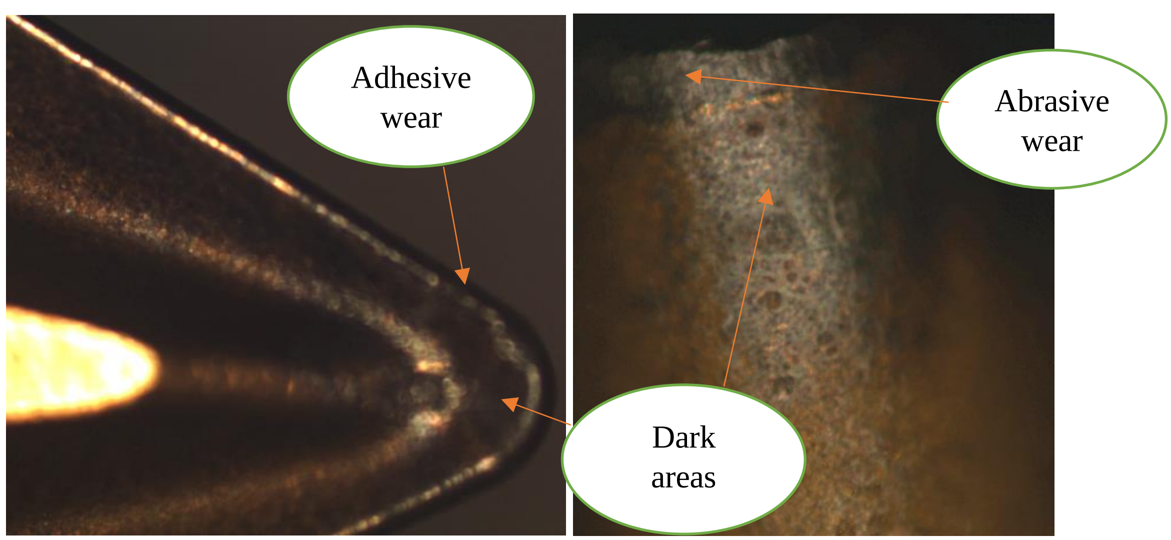

a) Crater wear   b) flank wear

Figure 4. 31 Crater and Flank Wear at 250 m/min, 2.5 mm, and 0.25 mm/rev (Exp. 9)

Due to the small chip–tool contact area during machining, high temperatures are concentrated at the tooltip, and hence, the adhesion between the tool and the workpiece can easily be enhanced. The wear morphologies of the cutting tool in this condition revealed an adhered chip on the cutting edge near the rake face and an abrasion in the flank face. In this experiment, the highest crater wear is observed at the nose. This leads one to the conclusion in this case that as cutting velocity increased, crater and flank wear also did so. In the flank, the rapid chipping action caused by high temperatures and a lack of lubrication was also observed. This also happened as a result of the chips twisting together, which raised the vibration intensity.

Figure 4.12 indicates the crater and flank wear of experimental run nine at 250 m/min cutting speed, 2.5 depth of cut, and 0.25 mm/rev feed. This result occurred at the highest tool temperature which is 148.7 °C and is the second largest wear faced in this investigation. abrasive wear and chipping are the wear mechanism observed. The dark areas observed are due to the effect of high temperature on the tool during turning. The analysis also reveals that the tool wear is concentrated in the nose region due to higher stress and material thermal softening brought on by the higher temperature in this area (Suresh, 2014)

Generally, from the lowest to highest wear observed in figures 4.29 to 4.31, the top rake face and the flank of a cutting tool are typically where the gradual wear occurs. As a result, crater wear and flank wear can be classified as two different types of tool wear. The crater can be measured either by its depth or its area. The width of the wear band is used to calculate flank wear. The rest of the experimental results of the tool wear micrographs are shown in between these minimum and maximum values (Appendix C). These experiments show that the flank face experiences higher wear depth, which significantly affects the tool. However, larger crater wear that covers a broader area was also observed in the rake face. As expected, and observed from the wear morphologies, the tool wear was highly influenced by the cutting speed. At high cutting speed, larger tool wear mechanisms were observed.

4.6.1.2 Wear amount (wear rate)

Equation 3.13 was used to determine the experimentally measured tool wear rates for each run. For instance, for an experiment run one as shown in Figure 4.32 the mass loss is obtained as;

The density of tool material is 0.01563 g/mm^3 (section 3.5.1)

$$\text{Tool wear rate} = \frac{55.5678\ g - 55.56.29\ g}{21\ s \times 0.01563\ g/mm^3} = 0.01494\ mm^3/s$$

Figure 4. 32 Weight Loss of Insert at 90 m/min, 0.5 mm, and 0.15 mm/rev (Exp. 1)

Table 4. 27 Experimental Results of Tool Wear Rate

Experimental result					
Exp. No.	A Cutting speed (m/min)	B Depth of cut (mm)	C Feed (mm/rev)	Tool wear rate (mm^3/s)	$^{S}/_{N_L}$
1	90	0.5	0.15	0.01494	36.51
2	90	1.5	0.25	0.06303	24.01
3	90	2.5	0.35	0.1169	18.64
4	170	0.5	0.25	0.1320	17.58
5	170	1.5	0.35	0.1865	14.58
6	170	2.5	0.15	0.1095	19.21
7	250	0.5	0.35	0.2972	10.54
8	250	1.5	0.15	0.1916	14.35
9	250	2.5	0.25	0.2374	12.49
Average				0.1498	18.66

The same way the results of the rest experiments are reported in Table 4.27 and are described in Figure 4.33. In Table 4.27 the mean and signal-to-noise ratio (S/N) for each run are also calculated.

Due to the high temperature experiment seven showed highest tool wear rate. Minimum tool wear was observed in experiment number one this is because of minimum temperature occurred in experiment one at lower cutting speed

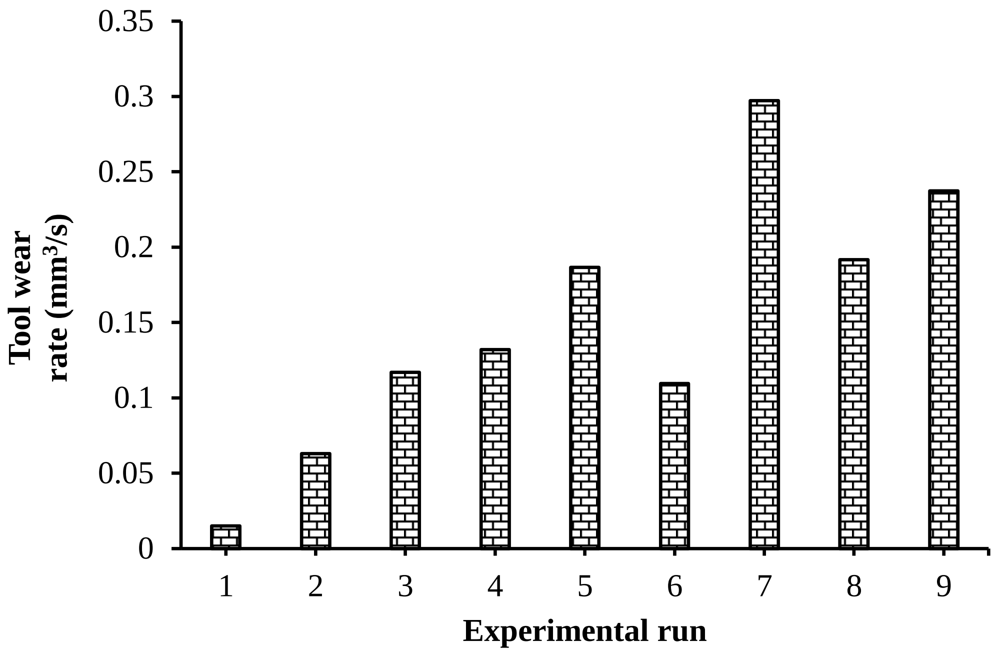

Figure 4. 33 Experimental Results of Tool Wear Rate

4.6.1.3. ANOVA for tool wear rate

The statistical ANOVA tables for tool wear rate are shown in Table 4.28. Cutting speed is the most important factor that influences the rate of tool wear, according to the ANOVA tables. The second most important component is the feed rate.

Table 4. 28 Analysis of Variance for Means

Source	DF	SST	SSTR	MSE	F	P	Percent contribution P (%)	Significance (α=0.05)
Cutting speed	2	0.0473	0.0473	0.0236	234.96	0.004	77.22	Highly Significant
Depth of cut	2	0.0001	0.0001	0.0001	0.50	0.666	0.16	Less Significant
Feed	2	0.0136	0.0136	0.0068	67.80	0.015	22.28	Significant
Residual Error	2	0.0002	0.0002	0.0001			0.33	
Total	8	0.0612					100%	

Figure 4.34 the percent contributions of the A, B, and C factors to the tool wear rate were found to be 77.22%, 0.16%, and 22.28%, respectively. An increase in the cutting speed of tungsten carbide-coated tools means an increase in wear rate. By increasing the temperatures in the cutting

area, an increase in cutting speed increases the thermal and mechanical loads, which accelerates the deformation of the cutting tools (Kıvak, 2014). Thus, the most important factor affecting the tool wear rate was cutting speed (factor A, 77.22%), followed by Feed (Factor C, 22.28%). The percent error was considerably lower at 0.33%.

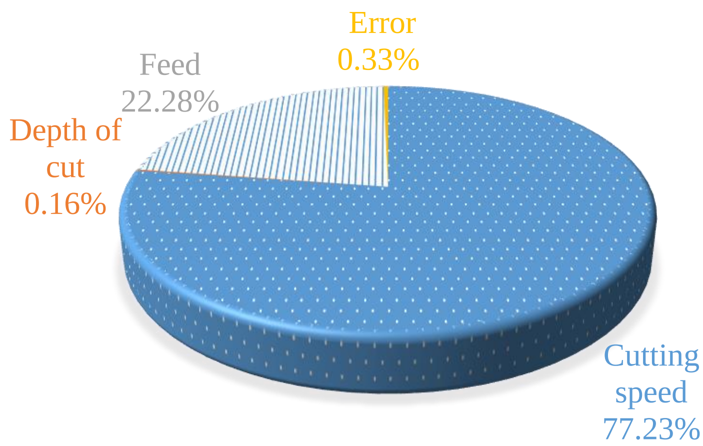

Figure 4. 34 Contribution of Cutting Parameters on Tool Wear Rate

4.3.1.4 Optimization of Cutting Parameters

The effect of cutting parameters on the tool wear rate and the optimum parameter combination was described as follows.

Analysis of mean

The average mean tool wear rate values for each factor, such as spindle speed, depth of cut, and feed rate, were determined using Minitab 17 software. The results are displayed in the response table for means Table 4.29. from the table Tool wear rate is primarily influenced by cutting speed (delta 0.177), then by feed rate (delta 0.09485). The rate at which a cutting tool wears out increases with increasing cutting speed and feed rate.

A minimum tool wear rate was obtained at the lowest spindle speed and feed. Figure. 4.35 displays the main effect plot for the means of wear rate. In this instance, lower levels of spindle speed, feed, and medium Depth of cut yielded lower values of tool war rate. The graph demonstrates how the tool wear rate increases with spindle speed. The factors with the levels and means that resulted in the lowest tool wear were Factor A (Level 1, mean = 0.06496), Factor B (Level 2, mean = 0.14704), and Factor C (Level 2, mean = 0.10535), or a lower cutting speed, medium depth of cut, and lower feed **A1B2C1** combination. Figure 4.35 shows that when turning AISI 1030 with coated tungsten tools, tool wear increased with increasing cutting speeds. High cutting speeds during the turning process have resulted in a high cutting temperature (Çelik et al., 2017). In addition, the tool wear rose as the feed rate and depth of cut increased. It is well known that as feed rate and cut depth rise, so do the pressures operating on the tool. Therefore, it is believed that increasing the feed rate, the depth of cut, and the cutting time will accelerate tool wear.

Table 4. 29 Response Table for Means of Tool Wear

Level	Cutting speed	Depth of cut	Feed
1	**0.06496**	0.14805	**0.10535**
2	0.14267	**0.14704**	0.14414
3	0.24207	0.15460	0.20020
Delta	0.17711	0.00756	0.09485
Rank	1	3	2

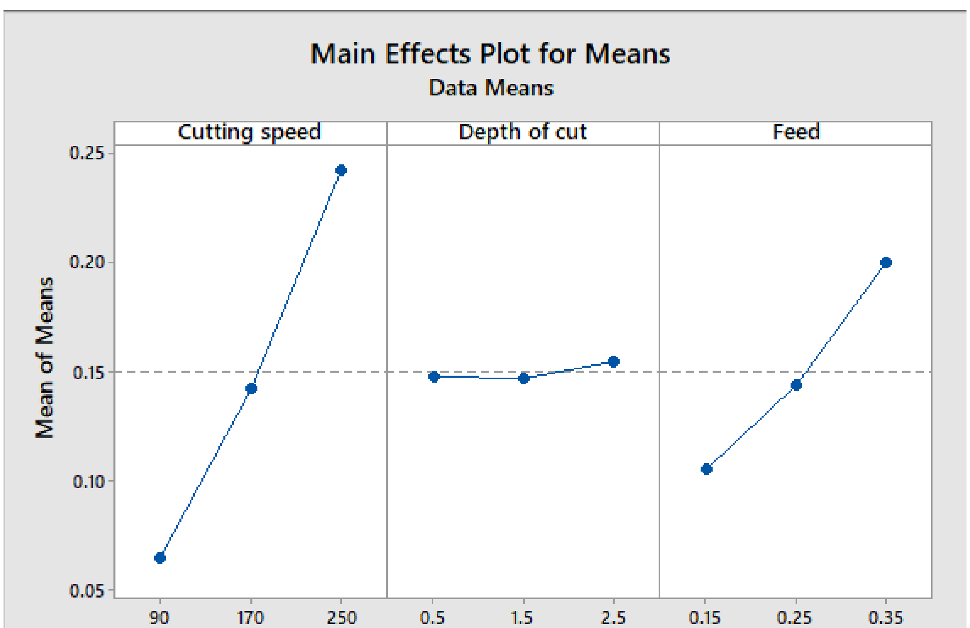

Figure 4. 35 Main Effects Plot for Means Tool Wear Rate

Interaction Effect

Figure 4.36 depicts the interaction effect of cutting speed and depth of cut on tool wear rate. When the depth of cut was 2.5 mm, the tool wear rate increases from 0.01494 mm^3/s to 0.132 mm^3/s as the cutting speed was increased from 90 to 170 m/min and further increased to 0.2972 mm^3/s as cutting speed increased to 250 m/min. When the depth of cut was set to 1.5 mm, the tool wear rate gradually rises from 0.06303 mm^3/s to 0.1865 mm^3/s as the cutting speed rises from 90 m/min to 170 m/min, and continue to rise to 0.1916 mm^3/s when the cutting speed rises to 250 m/min. Maintaining depth of cut at 2.5 mm and increasing the cutting speed from 90 to 170 m/min results in a decrease in wear rate from 0.1169 mm^3/s to 0.1095 mm^3/s then rises to 0.2374 mm^3/s when the cutting speed reaches 250 m/min.

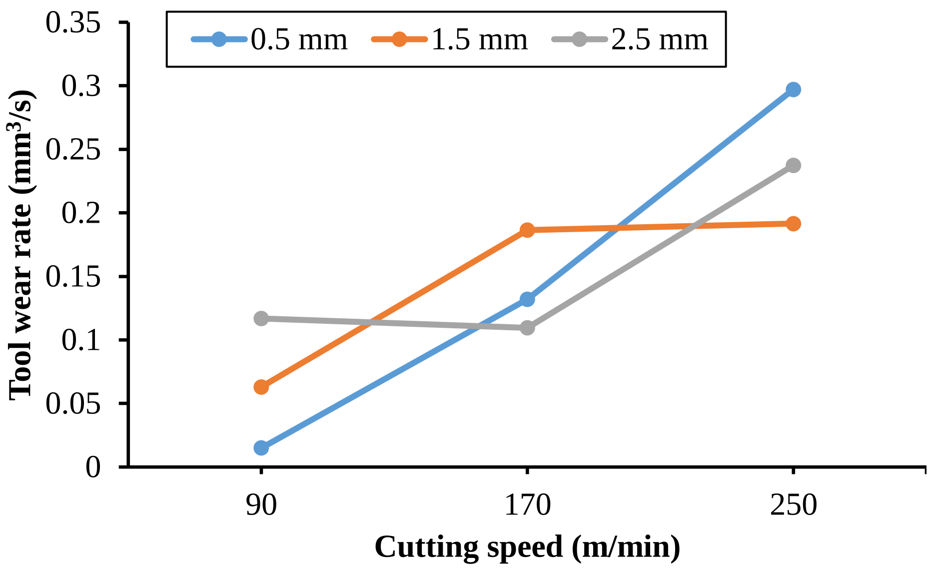

Figure 4. 36 Effect of cutting speed on tool wear rate at different depth of cut

The interaction effect of feed rate and cutting speed on tool wear rate is depicted in Figure 4.37. The rate of tool wear increases as the feed rate and cutting speed increase. When cutting speed is kept at 90 m/min, the tool wear rate increases from 0.01494 to 0.06303 and subsequently to 0.1169 mm^3/s as the feed rate increases from the lowest level to the maximum level. According to (Rashid et al., 2012), feed rate had an impact on the amount of wear. Increasing the feed rate from low to high causes the tool wear rate to steadily increase from 0.06303 to 0.2374 mm^3/s while the cutting speed is set to 170 m/min. The maximum cutting speed causes the tool wear rate to increase from 0.1169 to 0.292 mm^3/min. The result reveals that increasing the feed rate while keeping the cutting speed constant results in an increase in tool wear rate.

The interaction effect of cutting speed on tool wear rate at different feed rates is shown in Figure 4.38. The rate of tool wear increases from 0.01494 to 0.1916 mm^3/s when feed is held constant at

0.15 mm/rev while cutting speed is increased from a lower to a higher level. When the feed was changed to 0.25 and the cutting speed was raised from 90 to 170 and then to 250, the tool wear rate increased from 0.06303 to 0.132 and finally to 0.2374 mm^3/s.

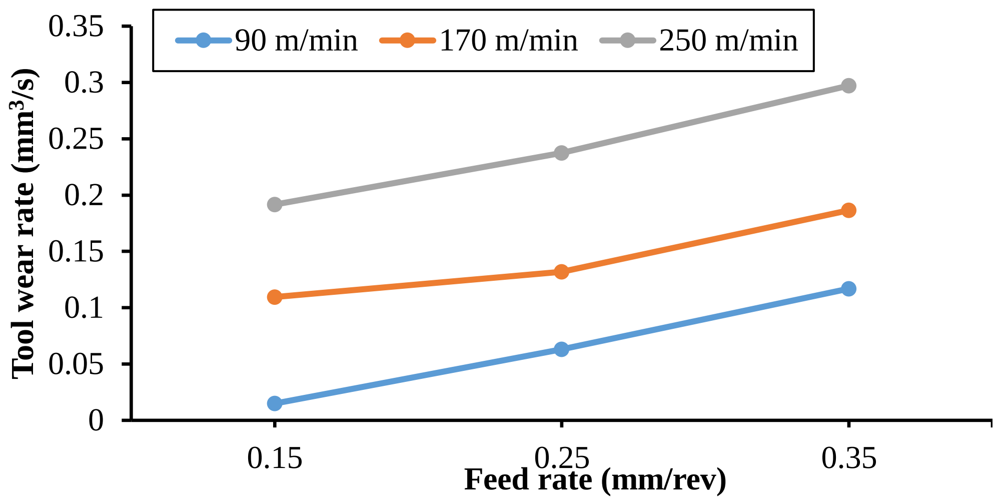

Figure 4. 37 Effect of feed rates on tool wear rate at different cutting speeds

When the feed rate is maintained at 0.35 mm/rev and the cutting speed is increased from the lowest to the highest setting, the tool wear rate rises from 0.1169 to 0.2972 mm^3/s. The coated layer on the tool face softens when the cutting temperature is particularly high as a result of the increased cutting speed and feed rate. In these circumstances, tool wear is accelerated and it is easily abraded by the hard particles of the workpiece material. Consequently, a coated tungsten carbide tool's life would eventually be reduced (Suresh & Basavarajappa, 2014).

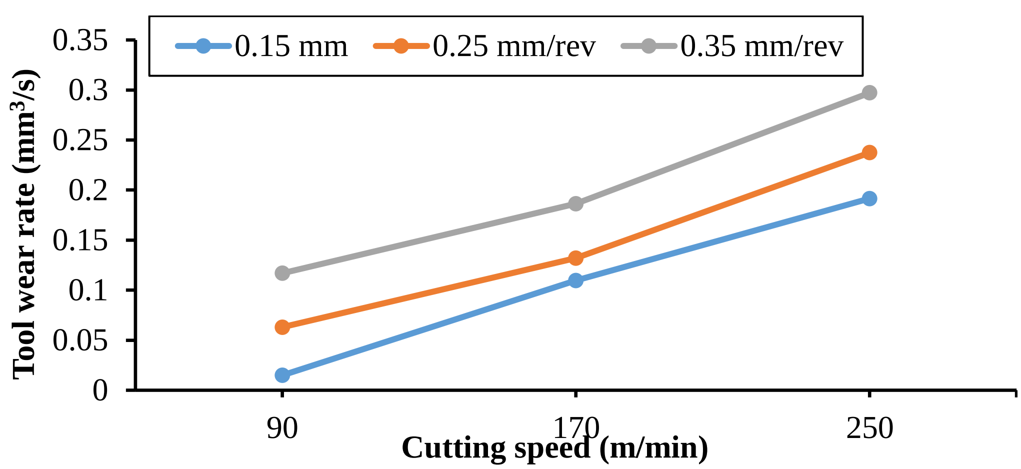

Figure 4. 38 Effect of cutting speeds on tool wear rate at different feed rates

Analysis of the S/N ratio for tool wear rate

When comparing the level of the desired signal to the level of background noise, a signal-to-noise ratio is used. Therefore, Taguchi S/N uses for optimization, helping in data analysis and predicting the optimal results. In the Taguchi method, response variation is studied with the help of S/N. Table 4.30 contains the S/N of the tool wear rate for each run of the experiment. The highest S/N ratio point on the main effect plot Figure 4.39 served as the benchmark for determining the optimal level for each control factor.

Table 4. 30 Response Table of Tool Wear Rate For S/N Smaller is Better

Level	Cutting speed	Depth of cut	Feed
1	**26.39**	**21.55**	**23.36**
2	17.13	17.65	18.03
3	12.46	16.78	14.59
Delta	13.93	4.76	8.77
Rank	1	3	2

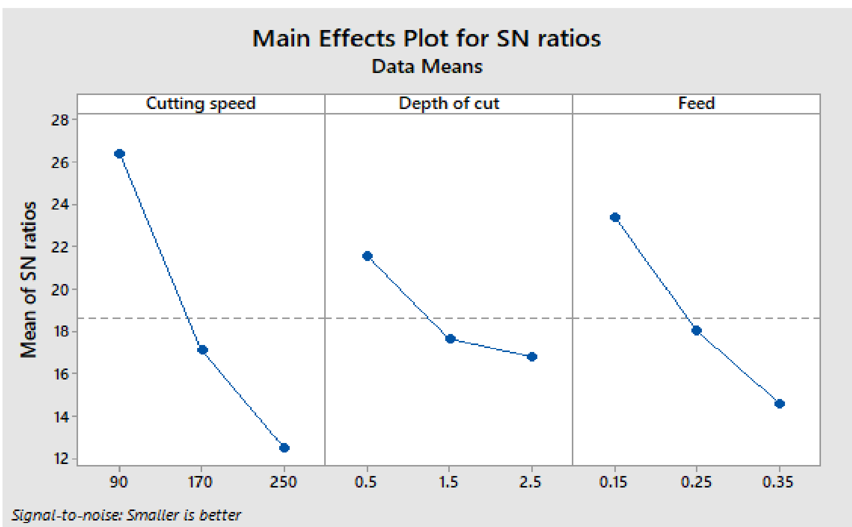

Figure 4. 39 Main Effect Plot for Signal-To-Noise Ratio

The graph revealed that factor A (Level 1, S/N = **26.39**), factor B (Level 1, S/N = **21.55**), and factor C (Level 1, S/N = **23.36**), or a lower cutting speed, lower depth of cut, and lower feed **A1B1C1** combination, were the best combinations to minimize tool wear rate. For optimization of cutting parameters using the Taguchi method, the S/N ratio approach is preferred. So, we can conclude that the optimum combination of cutting parameters that gives the minimum tool wear rate is the lowest level cutting speed (**A1=90 m/min),** lowest level depth of cut (**B1=0.5 mm**), and lowest level feed (**C1=0.15 mm/rev**). The optimum parameter setting and their values are displayed in Table 4.31.

Table 4. 31 Optimum Parameters Setting Levels and Their Values

Factors	Level selected	Value of level	The rank affecting the response
Cutting speed	1	90 m/min	1
Depth of cut	1	0.5 mm	3
feed	1	0.15 mm/rev	2

Prediction of Performance at Optimal Levels of Mean and S/N Result

Using Minitab 17 for predicting the optimum response of tool wear rate in the Taguchi method and obtaining the result in Table 4.32,

Table 4. 32 Predicted Optimum Mean And S/N For Tool Wear Rate

Response	Optimal parameter	Predicted value	
Tool wear rate (mm^3/s)	**A1B1C1**	Mean	S/N
		0.018557	33.97571

4.6.2 Tool Wear Simulation Result

Numerous techniques have been tested to predict the morphology and amount of tool wear. One of the strategies was the development of numerical wear models. When calculating wear rate, cutting parameters such as cutting speed, feed, and depth of cut were taken into account. The effect of the cutting parameters on tool wear rate is taken into account in a three-dimensional model. More meshes would help simulations run more accurately but take a lot of computing time. A medium quantity of mesh was chosen to balance the simulation's accuracy and time consumption.

4.6.2.1 Calibration of The Tool Wear Model

As shown in Figure 4.40, experiments and FEM chip formation simulations were used to calibrate the Usui wear model. On the one hand, experiments are done to measure the wear rate under various cutting conditions and cutting times. On the other hand, simulations using a validated model are carried out at various wear stages to determine values for the interface pressure σ, interface temperature T, and sliding velocity Vs. Both the experimental and simulation have identical input parameters. The Usui tool wears equation 3.16 constants A and B were found using a regression analysis that combines experimental and numerical results.

For the regression analysis, Equation 3.16 can be rewritten as

$$\left(\frac{dw}{\sigma\, V dt}\right) = A\ \exp\left(\frac{-B}{T}\right) \qquad (4.6)$$

By taking the logarithm of this expression, the following equation is obtained:

$$ln\left(\frac{dw}{\sigma\, V dt}\right) = \ln(A) - \left(B\frac{1}{T}\right) \qquad (4.7)$$

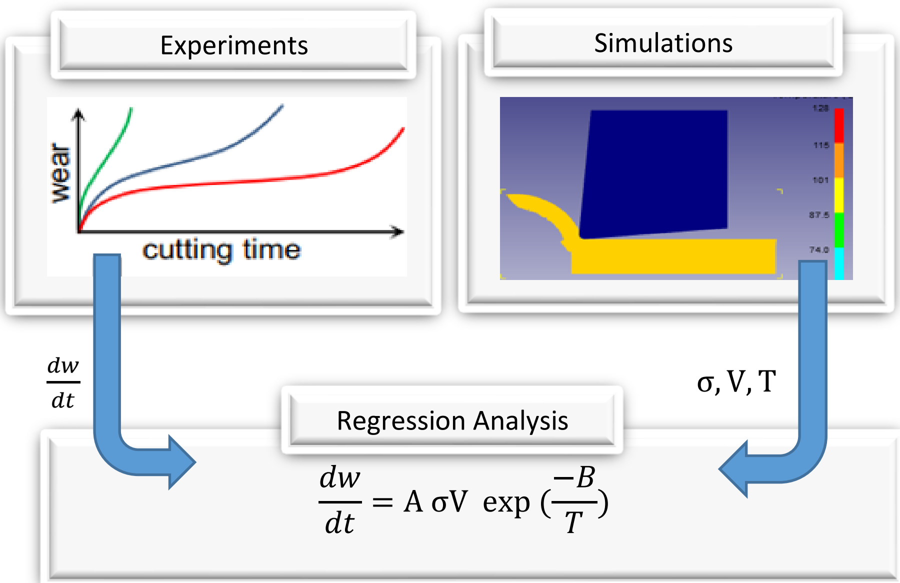

Figure 4. 40 Schematic Calibration Steps for Tool Wear Constants

A linear equation describes this expression. This linear equation's axis intercept produces the value ln (A). The slope of that equation yields the constant B. As shown in Figure 4.40., the models offer the contact pressure σ, temperature T, and sliding velocity Vs, whereas the measurements provide the wear rate. The simulation result for the regression analysis is shown in Figure 4.41.

Figure 4.42 then displays the regression outcome of the wear amount measurements utilized to calibrate constants A and B. From the regression plot Figure 4.43 the constants A and B are then obtained and the Usui tool wear equation. (3.16) can be rewritten as:

$$\left(\frac{dw}{\sigma\, V dt}\right) = 3.775 \times 10^{-11}\ \exp\left(\frac{-1200}{T}\right) \qquad (3.8)$$

The tool wear rate can now be calculated using this equation by obtaining $\sigma, V,$ and T from the simulation. For all of the provided experimental runs, deform 3D was utilized to simulate the turning process.

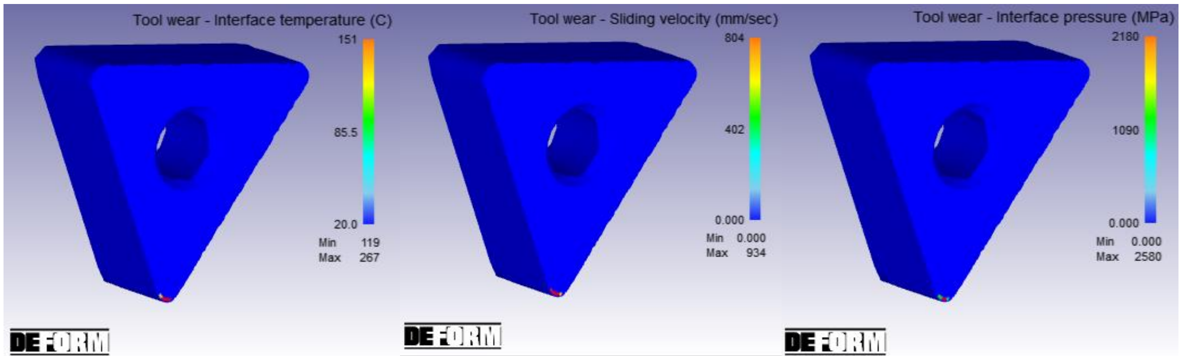

Figure 4. 41 3D Simulations Used for Model Calibration.

The simulation modelling used the same parameters as the experiment. Results of the tool wear simulation for the fifth experimental run at 170 m/min, 1.5 mm, and 0.35 mm/rev are shown in Figure.4.43 (see appendix C for the rest simulation results). Table 4.33 shows the simulation result of the tool wear rate for each run and their S/N ratios.

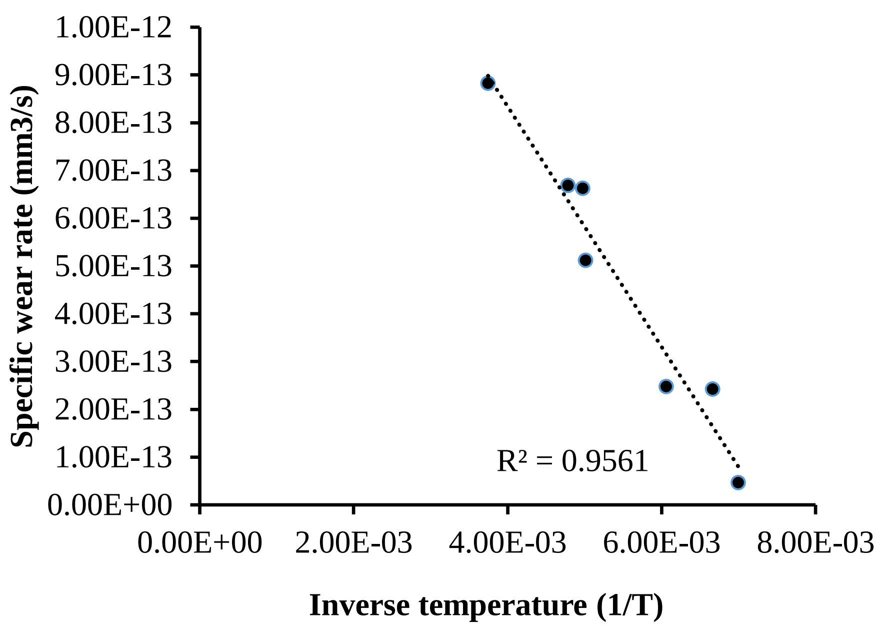

Figure 4. 42 Regression for Calibration of AISI1030 And Tungsten Carbide Tool.

From the table, the average values of the tool wear rate for mean and S/N ratio were obtained to b e 0.1537 mm^3/s and 18.41 respectively.

Table 4. 33 Simulation Results of Tool Wear Rate

Simulation result					
Exp. No.	A Cutting speed (m/min)	B Depth of cut (mm)	C Feed (mm/rev)	Tool wear rate (mm^3/s)	S/N_L
1	90	0.5	0.15	0.01559	36.14
2	90	1.5	0.25	0.0665	23.54
3	90	2.5	0.35	0.1040	19.66
4	170	0.5	0.25	0.1410	17.02
5	170	1.5	0.35	0.1710	15.34
6	170	2.5	0.15	0.1290	17.79
7	250	0.5	0.35	0.3066	10.27
8	250	1.5	0.15	0.2060	13.72
9	250	2.5	0.25	0.2440	12.25
Average				0.1537	18.41

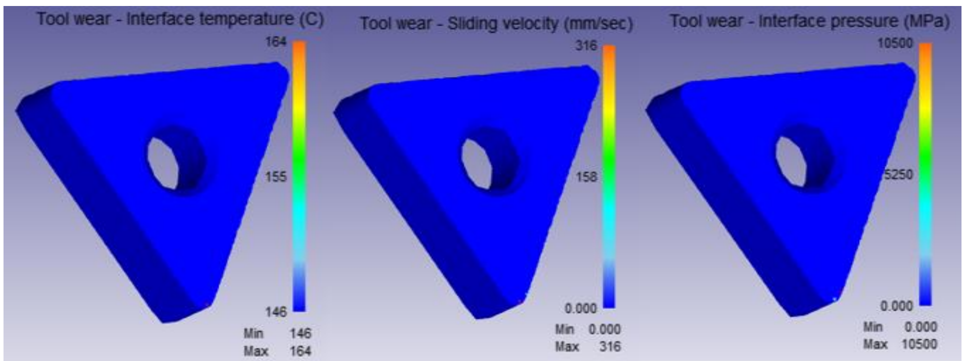

Figure 4. 43 Tool Wear Simulation At 170 m/min, 1.5 mm, And 0.35 mm/rev (EXP .5)

4.6.3 Comparison

The simulation result obtained for the optimum conditions and all runs were compared with the experimental result and discussed in this section.

4.6.3.1 Confirmation tests of optimum result

A confirmation experiment was conducted to validate the optimum result. The confirmation experiment for the optimum result and its comparison with the predicted and simulated result is then shown in Table 4.34. In this table, a comparison of the optimum mean and S/N of confirmation experimental results with simulation results for tool wear rate was done. The results of the simulation closely match those of the experiment. The error value was within acceptable bounds. As a result, the results of the validation tests show that optimization was successful.

Table 4. 34 Confirmation of Optimum Result for Tool Wear Rate

Level	Confirmation Experimental Result (mm^3/s)		Simulation	
			Sim.	Error (%)
A1B1C1 (optimum)	Mean	0.01494	0.01559	4.35
	S/N	36.51	36.14	1.004
A1B2C2 (Random)	Mean	0.06303	0.0665	5.51
	S/N	24.01	23.54	1.94

4.6.3.2 Comparison of numerical and experimental results

The results obtained from the simulation were compared with experimental results for all experimental runs and the relative percentage error was determined using equation 4.3. Table 4.35 shows the comparison of experimental results with simulation results. The table shows the typical relative error for tool wear rate between experimental data and simulation data.

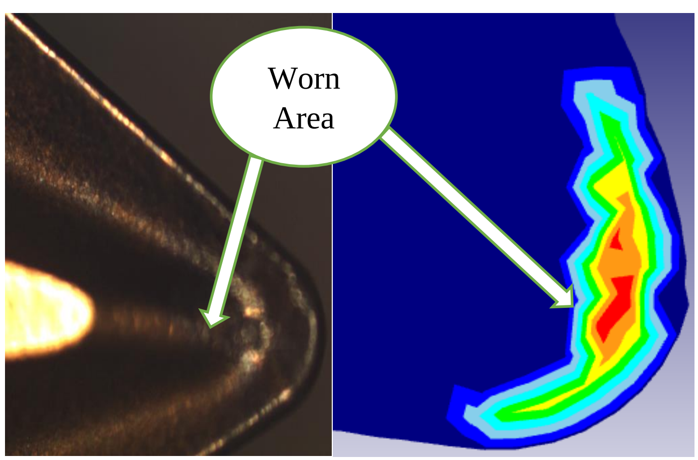

a) Experimental result b) simulation result

Figure 4. 44 Comparison of Crater Wear (Exp. 9)

Figure 4.44 compares the simulated output from DEFORM-3D at 250 m/min Cutting Speed, 2.5 mm Depth of Cut, and 0.25 mm/rev Feed to the experimental crater wear obtained using an optical microscope at the same cutting parameters. The Figure illustrates how the outcomes of the two approaches are comparable. The comparison of simulation and experiment demonstrates the created simulation model's applicability, allowing the impact of various process parameters on wear growth to be investigated. These results also validate Usui's wear model and the model parameters used for machining AISI 1030 steel alloy. The simulation results agreed well with the experimental results that tool wear is higher when cutting speed is increased, which leads to an increase in the cutting tool temperature in turn. This is because of material softening due to higher temperatures.

Figure 4.45 illustrates the comparison of the tool wear rate results from simulation and experiment approaches for all experimental runs. As a result, it can be said that the tool wear simulation of the turning process yields findings that are in a fair deal of agreement with the outputs of experiments.

Table 4. 35 Comparison of Experimental Result with Simulation Result

Exp. No.	Experimental tool wear rate (mm^3/s)	Comparison of experimental and simulation	
		simulation	Error (%)
1	0.01494	0.01559	4.35
2	0.06303	0.0665	5.51
3	0.1169	0.104	11.04
4	0.132	0.141	6.82
5	0.1865	0.171	8.31
6	0.1095	0.129	17.81
7	0.2972	0.3066	3.16
8	0.1916	0.206	7.52
9	0.2374	0.244	2.78

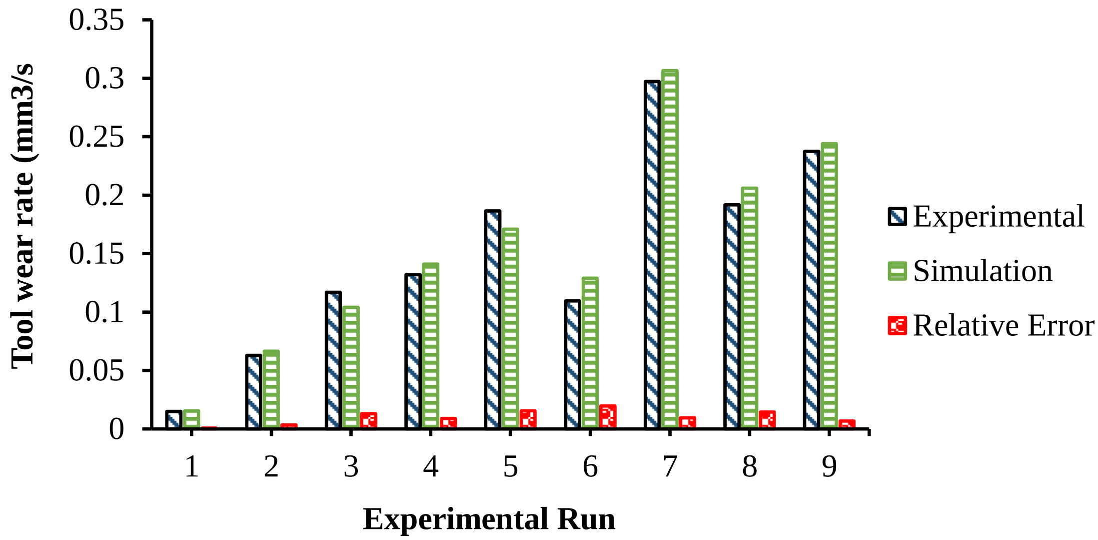

Figure 4. 45 Comparison of Simulation and Experimental Results

4.7 The Effect of Temperature on Tool Wear Rate

Heat is produced during machining operations as a result of friction between the cutting tool and the object being machined. Tool wear and the quality of the workpiece's surface are both significantly impacted by the heat generated in the cutting zone. Additionally, the thermal expansion of the work material leads to inaccurate work part dimensions and it can also produce hot chips that endanger the machine operator's safety. This section discusses the impact of tool temperature on tool wear rate when turning AISI 1030 steel under dry conditions. Tables 4.36 illustrate the relationship between tool temperature and tool wear rate. As is observed in Figure. 4.46, the tool wear rate increases as the tool temperature increases.

Table 4. 36 The Effect of Tool temperature on the Tool wear rate

Tool Temperature (^{0}C)	77.6	83	102	104.5	115.9	121.3	134.7	139.1	148.7
Tool wear rate (mm^3/s)	0.01559	0.0665	0.104	0.141	0.171	0.129	0.3066	0.206	0.244

The variables that influence tool temperature also have an impact on how quickly tools wear out. The primary factor that affects both the temperature of the cutting tool and the rate of tool wear is cutting speed. High cutting speeds cause the cutting temperature to rise, which causes tool wear, welding, adhesion, and BUE (Varghese et al., 2018). Therefore, parameters that produce a minimum temperature must be chosen to reduce the tool wear rate.

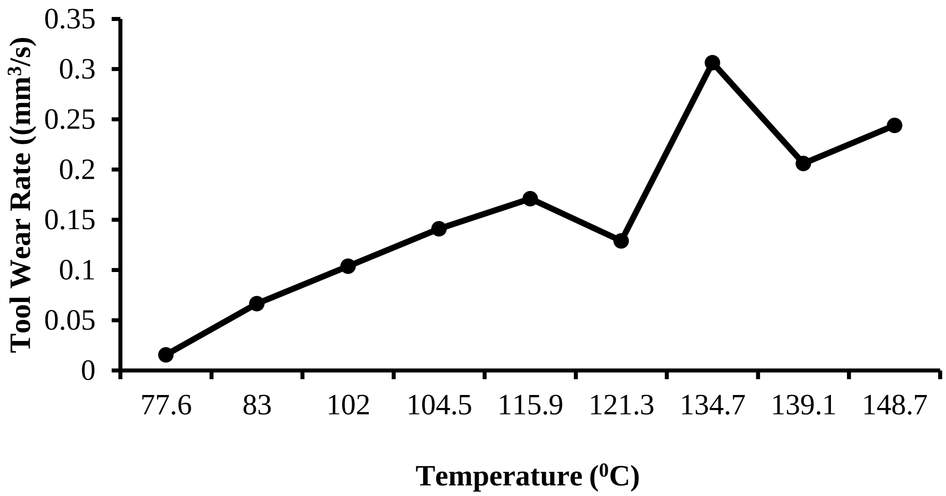

Figure 4. 46 Effect of Tool Temperature on The Tool Wear Rate

4.8 Chip Analysis

This section discussed the type of chip produced when turning AISI 1030 steel. A chip created during the turning process was gathered for each of the nine experiments during this experimental study. The kind of chip that had formed was determined once the chips had been gathered. Figure. 4.47 depicts photographic images of chips produced during the dry turning of AISI 1030 steel.

The types of chips formed in this study are classified as continuous chips, continuous chips with a built-up edge, and discontinuous chips. In experiment runs 6, 7, 8, and 9, as seen in Figure 4.47, a continuous chip was produced due to an increase in the cutting speed and increasing material ductility due to rising in temperature (Das et al, 2018). The chips are removed unbroken in a long string or bent into a tight coil. Continuous chip machining produces a high surface finish, low power consumption, steady cutting force, and low friction which extends tool life and for AISI 1030, it is preferred since it is fairly ductile. As shown in Figure 4.47, the chips took on a helical structure the same as stated by Das et al. (2018) as the feed and depth of cut were increased. In experiments 3, 4, and 5, it was produced similar to the continuous chip but with a built-up edge at the tool's nose, as shown in Figure 4.47. This is due to High friction at the tool face. A "built-up edge" is formed when the chip material attaches or welds to the cutting edge and tool face close to the nose at high temperatures and pressure. This built-up edge initially gives strength to the cutting edge. But as the cutting process goes on, the built-up edge gets bigger and the tool geometry is altered.

Figure 4. 47 Chip Formed During Turning AISI 1030 Steel Experiments

Adhesion wear may cause a portion of the tool to be lost. A built-up edge is undesirable because it results in poor surface finish, excessive power consumption, and shortened tool life. Figure 4.47 for experiment number 1 and 2 illustrates discontinuous chips. This is due to the low cutting speed and high friction. Discontinuous chips are the pieces of the plastically deformed workpiece that are either completely separate or loosely attached (they adhere to one another). The chip dissipates the majority of the heat produced, while the tool's edge has a lower temperature. However, a discontinuous chip results in a poor surface finish for ductile materials.

4.9 Grey Relational Analysis

The experimental data have been normalized which is grey relational generations for MRR, surface roughness, tool temperature, and tool wear rate using Equation 3.6 and presented in Table 4.37. Using Equation 3.6, the experimental data for MRR, surface roughness, tool temperature, and tool wear rate have been normalized, resulting in grey relational generations, and are shown in Table 4.37. Equation 3.8 has been used to calculate the grey relational coefficients from the normalized data set in Table 4.37.

Table 4. 37 Grey Relational Generation Values

EXP. No	Responses				Data normalization			
	MRR (mm^3/sec)	Ra (μm)	Temp (^{0}C)	Wear rate (mm^3/s)	MRR (mm^3/sec)	Ra (μm)	Temp (^{0}C)	Wear rate (mm^3/s)
1	43.944	3.24	78.5	0.01494	0.000	0.448	1.000	1.000
2	161.468	3.85	83	0.06303	0.287	0.236	0.924	0.830
3	453.567	4.53	102	0.1169	1.000	0.000	0.657	0.639
4	54.285	1.82	104.5	0.132	0.025	0.941	0.622	0.585
5	274.45	3.53	115.9	0.1865	0.563	0.347	0.461	0.392
6	215.95	1.89	121.3	0.1095	0.420	0.917	0.385	0.665
7	92.284	2.3	134.7	0.2972	0.118	0.774	0.197	0.000
8	130.71	1.65	139.1	0.1916	0.212	1.000	0.135	0.374
9	251.71	1.73	148.7	0.2374	0.507	0.972	0.000	0.212

Due to the responses being given equal weight, the distinguishing coefficient was taken to be 0.5. Table 4.38 presents the outcomes.

Equation 3.10 has been used to derive the grey relational grade (GRG) from the findings of the grey relational coefficients.

Table 4. 38 Grey Relational Coefficient and Grey Relational Grade Values

Exp. No	Deviation sequence				Grey Relational Coefficient				Grey Relational Grade	
	MRR (mm^3/sec)	Ra (μm)	Temp (^0C)	Wear rate (mm^3/s)	MRR (mm^3/sec)	Ra (μm)	Temp (^0C)	Wear rate (mm^3/s)	GRG	RANK
1	1.000	0.552	0.000	0.000	0.333	0.475	1.000	1.000	0.702	1
2	0.713	0.764	0.076	0.170	0.412	0.396	0.868	0.746	0.605	3
3	0.000	1.000	0.343	0.361	1.000	0.333	0.593	0.581	0.627	2
4	0.975	0.059	0.378	0.415	0.339	0.894	0.569	0.547	0.587	5
5	0.437	0.653	0.539	0.608	0.533	0.434	0.481	0.451	0.475	8
6	0.580	0.083	0.615	0.335	0.463	0.857	0.449	0.599	0.592	4
7	0.882	0.226	0.803	1.000	0.362	0.689	0.384	0.333	0.442	9
8	0.788	0.000	0.865	0.626	0.388	1.000	0.366	0.444	0.550	6
9	0.493	0.028	1.000	0.788	0.504	0.947	0.333	0.388	0.543	7

Table 4.38 presents the GRG's findings. As the multi-responses are reduced to a single grade, this result is used to optimize the multi-responses.

4.9.1 Analysis of Mean of GRG

The effects of each process parameter at various levels are plotted and illustrated in Figure 4.48 from the value of GRG, and Table 4.39 presents the mean grey relational grade. Based on Table 4.39's higher mean grey relational grade values, the optimal parametric combination is selected. As a result, A1B3C1 (90 m/min cutting speed, 2.5 mm depth of cut, and 0.15 mm/rev feed) are the settings that are optimal for multi-responses.

The lower values of surface roughness, flank wear, tool temperature, and higher material removal rate are given by the higher values of mean grey relational grade (Figure 4.48). This finding suggests that, in dry turning operations, cutting speed, as compared to the depth of cut and feed, has the greatest influence on multi-responses.

Table 4. 39 Response Table for Means of GRG

Level	Cutting speed	Depth of cut	Feed
1	**0.6447**	0.5770	**0.6147**
2	0.5513	0.5433	0.5783
3	0.5117	**0.5873**	0.5147
Delta	0.1330	0.0440	0.1000
Rank	1	3	2

Total mean grey relational grade =0.56922

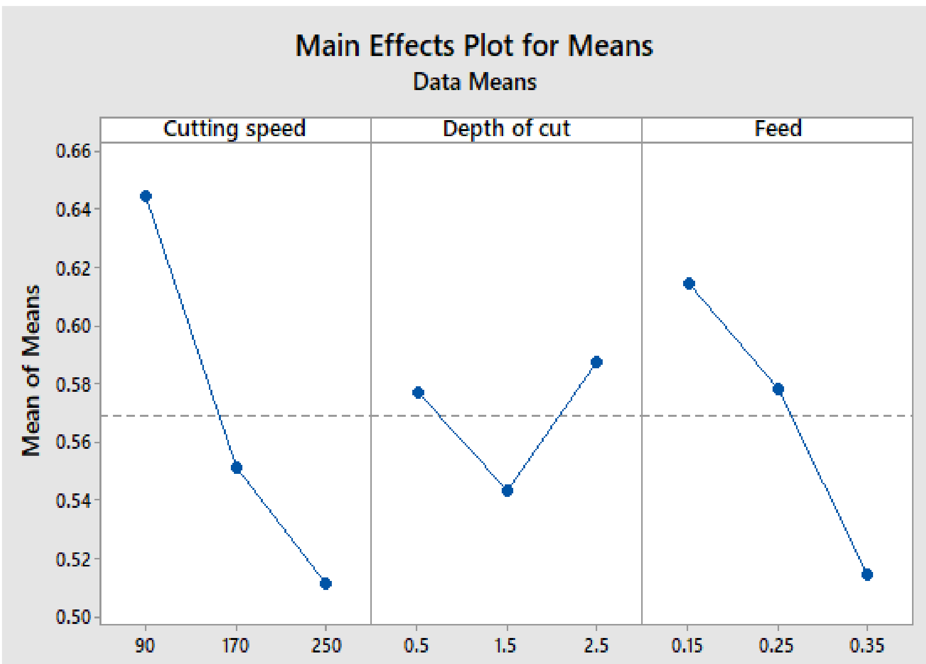

Figure 4. 48 Main Effects Plot for Means of GRG

4.9.2 Analysis of Variance (ANOVA) OF GRG

Analysis of variance is created by taking into account the grey relational grade value that is displayed in Table 4.40. The significance of process parameters on multi-responses is provided in this table. The cutting speed with a contribution of 56.85 % is the significant process parameter affecting multi-responses, according to Figure 4.51. There is little significance in the feed, and the depth of cut shows no significance in the responses.

Table 4. 40 Analysis of Variance for Means of GRG

Source	DF	SST	SSTR	MSE	F	P	Percent contribution P (%)	Significance (α=0.05)
Cutting speed	2	0.027974	0.027974	0.013987	10.44	0.087	56.85	Highly Significant
Depth of cut	2	0.003176	0.003176	0.001588	1.19	0.458	6.45	Significant
Feed	2	0.015374	0.015374	0.007687	5.74	0.148	31.25	Significant
Residual Error	2	0.002680	0.002680	0.001340			5.45	
Total	8	0.049204					100%	

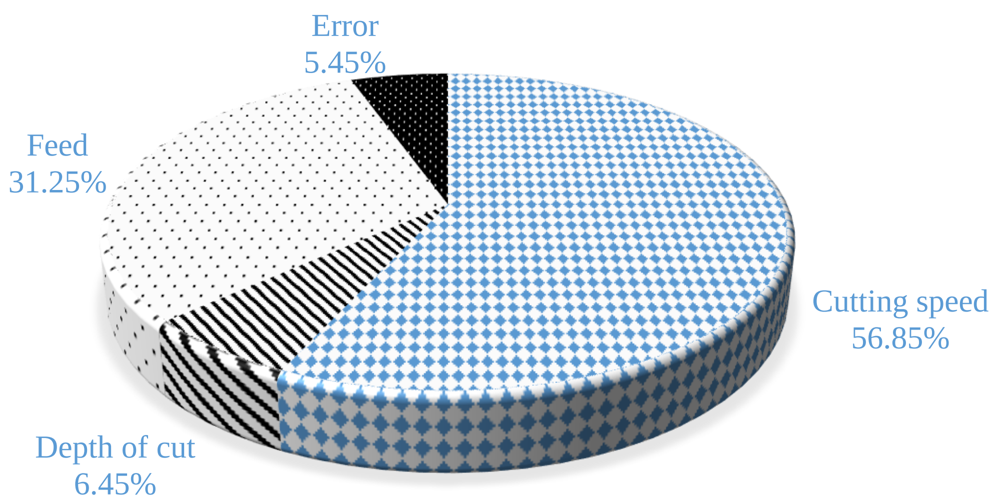

Figure 4. 49 Contribution of cutting parameters on the multi-response

4.9.3 Confirmation test

When dry-machining AISI 1030 steel with tungsten carbide inserts, a confirmation test was performed to determine how the grey relational grade has improved from the initial parameter setting to the optimal parameters. Equation 3.11 can be used to determine the predicted GRG. The grey relational grade changes to 0.728 at the optimum setting, which is near the predicted value of 0.7081.

Table 4.41 of the confirmation run shows that by choosing the optimal parametric combination, the grey relation grade of the responses is improved (0.026). The parameters are optimized based on the analysis mentioned above.

Table 4. 41 Confirmation Experiment

	Initial Factor Setting	Optimum Factor Setting	
		Prediction	Experimental
combination	A1B1C1	A1B3C1	A1B3C1
Surface roughness Ra (μm)	3.24		3.27
Material removal rate (mm^3/sec)	43.944		405.23
Tool temperature (^0C)	77.6		81.5
Tool wear rate (mm^3/s)	0.01494		0.0665
Grey relational grade	0.702	0.7081	0.728
Improvement in GRG = 0.026			

CHAPTER 5

CONCLUSIONS AND RECOMMENDATIONS

Conclusions

The main objective of this study was to investigate experimentally and numerically the effects of cutting parameters on surface roughness, material removal rate, tool temperature, tool wear rate, chip, and parameter optimization during dry turning of AISI 1030 steel with coated tungsten carbide tool inserts in CNC Lathe. Three primary cutting parameters (cutting speed, depth of cut, and feed rate) each with three levels were chosen and investigated Their effects on the responses.

Parameters were investigated and optimized using a Taguchi L9 orthogonal array. An ANOVA was used to establish the significance of each element. The effect of cutting parameters on responses was predicted using finite element simulation with the aid of DEFORM. The DEFORM 3D model was employed for the simulation of material removal rate, tool temperature, and tool wear rate. Finally, the multi-optimization technique, which is a grey relational analysis, was used for the overall optimization. This is done by integrating grey relational analysis with an orthogonal array of the Taguchi approach. Based on the results presented, the following conclusions are drawn from the study:

- According to the results of statistical analyses, the depth of cut, which contributed 66.13% to the material removal rate (MRR), was shown to be the most important parameter, followed by feed rate (26.01%). Cutting speed did not show any contribution to the material removal rate.
- The optimal condition for MRR was observed at A1B3C3, i.e., medium cutting speed (170 m/min), higher depth of cut (2.5 mm) and higher feed rate (0.35 mm/rev). A confirmation experiment was carried out and obtained 453.57 mm^3/s.
- Surface roughness was significantly influenced by cutting speed, which contributes 67.21%, followed by feed rate, which contributes 26.91%, and depth of cut, which contributes 3.96%.
- With an A3B1C1 combination i.e., 250 m/min cutting speed, 0.5 mm depth of cut, and 0.15 mm/rev feed rate, a minimum (optimal) surface roughness of 1.21 µm was achieved. Since the orthogonal array design does not include this combination of levels, a Taguchi prediction and conformation test was carried out. The fact that there was only a small

(4.96%) difference between the predicted value and the confirmation test indicates that Taguchi-based orthogonal array experimentation was an effective method for performing analysis and prediction with the least number of experiments. The prediction for all experimental runs was also done and compared with the experimental result; the result demonstrates that the prediction was close to the experiment with an average of all errors of 2.9 %.

- The results of an ANOVA study show that cutting speed was the most significant parameter followed by the depth of cut, which had an impact on tool temperature by about 88.05% and 10.68%, respectively. With an increase in cutting speed, the tool temperature raised significantly.
- According to Taguchi's analysis, the optimum conditions for minimizing cutting tool temperature, which is 77.6 ^{0}C, include a cutting speed of 90 m/min, a cut depth of 0.5 mm, and a feed rate of 0.25 mm/rev.
- A coated tungsten carbide tool was observed under an optical microscope, and it was determined that abrasion and adhesion were the main wear mechanisms. The micrograph taken with an optical microscope revealed significant wear damage on the flank face. When compared to flank wear, crater wear covered a larger area of the rake face but had a smaller depth.
- The cutting condition with the greatest impact on tool wear rate was cutting speed (77.22%), followed by feed (22.28%), and depth of cut (0.16%). The tool wear was positively impacted by an increase in all three factors.
- For the A1B1C1 combination of parameters, i.e., cutting speed of 90 m/min, depth of cut of 0.5 mm, and a feed rate of 0.15 mm/rev, the wear rate of the tungsten carbide cutting tool insert was minimal (0.01494).
- The tool wear rate rises as the cutting tool temperature rises, and the parameters that affect the tool temperature affect the tool wear rate in a directly proportional way.
- Turning of AISI 1030 steel resulted in the formation of continuous chips, continuous chips with a built-up edge, and discontinuous chips. In experiments 6, 7, 8, and 9, a continuous chip was produced, which resulted in a better surface finish, lower power usage, and lower friction for this material. In experiments 3, 4 and 5, a continuous with a built-up edge and

in experiments 1 and 2, 3 discontinuous chips were developed, resulting in a poor surface finish and a shorter tool life.

- According to the ANOVA table of grey relational analysis, cutting speed is the controlled process parameter that has the greatest influence on multiple responses, with a significance of 56.85% followed by feed rate (31.25%), and depth of cut (6.45%).
- A1B3C1, or a cutting speed of 90 m/min, a depth of cut of 0.25 mm, and a feed of 0.15 mm/rev, is the optimum parametric combination for multi-responses. Setting the optimum parametric combination results in a considerable improvement in the grey relation grade (0.026).
- The developed simulation model and Taguchi prediction were closely related to the experimental results, with smaller relative errors, the comparison of simulation and prediction data with experimental data showed that both are in good agreement. As a result, the simulation model and Taguchi prediction were shown to be successful in the estimation of the dry-turning AISI 1030 steel.

Recommendations

The researcher submits the following recommendations for dry turning of AISI 1030 steel in light of the findings and conclusions drawn from this investigation.

- AISI 1030 medium carbon steel has been employed in this study. To explore the impact of cutting parameters on surface roughness under the same dry turning parameter, this can be expanded to additional material types.
- In the future, these parametric optimization outcomes can be applied for academic research as well as for the automotive, machining sector, and manufacturing industries to save production costs and improve machining effectiveness.

Scope For Future Work

- This research examined the impact of cutting parameters such as feed rate, depth of cut, and spindle speed. Further research could take into account additional elements like the nose radius, cutting tool geometry, material composition, coating material, lubricants, chip breakers, etc.
- Future experiments could be performed by measuring cutting forces and power usage.

- In the future, numerical simulation and modelling may be used to study stress, strain, and tooltip deformation. because it is difficult to experimentally investigate those characteristics.
- The study of chip morphology could be considered as part of further research using an optical or electron microscope, for deep investigation of the behaviour of chips.
- Further study may consider the effect of mesh change on the accuracy of simulation result

REFERENCES

Alabi, A., Ajiboye, T., & Olusegun, H. (2010). Measuring the stress, strain and strain rate in heat-treated medium carbon steel samples and finding the constituted material-related properties. African Journal of Mathematics and Computer Science Research, 3(3), 038-048

Agrawal, S. M., & Patil, N. G. (2018b). Experimental study of non-edible vegetable oil as a cutting fluid in the machining of M2 Steel using MQL. Procedia Manufacturing, 20, 207–212. https://doi.org/10.1016/j.promfg.2018.02.030

Achuthamenon Sylajakumari, P., Ramakrishnasamy, R., & Palaniappan, G. (2018, September 16). Taguchi Grey Relational Analysis for Multi-Response Optimization of Wear in Co-Continuous Composite. Materials, 11(9), 1743. https://doi.org/10.3390/ma11091743

Akram, S., Jaffery, S. H. I., Khan, M., Fahad, M., Mubashar, A., & Ali, L. (2018, September). Numerical and experimental investigation of Johnson–Cook material models for aluminium (Al 6061-T6) alloy using orthogonal machining approach. Advances in Mechanical Engineering, 10(9), 168781401879779.

Aouici, H., Yallese, M., Belbah, A., Ameur, M., & Elbah, M. (2013). Experimental investigation of cutting parameters influence on surface roughness and cutting forces in hard turning of X38CrMoV5-1 with CBN tool. Sādhanā, 38(3), 429-445. https://doi.org/10.1007/s12046-013-0147-z

Attanasio, A., Ceretti, E., Outeiro, J., & Poulachon, G. (2020). Numerical simulation of tool wear in drilling Inconel 718 under flood and cryogenic cooling conditions. Wear, 458, 203403. https://doi.org/10.1016/j.wear.2020.203403

Badiger, P. V., Desai, V., Ramesh, M. R., Prajwala, B. K., & Raveendra, K. (2018, October 3). Effect of cutting parameters on tool wear, cutting force and surface roughness in machining of MDN431 alloy using Al and Fe coated tools. Materials Research Express, 6(1), 016401. https://doi.org/10.1088/2053-1591/aae2a3

Bashir, K., Alkali, A. U., Elmunafi, M. H. S., & Yusof, N. M. (2018, April). Experimental investigation into the effect of cutting parameters on surface integrity of hardened tool steel. IOP Conference Series: Materials Science and Engineering, 344, 012020. https://doi.org/10.1088/1757-899x/344/1/012020

Bhemuni, V., Chelamalasetti, S. R., & Kondapalli, S. P. (2014). Effect of Machining Parameters on Tool Wear and Nodal Temperature in Hard Turning of AISI D3 Steel. OALib, 01(06), 1–12. https://doi.org/10.4236/oalib.1100627

Binder, M., Klocke, F., & Lung, D. (2015). Tool wear simulation of complex shaped coated cutting tools. Wear, 330, 600-607.

Bovas Herbert Bejaxhin, A., Paulraj, G., Jayaprakash, G., & Vijayan, V. (2021). Measurement of roughness on hardened D-3 steel and wear of coated tool inserts. Transactions of the Institute of Measurement and Control, 43(3), 528-536. https://doi.org/10.1177/0142331220938554

Çelik, B., & Kaçal, A. (2020). Effect of Machining Parameters on Turning of Inconel X750 Using PVD Coated Carbide Inserts. https://dx.doi.org/10.18505/cuid.777716

Çelik, Y. H., Kilickap, E., Güney, M. J. J. o. t. B. S. o. M. S., & Engineering. (2017). Investigation of cutting parameters affecting tool wear and surface roughness in dry turning of Ti-6Al-4V using CVD and PVD coated tools. 39(6), 2085-2093. https://doi.org/10.1007/s40430-016-0607-6.

Das, D., Prasanna Sahoo, B., Bansal, S., & Mishra, P. (2018). Experimental investigation on material removal rate and chip forms during turning T6 tempered Al 7075 alloy. Materials Today: Proceedings, 5(2), 3250–3256. https://doi.org/10.1016/j.matpr.2017.11.566

Dhandapani, K., Vasanthkumar, P., & Nagarajan, S. (2014). A meta-heuristic evolutionary algorithm to optimize machining parameters in turning AISI 4340 steel. Journal of Advanced Engineering Research, 1(2), 105-113.

Dijmărescu, M. R., & Tiriplica, P. G. (2019). Development of cutting forces and surface roughness prediction models for turning a CoCrWNi alloy. Materials Science Forum, https://doi.org/10.4028/www.scientific.net /MSF.957.148

Ejieji, T., Adedayo, S. M., Bello, O.W., Abdulkareem, S., (2018). Effect of machining variables and coolant application on HSS tool temperature during turning on a CNC lathe, IOP Conference Series, Mat. Sci and Eng, 413(012004), 1-9.

Engineering ToolBox, AISI/SAE Steel and Alloys - Designation System. (n.d.). Engineering ToolBox. Retrieved 2021, from https://www.engineeringtoolbox.com/aisi-sae-steel-numbering-systemd_1449.html

Feng, C.-X., & Wang, X.-F. (2003). Surface roughness predictive modelling: neural networks versus regression. IIE Transactions, 35(1), 11-27.

Gohil, V., & Puri, Y. M. (2016, October 11). Statistical analysis of material removal rate and surface roughness in electrical discharge turning of titanium alloy (Ti-6Al-4V). Proceedings of the Institution of Mechanical Engineers, Part B: Journal of Engineering Manufacture, 232(9), 1603–1614. https://doi.org/10.1177/0954405416673104

Gunjal, S. U., & Patil, N. G. (2018). Experimental Investigations into Turning of Hardened AISI 4340 Steel using Vegetable-based Cutting Fluids under Minimum Quantity Lubrication. Procedia Manufacturing, 20, 18–23. https://doi.org/10.1016/j.promfg.2018.02.003

Gupta, S., Chandra, V., & Kumar, P. (2019). Assessment of machining parameters on EN24 steel under dry, wet and MQL condition using multi coated inserts. *Journal of Physics: Conference Series*, *1240*, 012141. https://doi.org/10.1088/1742-6596/1240/1/012141

Gopal, M. (2021, February 22). The Effect of Machining Parameters and Optimization of Temperature Rise in Turning Operation of Aluminium-6061 Using RSM and Artificial Neural Network. Periodica Polytechnica Mechanical Engineering, 65(2), 141–150. https://doi.org/10.3311/ppme.16625

Hosseinkhani, K., & Ng, E. (2018). A hybrid experimental and simulation approach to evaluate the calibration of tool wear rate models in machining. The International Journal of Advanced Manufacturing Technology, 96(5), 2709-2724. https://doi.org/10.1007/s00170-018-1687-5

Jafarian, F., Masoudi, S., Soleimani, H., & Umbrello, D. (2018, January 19). Experimental and numerical investigation of thermal loads in Inconel 718 machining. Materials and Manufacturing Processes, 33(9), 1020–

Jafarian, F., Umbrello, D., & Jabbaripour, B. (2016, August). Identification of new material model for machining simulation of Inconel 718 alloy and the effect of tool edge geometry on microstructure changes. Simulation Modelling Practice and Theory, 66, 273–284. https://doi.org/10.1016/j.simpat.2016.05.001

Jebaraj, M., Pradeep Kumar, M., Yuvaraj, N., & Mujibar Rahman, G. (2019, March 20). Experimental study of the influence of the process parameters in the milling of Al6082-T6 alloy. Materials and Manufacturing Processes, 34(12), 1411–1427.

Jhodkar, D., Amarnath, M., Chelladurai, H., & Ramkumar, J. (2018, November 26). Experimental Investigations to Study the Effects of Microwave Treatment Strategy on Tool Performance in Turning Operation. Journal of Materials Engineering and Performance, 27(12), 6374–6388. https://doi.org/10.1007/s11665-018-3742-7

Kaçal2, B. Ç. a. A. (2020). Experimental Investigation on Nano MoS2Application in Milling of EN-GSJ 700-02 Cast Iron with Minimum Quantity Lubrication. Journal of Scientific & Industrial Research, 479-483.

Kam, M., & Şeremet, M. (2021, April 20). Experimental investigation of the effect of machinability on surface quality and vibration in hard turning of hardened AISI 4140 steels using ceramic cutting tools. Proceedings of the Institution of Mechanical Engineers, Part E: Journal of Process Mechanical Engineering, 235(5), 1565–1574. https://doi.org/10.1177/09544089211007366

Kamaruddin, A. M. N. A., Hosokawa, A., Ueda, T., & Furumoto, T. (2016, May 2). Cutting Characteristics of Binderless Diamond Tools in High-Speed Turning of Ti-6Al-4V – Availability of Single-Crystal and Nano-Polycrystalline Diamond –. International Journal of Automation Technology, 10(3), 411–419. https://doi.org/10.20965/ijat.2016.p0411

Kannan, A., Mohan, R., Viswanathan, R., & Sivashankar, N. (2020, November). Experimental investigation on surface roughness, tool wear and cutting force in turning of hybrid (Al7075 + SiC + Gr) metal matrix composites. Journal of Materials Research and Technology, 9(6), 16529–16540. https://doi.org/10.1016/j.jmrt.2020.11.074

Karazi, S. M., Moradi, M., & Benyounis, K. Y. (2019). Statistical and Numerical Approaches for Modeling and Optimizing Laser Micromachining Process-Review. Reference Module in Materials Science and Materials Engineering. https://doi.org/10.1016/b978-0-12-803581-8.11650-9

Karim, Z. A., Azuan, S., & Yasir, A. (2013). A study on tool wear and surface finish by applying positive and negative rake angle during machining.

Karthik, M., Raju, V., Reddy, K. N., Balashanmugam, N., & Sankar, M. (2020). Cutting parameters optimization for surface roughness during dry hard turning of EN 31 bearing steel using CBN insert. Materials Today: Proceedings, 26, 1119–1125. https://doi.org/10.1016/j.matpr.2020.02.224

Kesavan, J., Senthilkumar, V., & Dinesh, S. (2020). Experimental and numerical investigations on machining of Hastelloy C276 under cryogenic conditions. Materials Today: Proceedings, 27, 2441-2444. https://doi.org/10.1016/j.matpr.2019.09.214

Kıvak, T. (2014). Optimization of surface roughness and flank wear using the Taguchi method in milling of Hadfield steel with PVD and CVD coated inserts. Measurement, 50, 19-28. https://doi.org/10.1016/j.measurement.2013.12.017

Korkmaz, M. E., Yaşar, N., & Günay, M. (2020). Numerical and experimental investigation of cutting forces in turning of Nimonic 80A superalloy. Engineering Science and Technology, an International Journal, 23(3), 664-673. https://doi.org/10.1016/j.jestch.2020.02.001

Krishankant, J. T., Bector, M., & Kumar, R. (2012). Application of Taguchi method for optimizing turning process by the effects of machining parameters. International Journal of Engineering and Advanced Technology, 2(1), 263-274.

Kumar, S., Singh, D., & Kalsi, N. S. (2017). Experimental Investigations of Surface Roughness of Inconel 718 under different Machining Conditions. Materials Today: Proceedings,4(2),1179–1185. https://doi.org/10.1016/j.matpr.2017.01.135

Kumar Gupta, M., Korkmaz, M. E., Sarıkaya, M., Krolczyk, G. M., & Günay, M. (2022, April). In-process detection of cutting forces and cutting temperature signals in the cryogenic assisted turning of titanium alloys: An analytical approach and experimental study. Mechanical Systems and Signal Processing, 169,

Kuntoğlu, M., Aslan, A., Pimenov, D. Y., Giasin, K., Mikolajczyk, T., & Sharma, S. (2020). Modelling of cutting parameters and tool geometry for multi-criteria optimization of surface roughness and vibration via response surface methodology in turning of AISI 5140 steel. Materials, 13(19), 4242. https://doi.org/10.3390/ma13194242

Kuram, E., & Ozcelik, B. (2013). Multi-objective optimization using Taguchi-based grey relational analysis for micro-milling of Al 7075 material with ball nose end mill. Measurement, 46(6), 1849-1864. https://doi.org/10.1016/ j.measurement.2013.02.002

Kuo, Y., Yang, T., & Huang, G. W. (2008, August). The use of grey relational analysis in solving multiple attribute decision-making problems. Computers &Amp; Industrial Engineering, *55*(1), 80–93. https://doi.org/10.1016/j.cie.2007.12.002

Laakso, S. V. A., & Niemi, E. (2015, January 8). Determination of material model parameters from orthogonal cutting experiments. Proceedings of the Institution of Mechanical

Engineers, Part B: Journal of Engineering Manufacture, 230(5), 848–857. https://doi.org/10.1177/0954405414560620

Lalwani, D., Mehta, N., & Jain, P. (2008, September). Experimental investigations of cutting parameters influence on cutting forces and surface roughness in finish hard turning of MDN250 steel. Journal of Materials Processing Technology, 206(1–3), 167–179. https://doi.org/10.1016/j.jmatprotec.2007.12.018

Larson, M. G. (2008, January). Analysis of Variance. *Circulation*, *117*(1), 115–121. https://doi.org/10.1161/circulationaha.107.654335

Liu, D., Zhang, Y., Luo, M., & Zhang, D. (2019). Investigation of tool wear and chip morphology in dry trochoidal milling of titanium alloy Ti–6Al–4V. Materials, 12(12), 1937. https://doi.org/10.3390/ma12121937

Liu, G., Özel, T., Li, J., Wang, D., & Sun, S. (2020). Optimization and fabrication of curvilinear micro-grooved cutting tools for sustainable machining based on finite element modelling of the cutting process. The International Journal of Advanced Manufacturing Technology, 110(5), 1327-1338.

Liu, E., An, W., Xu, Z., & Zhang, H. (2020, May). Experimental study of cutting-parameter and tool life reliability optimization in inconel 625 machining based on wear map approach. Journal of Manufacturing Processes, 53, 34–42.

Li, L., Wu, M., Liu, X., Cheng, Y., & Yu, Y. (2017, November 17). Experimental study of the wear behavior of PCBN inserts during cutting of GH4169 superalloys under high-pressure cooling. The International Journal of Advanced Manufacturing Technology, 95(5–8), 1941–1951. https://doi.org/10.1007/s00170-017-1333-7

Liu, L., Sun, J., Chen, W., & Zhang, J. (2016, June 20). Finite element analysis of machining processes of turbine disk of Inconel 718 high-temperature wrought alloy based on the theorem of minimum potential energy. The International Journal of Advanced Manufacturing Technology, 88(9–12), 3357–3369. https://doi.org/10.1007/s00170-016-9026-1

Masoudi, S., Vafadar, A., Hadad, M., & Jafarian, F. (2017, November 17). Experimental investigation into the effects of nozzle position, workpiece hardness, and tool type in MQL turning of AISI 1045 steel. Materials and Manufacturing Processes, 33(9), 1011–1019. https://doi.org/10.1080/10426914.2017.1401716

Ming, C., Fanghong, S., Haili, W., Renwei, Y., Zhenghong, Q., & Shuqiao, Z. (2003, July). Experimental research on the dynamic characteristics of the cutting temperature in the process of high-speed milling. Journal of Materials Processing Technology, 138(1–3), 468–471. https://doi.org/10.1016/s0924-0136(03)00120-1

Mohanraj, T., Shankar, S., Rajasekar, R., Sakthivel, N., & Pramanik, A. (2020, January). Tool condition monitoring techniques in milling process — a review. Journal of Materials Research and Technology, 9(1), 1032–1042. https://doi.org/10.1016/j.jmrt.2019.10.031

Nalbant, M., Gökkaya, H., & Sur, G. (2007). Application of Taguchi method in the optimization of cutting parameters for surface roughness in turning. Materials & Design, 28(4), 1379 1.

Ni, C., Zhu, L., Liu, C., & Yang, Z. (2018, July). Analytical modeling of tool-workpiece contact rate and experimental study in ultrasonic vibration-assisted milling of Ti–6Al–4V. International Journal of Mechanical Sciences, 142–143, 97–111.

Oberg, E. (2020). Machinery's Handbook Toolbox (Thirty-first ed.). Industrial Press, Inc.

Obiko, J. O., Mwema, F. M., & Bodunrin, M. O. (2021). Validation and optimization of cutting parameters for Ti-6Al-4V turning operation using DEFORM 3D simulations and the Taguchi method. Manufacturing Review, 8, 5. https://doi.org/10.1051/mfreview /2021001

Özel, T., Sima, M., Srivsastava, A., & Kaftanoglu, B. (2010). Investigations on the effects of multi-layered coated inserts in machining Ti–6Al–4V alloy with experiments and finite element simulations. CIRP annals, 59(1), 77-82.

ÖZSOY, N. (2019, November 30). Experimental Investigation of Surface Roughness of Cutting Parameters in T6 Aluminum Alloy Milling Process. International Journal of Computational and Experimental Science and Engineering, 5(3), 105–111.

Panda, A., Sahoo, A., & Rout, R. (2016). Multi-attribute decision making parametric optimization and modelling in hard turning using ceramic insert through grey relational analysis: A case study. Decision Science Letters, 5(4), 581-592.

Panneerselvam, T. (2019, February 12). Experimental Investigation on Cutting Tool Performance of Newly Synthesized P/M Alloy Steel Under Turning Operation. SpringerLink. Retrieved September 18, 2022, from https://link.springer.com/article/10.1007/s13369-019-03763-4?error=cookies_not_supported&code=4df73246-633f-4fe1-bd0b-573b9357f261

Parida, A., Rao, P., & Ghosh, S. (2020). Numerical analysis and experimental investigation in the machining of AISI 316 steel. Sādhanā, 45(1), 1-11.

Prakash, K. S., Gopal, P., & Karthik, S. (2020). Multi-objective optimization using Taguchi-based grey relational analysis in turning of Rock dust reinforced Aluminum MMC. Measurement, 157, 107664. https://doi.org/10.1016/j.measurement .2020.107664

Parthiban, A., Pugazhenthi, R., Ravikumar, R., & Vivek, P. (2017). Experimental Investigation of Turning Parameters on AA 6061-T6 Material. IOP Conference Series: Materials Science and Engineering, https://doi.org/10.1088/1757-899X/183/1/012013

Pervaiz, S., Deiab, I., Wahba, E., Rashid, A., & Nicolescu, M. (2017, August 21). A numerical and experimental study to investigate convective heat transfer and associated cutting temperature distribution in single point turning. The International Journal of Advanced Manufacturing Technology, 94(1–4), 897–910. https://doi.org/10.1007/s00170-017-0975

Rajesh, K. D., Shaik, A. M., Prasad, A. R., Buddi, T., & Mwema, F. (2021). Finite element simulation of AISI 1025 and Al6061 specimen with coated and uncoated tools on turning process using deform-3D. E3S Web of Conferences, DOI:10.1051/e3sconf/202130901095

Rashid, R. R., Sun, S., Wang, G., & Dargusch, M. (2012). An investigation of cutting forces and cutting temperatures during laser-assisted machining of the Ti–6Cr–5Mo–5V–4Al beta titanium alloy. International Journal of Machine Tools and Manufacture, 63, 58-69.

San-Juan, M., Martín, Tiedra, M. D. P. D., Santos, F., López, R., & Cebrián, J. (2015b). Study of Cutting Forces and Temperatures in Milling of AISI 316L. Procedia Engineering, 132, 500–506. https://doi.org/10.1016/j.proeng.2015.12.525

Shahid, M. (2020). Optimization of Turning Process Parameters in Machining Heat Treated Steel. International Journal for Research in Applied Science and Engineering Technology, 8(9), 121–125. https://doi.org/10.22214/ijraset.2020.31339

Shao, W., Li, X., Sun, Y., Huang, H., & Tang, J. (2018, July). An experimental study of temperature at the tip of point-attack pick during rock cutting process. International Journal of Rock Mechanics and Mining Sciences, 107, 39–47.

Shetty, R., Jose, T. K., Revankar, G. D., Rao, S. S., Shetty, D. S. (2014). Surface roughness analysis during turning of Ti-6Al-4V under near dry machining using statistical tool. International Journal of Current Engineering and Technology, 4(3):2061-2067.

Shihab, S. K., Khan, Z. A., Mohammad, A., & Siddiqueed, A. N. (2014). RSM based Study of Cutting Temperature During Hard Turning with Multilayer Coated Carbide Insert. Procedia Materials Science, 6, 1233–1242. https://doi.org/10.1016/j.mspro.2014.07.197

Singh, B., & Singh, G. (2018). Experimental investigation of cutting parameters influence on surface finish during turning of steel using Taguchi approach. International Journal of Manufacturing Research, 13(1), 49. https://doi.org/10.1504/ijmr.2018.092778

Siva Surya, M., Shalini, M., & Sridhar, A. (2017). Multi-Response Optimization On EN19 Steel Using Grey Relational Analysis Through Dry & Wet Machining. Materials Today: Proceedings, 4(2), 2157–2166. https://doi.org/10.1016/j.matpr.2017.02.062

Suhail, A. H., Ismail, N., Wong, S., & Jalil, N. A. (2010). Optimization of cutting parameters based on surface roughness and assistance of workpiece surface temperature in the turning process. American journal of engineering and applied sciences, 3(1), 102-108.

Suresh, R., & Basavarajappa, S. (2014). Effect of process parameters on tool wear and surface roughness during turning of hardened steel with a coated ceramic tool. Procedia Materials Science, 5, 1450-1459. https://doi.org/10.1016/j.mspro.2014.07.464

Syed Irfan, S., Vijay Kumar, M., & Rudresha, N. (2019). Optimization of Machining Parameters in CNC Turning of EN45 by Taguchi's Orthogonal Array Experiments. https://doi.org/10.1016/j.matpr.2019.07.165

Tamerabet, Y., Brioua, M., Tamerabet, M., & Khoualdi, S. (2018, March 15). Experimental Investigation on Tool Wear Behavior and Cutting Temperature during Dry Machining of Carbon Steel SAE 1030 Using KC810 and KC910 Coated Inserts. Tribology in Industry, 40(1), 52–65. https://doi.org/10.24874/ti.2018.40.01.04

Teng, X., Huo, D., Shyha, I., Chen, W., & Wong, E. (2018, February 19). An experimental study on tool wear behaviour in micro milling of nano Mg/Ti metal matrix composites. The International Journal of Advanced Manufacturing Technology, 96(5–8), 2127–2140. https://doi.org/10.1007/s00170-018-1672-z

Tiwari, R., Das, D., Kumar Sahoo, A., Kumar, R., Kumar Das, R., & Chandra Routara, B. (2018). Experimental investigation on surface roughness and tool wear in hard turning JIS S45C steel. Materials Today: Proceedings, 5(11), 24535–24540.

Uhlmann, E., Von Der Schulenburg, M. G., & Zettier, R. J. C. a. (2007). Finite element modeling and cutting simulation of Inconel 718. 56(1), 61-64. https://doi.org /10.1016/j.cirp.2007.05.017

Usui, E., Shirakashi, T., & Kitagawa, T. (1984, December). Analytical prediction of cutting tool wear. Wear, 100(1–3), 129–151. https://doi.org/10.1016/0043-1648(84)90010-3

Varghese, V., Ramesh, M., & Chakradhar, D. (2018, May 24). Experimental investigation and optimization of machining parameters for sustainable machining. Materials and Manufacturing Processes, 33(16), 1782–1792.

Verma, M., & Pradhan, S. K. (2020). Experimental and numerical investigations in CNC turning for different combinations of tool inserts and workpiece material. Materials Today: Proceedings, 27, 2736-2743. https://doi.org/10.1016/j.matpr.2019.12.193

Venkata Vishnu, A., Venkata Ramana, M., & Tilak, K. (2018). Experimental Investigations of Process Parameters Influence on Surface Roughness in Turning of EN-353 Alloy Steel under Different Machining Environments. Materials Today: Proceedings, 5(2), 4192–4200. https://doi.org/10.1016/j.matpr.2017.11.682

Valera, H. Y., & Bhavsar, S. N. J. P. T. (2014). Experimental investigation of surface roughness and power consumption in turning operation of EN 31 alloy steel. 14, 528-534.

Vaxevanidis, N., Fountas, N., Koutsomichalis, A., & Kechagias, J. (2018). Experimental investigation of machinability parameters in turning of CuZn39Pb3 brass alloy. Procedia Structural Integrity, 10, 333–341. https://doi.org/10.1016/j.prostr.2018.09.046

Yadav, R. K., Abhishek, K., & Mahapatra, S. S. (2015). A simulation approach for estimating flank wear and material removal rate in turning of Inconel 718. Simulation modelling practice and theory, 52, 1-14. Y https://doi.org/10.1016/j.simpat.2014.12.004

Yanda, H., Ghani, J. A., Rodzi, M. N. A. M., Othman, K., & Haron, C. H. C. (2010). Optimization of material removal rate, surface roughness and tool life on conventional dry turning of FCD700. International Journal of Mechanical and Materials Engineering, 5(2), 182-190

Younas, M., Jaffery, S. H. I., Khan, M., Khan, M. A., Ahmad, R., Mubashar, A., & Ali, L. (2019, August 27). Multi-objective optimization for sustainable turning Ti6Al4V alloy using grey relational analysis (GRA) based on analytic hierarchy process (AHP). The International Journal of Advanced Manufacturing Technology, 105(1–4), 1175–1188. https://doi.org/10.1007/s00170-019-04299-5

Yousuf Al Kindi, M. R., & Salim, R. K. (2018). Tool wear investigation in CNC turning operation. In Proceedings of the World Congress on Engineering (Vol. 2).

Yume, J. A. O., & Kwon, P. Y. (2007). Tool wear mechanisms in machining. International Journal of Machining and Machinability of Materials, 2(3/4), 316.

Yu, Q., Li, S., Zhang, X., & Shao, M. (2019, March 21). Experimental study on the correlation between turning temperature rise and turning vibration in dry turning on aluminium alloy. The International Journal of Advanced Manufacturing Technology, 103(1–4), 453–469. https://doi.org/10.1007/s00170-019-03506-7

Zhenyu, S., Xin, L., Ningmin, D., & Qibiao, Y. (2021). Evaluation of tool wear and cutting performance considering effects of dynamic nodes movement based on FEM simulation. Chinese Journal of Aeronautics, 34(4), 140-152.

Zhao, W., Gong, L., Ren, F., Li, L., Xu, Q., & Khan, A. M. (2018, March 17). Experimental study on chip deformation of Ti-6Al-4V titanium alloy in cryogenic cutting. The International Journal of Advanced Manufacturing Technology, 96(9–12), 4021–4027. https://doi.org/10.1007/s00170-018-1890-4

Zhou, T., He, L., Wu, J., Du, F., & Zou, Z. (2019). Prediction of surface roughness of 304 stainless steel and multi-objective optimization of cutting parameters based on GA-GBRT. Applied Sciences, 9(18), 3684.

Zhou, Y., Liu, C., Yu, X., Liu, B., & Quan, Y. (2022, July 23). Tool wear mechanism, monitoring and remaining useful life (RUL) technology based on big data: a review. *SN Applied Sciences*, *4*(8). https://doi.org/10.1007/s42452-022-05114-9

Zukeri, M. Z. M., & Zaim, M. (2010). Study on cutting Operation in turning process by 3d simulation using deform 3D Universiti Tun Hussein Onn Malaysia.

.

APPENDIXES

Publication: Gebremichael Haileselasse Alemayoh[1], Balkeshwar Singh[2*]**.** Experimental and numerical investigation of dry turning AISI 1030 carbon steel using CNC lathe machining. Journal of engineering research express (Scopus web of science). Manuscript reference: ERX-102163

Appendix A. Minitab 17 Software and all response results using L9 Orthogonal Array

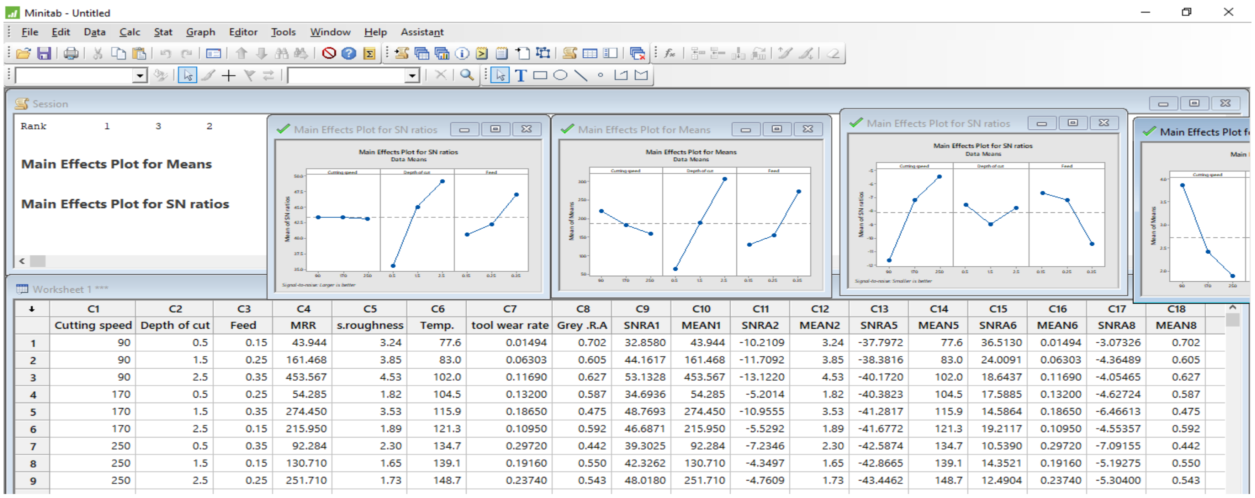

↓	C1	C2	C3	C4	C5	C6	C7	C8	C9	C10	C11	C12	C13	C14	C15	C16	C17	C18
	Cutting speed	Depth of cut	Feed	MRR	s.roughness	Temp.	tool wear rate	Grey .R.A	SNRA1	MEAN1	SNRA2	MEAN2	SNRA5	MEAN5	SNRA6	MEAN6	SNRA8	MEAN8
1	90	0.5	0.15	43.944	3.24	77.6	0.01494	0.702	32.8580	43.944	-10.2109	3.24	-37.7972	77.6	36.5130	0.01494	-3.07326	0.702
2	90	1.5	0.25	161.468	3.85	83.0	0.06303	0.605	44.1617	161.468	-11.7092	3.85	-38.3816	83.0	24.0091	0.06303	-4.36489	0.605
3	90	2.5	0.35	453.567	4.53	102.0	0.11690	0.627	53.1328	453.567	-13.1220	4.53	-40.1720	102.0	18.6437	0.11690	-4.05465	0.627
4	170	0.5	0.25	54.285	1.82	104.5	0.13200	0.587	34.6936	54.285	-5.2014	1.82	-40.3823	104.5	17.5885	0.13200	-4.62724	0.587
5	170	1.5	0.35	274.450	3.53	115.9	0.18650	0.475	48.7693	274.450	-10.9555	3.53	-41.2817	115.9	14.5864	0.18650	-6.46613	0.475
6	170	2.5	0.15	215.950	1.89	121.3	0.10950	0.592	46.6871	215.950	-5.5292	1.89	-41.6772	121.3	19.2117	0.10950	-4.55357	0.592
7	250	0.5	0.35	92.284	2.30	134.7	0.29720	0.442	39.3025	92.284	-7.2346	2.30	-42.5874	134.7	10.5390	0.29720	-7.09155	0.442
8	250	1.5	0.15	130.710	1.65	139.1	0.19160	0.550	42.3262	130.710	-4.3497	1.65	-42.8665	139.1	14.3521	0.19160	-5.19275	0.550
9	250	2.5	0.25	251.710	1.73	148.7	0.23740	0.543	48.0180	251.710	-4.7609	1.73	-43.4462	148.7	12.4904	0.23740	-5.30400	0.543

Appendix B. Simulation result of Tool Temperature for Experiments 1, 2,5,7,8, and 9

Simulation Result of Tool Temperature for Experimental Run Two

t(sec)	T(0C)	t(sec)	T(0C)	t(sec)	T(0C)	t(sec)	T(0C)	t(sec)	T(0C)
0.0000	37.22	0.0001	54.72	0.0001	58.15	0.0001	64.69	0.0001	53.46
0.0001	38.63	0.0001	55.58	0.0001	57.60	0.0001	64.69	0.0001	47.55
0.0001	40.04	0.0001	56.38	0.0001	57.34	0.0001	63.26	0.0001	42.89
0.0001	41.43	0.0001	56.38	0.0001	57.28	0.0001	64.16	0.0001	39.05
0.0001	42.80	0.0001	54.58	0.0001	57.31	0.0001	65.01	0.0001	36.71
0.0001	44.14	0.0001	55.13	0.0001	57.31	0.0001	65.61	0.0001	35.46
0.0001	45.43	0.0001	55.71	0.0001	57.11	0.0001	66.17	0.0001	34.35
0.0001	46.66	0.0001	56.31	0.0001	57.06	0.0001	66.77	0.0001	34.35
0.0001	47.82	0.0001	56.93	0.0001	57.28	0.0001	67.40	0.0001	31.71
0.0001	48.82	0.0001	57.64	0.0001	57.36	0.0001	68.02	0.0002	30.83
0.0001	49.68	0.0001	58.27	0.0001	57.87	0.0001	68.63	0.0002	30.09
0.0001	49.68	0.0001	58.89	0.0001	58.47	0.0001	69.28	0.0002	29.48
0.0001	47.07	0.0001	58.89	0.0001	58.47	0.0001	69.97	0.0002	28.92
0.0001	47.76	0.0001	57.10	0.0001	59.18	0.0001	70.71	0.0002	28.38
0.0001	48.64	0.0001	57.80	0.0001	59.94	0.0001	71.51	0.0002	27.87
0.0001	49.79	0.0001	58.49	0.0001	60.78	0.0001	72.35	0.0002	27.48
0.0001	50.92	0.0001	59.15	0.0001	61.62	0.0001	71.91	0.0002	27.57

0.0001	52.04	0.0001	59.14	0.0001	62.43	0.0001	71.91	0.0002	27.16
0.0001	52.98	0.0001	59.12	0.0001	63.22	0.0001	71.91	0.0002	27.16
0.0001	53.86	0.0001	59.05	0.0001	63.97	0.0001	61.41	0.0002	27.16
0.0002	29.61	0.0002	46.15	0.0003	55.66	0.0003	66.74	0.0004	73.88
0.0002	28.58	0.0002	46.95	0.0003	55.58	0.0003	62.82	0.0004	75.60
0.0002	32.01	0.0002	46.95	0.0003	56.63	0.0003	58.78	0.0004	78.63
0.0002	34.56	0.0002	46.34	0.0003	58.42	0.0003	56.35	0.0004	71.50
0.0002	36.51	0.0003	47.45	0.0003	58.42	0.0003	55.47	0.0004	61.91
0.0002	36.90	0.0003	48.16	0.0003	60.66	0.0003	56.14	0.0004	56.64
0.0002	37.80	0.0003	49.12	0.0003	62.52	0.0003	58.34	0.0004	56.64
0.0002	39.42	0.0003	50.24	0.0003	64.27	0.0003	58.34	0.0004	56.64
0.0002	41.32	0.0003	51.28	0.0003	64.27	0.0003	59.48	0.0004	56.64
0.0002	43.13	0.0003	52.05	0.0003	62.04	0.0003	63.00	0.0004	64.00
0.0002	44.86	0.0003	52.05	0.0003	62.83	0.0003	66.03	0.0004	68.42
0.0002	44.86	0.0003	50.90	0.0003	63.62	0.0003	68.32	0.0004	72.67
0.0002	43.62	0.0003	51.03	0.0003	64.18	0.0003	69.01	0.0004	72.67
0.0002	44.48	0.0003	51.03	0.0003	64.56	0.0003	70.46	0.0004	75.57
0.0002	44.96	0.0003	50.31	0.0003	63.81	0.0003	72.80	0.0004	76.30
0.0002	45.67	0.0003	51.60	0.0003	63.84	0.0003	72.80	0.0004	78.17
0.0002	46.50	0.0003	52.60	0.0003	64.67	0.0003	75.12	0.0004	81.51
0.0002	46.50	0.0003	53.89	0.0003	65.66	0.0003	75.12	0.0004	75.63
0.0002	47.35	0.0003	55.27	0.0003	65.66	0.0004	75.87	0.0004	71.94
0.0002	46.47	0.0003	56.43	0.0003	66.33	0.0004	74.29	0.0004	72.34
0.0005	53.36	0.0005	55.84	0.0006	71.86	0.0006	57.92	0.0007	64.93
0.0005	51.85	0.0005	57.91	0.0006	70.68	0.0006	57.00	0.0007	70.57
0.0005	52.13	0.0005	59.89	0.0006	71.31	0.0006	56.24	0.0007	68.50
0.0005	53.56	0.0005	61.58	0.0006	72.97	0.0006	55.60	0.0007	67.05
0.0005	55.66	0.0005	61.40	0.0006	74.17	0.0006	55.04	0.0007	68.38
0.0005	58.08	0.0005	61.14	0.0006	73.86	0.0006	57.15	0.0007	71.29
0.0005	60.44	0.0005	62.37	0.0006	72.11	0.0006	60.26	0.0007	74.68
0.0005	62.49	0.0005	64.50	0.0006	67.83	0.0007	52.70	0.0007	74.68
0.0005	62.49	0.0005	64.50	0.0006	65.59	0.0007	47.61	0.0007	73.81
0.0005	60.90	0.0006	65.67	0.0006	65.34	0.0007	46.14	0.0007	73.98
0.0005	58.66	0.0006	63.93	0.0006	65.83	0.0007	45.56	0.0007	72.51
0.0005	57.55	0.0006	63.41	0.0006	66.13	0.0007	45.75	0.0007	72.51
0.0005	58.27	0.0006	63.41	0.0006	66.13	0.0007	45.75	0.0007	71.69
0.0005	58.27	0.0006	58.03	0.0006	65.23	0.0007	46.79	0.0007	71.47
0.0005	58.68	0.0006	57.97	0.0006	66.56	0.0007	46.79	0.0007	71.63
0.0005	54.54	0.0006	59.92	0.0006	66.51	0.0007	46.41	0.0007	71.94
0.0005	51.45	0.0006	62.98	0.0006	65.07	0.0007	46.24	0.0007	72.15
0.0005	51.29	0.0006	66.33	0.0006	62.79	0.0007	50.02	0.0007	71.99

Temperature Simulation Graphs for all Experiments

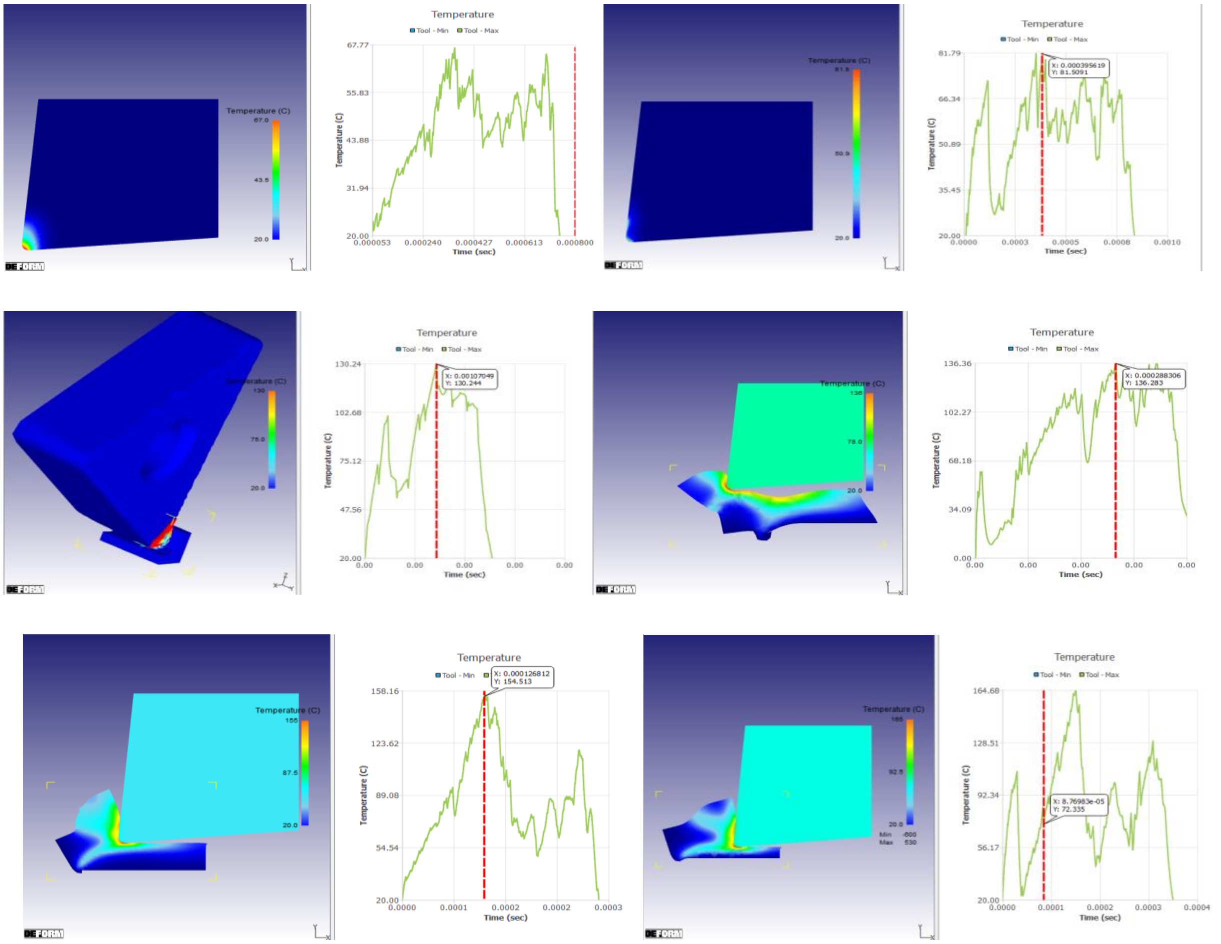

Appendix C. Experimental and simulation result of Tool wear

I. Crater wears for experiments runs eight, five, four, three, six, and two respectively, sequentially from the highest to the lowest.

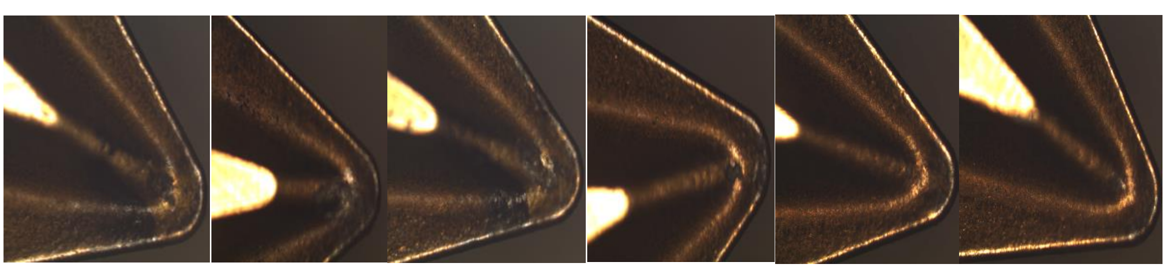

a) Exp.8 b) Exp.5 c) Exp.4 d) Exp.3 e) Exp.6 f) Exp.2

II. Weight loss of tool during machining

Run	Initial Weight of tool W_i (g)	Final Weight of tool W_f (g)	Machining time T_m(sec)
1	55.5678	55.5629	21
2	55.5867	55.5700	17
3	55.6173	55.5991	10
4	55.6230	55.5880	17
5	55.6023	55.5732	10
6	55.5471	55.5112	21
7	55.6107	55.5643	10
8	55.6709	55.6080	21
9	55.6678	55.6011	18
The density of tungsten carbide WC =15.63 g/cm^3			

III. Experimental And Simulation Results of The Specific Wear Rate for calibration.

Experiment and simulation at 90 m/min, 0.5 mm, and 0.15 mm/rev						
Exp.	Inverse temperature (1/T) K^{-1}	Interface pressure P (Mpa)	Sliding velocity V (mm/sec)	Specific wear rate (mm^3/s) $\frac{dw}{pvdt}$	Machining time T_m (sec)	The logarithm of the Specific wear rate $(ln\frac{dw}{pvdt})$
1	3.75E-03	2580	934	8.83E-13	160	-27.755
2	4.78E-03	2950	766	6.69E-13	150	-28.033
3	4.98E-03	3240	1080	6.63E-13	140	-28.042
4	5.07E-03	2920	904	5.12E-13	130	-28.29935
5	6.06E-03	3020	1080	2.48E-13	120	-29.024
6	6.66E-03	3090	957	2.42E-13	110	-29.04838
7	6.99E-03	8340	1640	4.68E-14	100	-30.69

IV. Simulation result at 90 m /min cutting speed, 0.5 depth of cut, and 0.15 feed for calibration of tool wear at different simulation times.

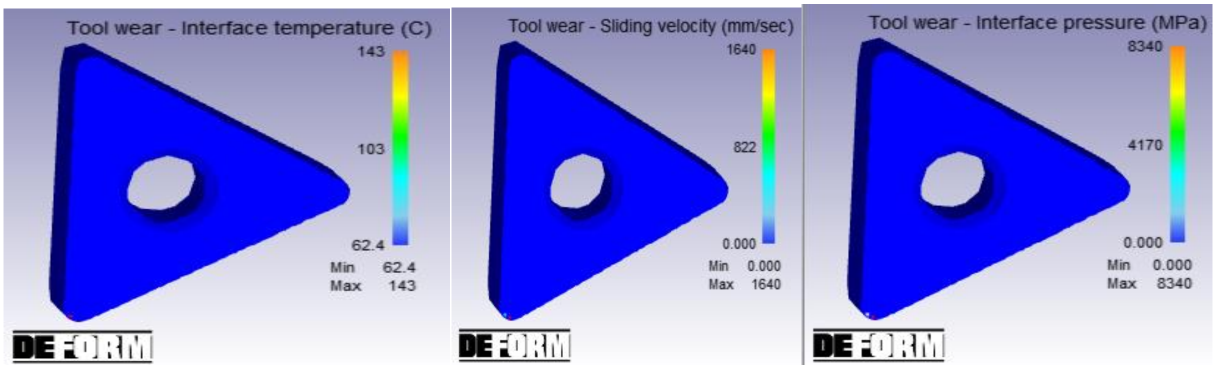

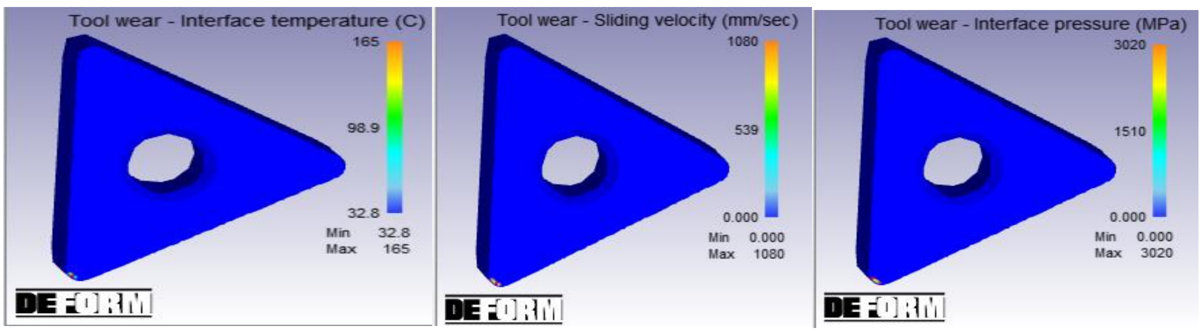

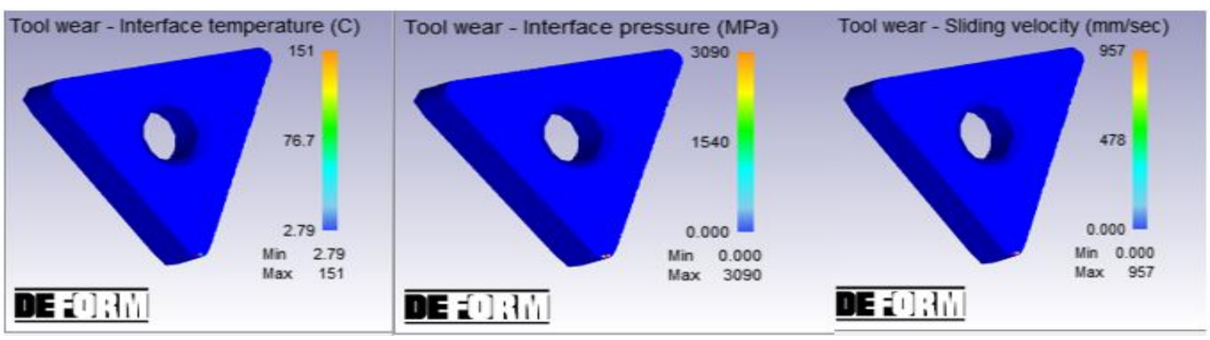

V. Regression of simulation and experimental result $(\frac{dw}{\sigma\, V dt}) = -1200\frac{1}{T} - 24$

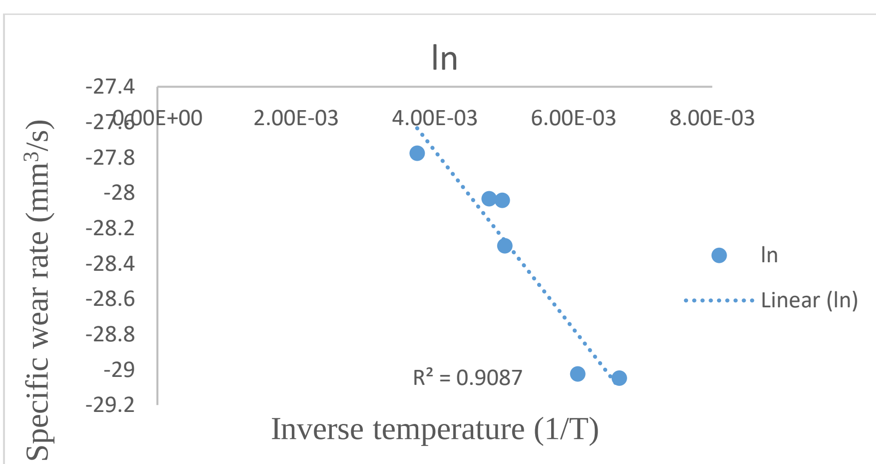

VI. Simulation results of tool wear rate for an orthogonal array of parameters

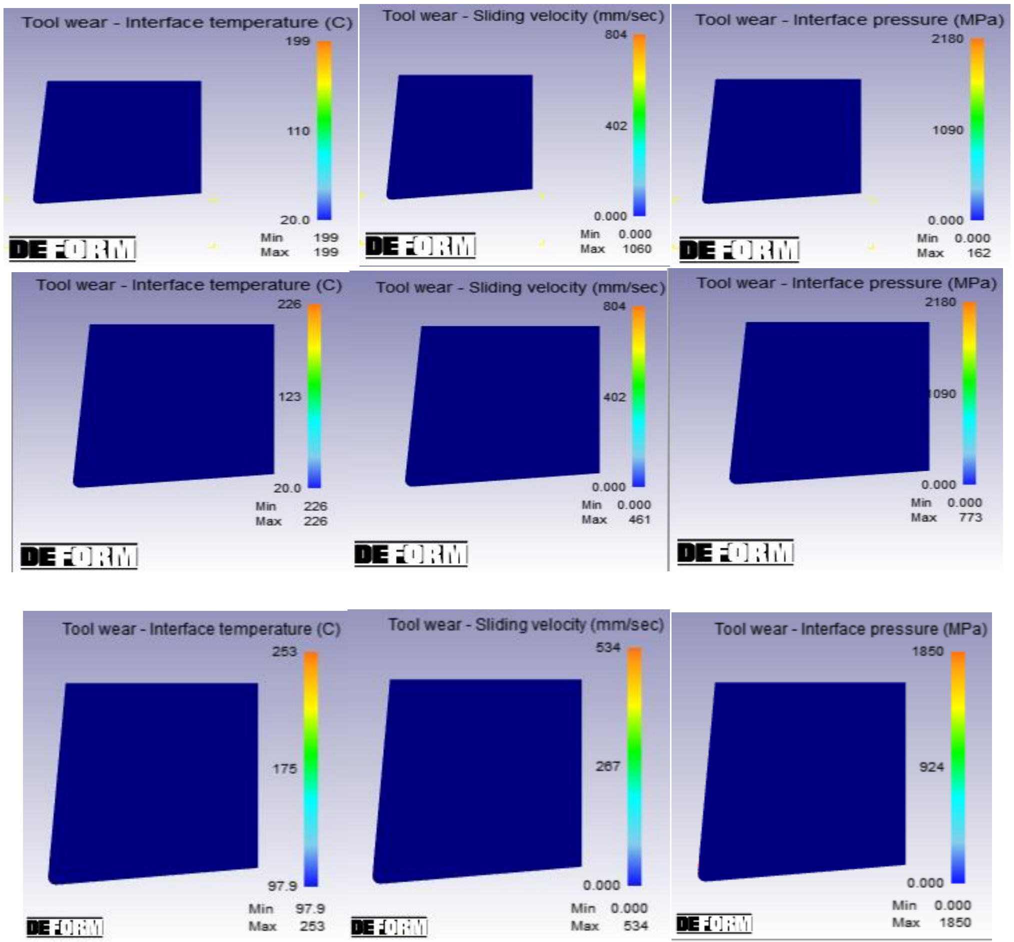

Appendix D. Chip Thickness

Cutting speed	Depth of cut	Feed	Average Chip Thickness (mm)
90	0.5	0.15	0.5
90	1.5	0.25	1
90	2.5	0.35	1.5
170	0.5	0.25	0.8
170	1.5	0.35	1.25
170	2.5	0.15	1.5
250	0.5	0.35	0.8
250	1.5	0.15	0.5
250	2.5	0.25	1.75

Appendix E. Interaction plot